GENERALIZED VORONOI TESSELLATIONS

Robert James Maillardet

B.Sc.(Hons) Monash

This thesis is submitted for the degree
of Doctor of Philosophy of the
Australian National University.

April, 1982

ORIGINALITY STATEMENT

This thesis represents the original work of the candidate, except for sections 2.4, 3.6 and 4.7, which contain joint work with Dr R.E. Miles.

Robert Maillardet

ROBERT MAILLARDET

ACKNOWLEDGEMENTS

I would like to thank Dr Roger Miles, who was a continual source of ideas and encouragement, and whose work forms the basis for so much of this thesis; Professor Moran, for his friendly guidance and advice, and Dr Geoff Watterson, who, in a sense, initiated the whole project.

Of my many Canberra friends, I particularly wish to mention Simon, Roger, Yasser, Cezary and the Murray family for their hospitality, support, advice and friendship. I especially wish to thank Miranda and Elizabeth, to both of whom I owe much more than I can express.

Returning to Melbourne, thanks go to Barbara Innes for her splendid typing and presentation. I sincerely wish to thank my family, and in particular my parents, whose support and assistance have never waned, and to whom I now dedicate this thesis.

To My Parents

ABSTRACT

This thesis is concerned with the Generalized Voronoi Tessellations V_n, a natural generalization of the well known Voronoi Tessellation $V \equiv V_1$, which is discussed in detail in Chapter 2. The Voronoi cells associated with random particles distributed over some space are the regions of that space where a particular particle is the closest particle. Generalized Voronoi cells are regions where a particular n particles are the closest n.

We undertake a comprehensive study of the geometry of these tessellations, particularly the particle arrangements around cells, and give stochastic constructions for vertices, sides and polygons (Chapter 3). These investigations form the basis for our main results. We find the mean area of Generalized Voronoi cells, for the general homogeneous case, and a wide collection of moment results (including the variance of the area for V_n cells), the probability of a quadrilateral in V_2, and certain conditional distributions for the area and perimeter, for the case when the generating point process is Poisson (Chapter 4).

Essential to our understanding of the geometry of V_n are plots of realizations of the tessellation. The computation of V_n is discussed (Chapter 5), together with a review of work dealing with the computation of V_1. Scaled realizations of a sequence of V_n's suggested that the tessellation converges fairly rapidly to a limit; in Chapter 6 we establish limiting distributions for the length of a typical V_n side, and for the interval length on an arbitrary linear transect of V_n.

Chapter 1 contains a review of tessellation models in general, discusses the ergodic definition of 'typical' cells, and presents a

summary of methods for moment calculations, which also contains some new moment results.

TABLE OF CONTENTS

GLOSSARY

$\mathbb{E}^n$	Euclidean n-space
$\underline{x},\underline{y}$	points in $\mathbb{E}^n$
∂X	boundary of a set X
ϕ	null set
$\omega_1,\omega_2,..,\Omega_1,\Omega_2,..$	*particles* of a point process (as opposed to *points* in $\mathbb{E}^n$)
$<\omega_1\omega_2>$	perpendicular bisector of particles ω_1 and ω_2
$<\omega_1\omega_2\omega_3>$	circumcentre of particles ω_1, ω_2 and ω_3
$<\omega_1\omega_2\omega_3>_i$	i-filled circumdisk of particles ω_1, ω_2 and ω_3
$Q(\underline{x},r)$	disk radius r centered at point $\underline{x}$
$Q(r)$	disk radius r
$\mathcal{V}_n$	aggregate of cells (convex polygons) in Generalized Voronoi Tessellation
P_n,R_n	elements of $\mathcal{V}_n$
$[\omega_1\omega_2..\omega_n]$	element of $\mathcal{V}_n$ with proximity set $\{\omega_1,\omega_2,..,\omega_n\}$
$A_{\omega,n}$	n-Area of particle ω
$C_{\omega,n}$	n-Circuit of particle ω
$\mathcal{L}_n$	aggregate of sides of $\mathcal{V}_n$ cells
$\mathcal{L}_n(\pm,\pm)$	sub-aggregate of sides of $\mathcal{V}_n$ cells with neighbouring segments from $\mathcal{V}_{\substack{n+1\\n-1}}$ on either side
$\sigma_n(\pm,\pm)$	density of $\mathcal{L}_n(\pm,\pm)$ sides
$p_n(\pm,\pm)$	ergodic probability that $\mathcal{L}_n$ side is member of $\mathcal{L}_n(\pm,\pm)$
$\sigma_n(i)$	density of $\mathcal{V}_n$ i-gons
$p_n(i)$	ergodic probability that $\mathcal{V}_n$ cell is i-gon
σ_n	density of $\mathcal{V}_n$ cells
$\nu_1,\nu_2,..$	vertices in $\mathcal{V}_n$

$\sigma(n,n+1)$	density of $(n,n+1)$ vertices
$\sigma(n)$	density of $\mathcal{V}_n$ vertices
$\mathcal{V}_{i-1,i}$	superposition of $\mathcal{V}_{i-1}$ and $\mathcal{V}_i$
a.s.	almost surely
$\xrightarrow{p}$	convergence in probability

Equations are numbered sequentially in each Section, and referenced by (Section. N), or (Chapter. Section. N), if reference is to another Chapter.

Figures are numbered sequentially in each Chapter, and referenced as Figure N, or Figure Chapter. N, if reference is to another Chapter. Lemmas and Theorems are treated the same way.

The following line conventions are followed when a figure contains cells or segments from $\mathcal{V}_1$, $\mathcal{V}_2$, $\mathcal{V}_3$ or $\mathcal{V}_4$:-

$\mathcal{V}_1$

$\mathcal{V}_2$

$\mathcal{V}_3$

$\mathcal{V}_4$

If a figure refers to a general V_i and V_{i-1} the conventions are:-

V_i

V_{i-1}

The following convention is sometimes used to emphasize a particular perpendicular bisector:-

perpendicular bisector

Crosses are used on diagrams to represent the *particles* of a point process.

CHAPTER 1

RANDOM TESSELLATIONS

1.1 Introduction

This thesis is concerned with the study of generalized Voronoi tessellations, which are a particular class of random tessellations of the plane.

Definition

A *tessellation* of a space X is an aggregate of disjoint sets C_i whose union is X. The C_i are called the cells of the tessellation. These cells may share a common boundary set which is null.

In the theoretical tessellation models we consider, the cells fall into a very limited class of types. In most models for the tessellation of d-dimensional Euclidean space $\mathbb{E}^d$, the cells are convex polytopes (polygons in $\mathbb{E}^2$, polyhedra in $\mathbb{E}^3$). Some models produce non-convex cells, and even unconnected cells. However connectedness is really a minimal assumption to permit the practical interpretation of the cells of a tessellation as the zone of influence, territory or actual shape of entities occupying X and competing for a share of its space.

For any given X there are numerous ways to partition it to form a tessellation. The established mathematical techniques can be divided into two general categories - (i) where we define the partitioning of X by a direct prescription of the boundaries between cells and (ii) where we specify a random framework of some description on X (often a point process) and a set of rules which partition the space using that random framework. To introduce a range of tessellation models and their generating mechanisms we now list a number of examples from both categories.

Category (i) - Direct Specification of Boundaries

(a) Box and Grid Tessellations

On a first attempt at defining cell boundaries we may think of associating vertical and horizontal lines with random points distributed on two orthogonal axes (in two dimensions) or similarly associating planes with random points distributed on three axes (in three dimensions). We thus generate the grid tessellation of the plane into rectangles and the box tessellation of $\mathbb{E}^3$ into rectangular cells.

However we may be interested in a truly random distribution of lines or planes in the sense that the probability that a subset X of $\mathbb{E}^2$ is hit by a line or plane of our process is invariant under Euclidean translations and rotations of X. From Integral Geometry, (Santalo [1976]) we know that the measures for lines and planes are uniquely determined (up to a constant) by this condition. By defining appropriate point processes on the parameter space for these geometric objects, a random tessellation results.

(b) Poisson Line Process

If we parametrize a line by the polar co-ordinates of the perpendicular bisector to the line from the origin (p,θ), then a standard Poisson point process with constant intensity ρ (denoted henceforth by $\mathbb{P}$) defined on the parameter space $(0 \leq \theta < 2\pi,\ p > 0)$ produces a random distribution of lines. Each realization of the point process corresponds to a tessellation of the plane into convex polygons by the associated lines. For any bounded convex domain K in $\mathbb{E}^2$, the number of lines which hit K is Poisson with mean proportional to the perimeter of K. For details see Miles [1964, 1973], Solomon [1978, Ch 3]. Distributional properties of this process which are beyond theoretical treatment have been estimated by Monte Carlo methods (Crain and Miles [1976]).

(c) Poisson Plane Process, Poisson Hyperplane Process

If we parametrize a plane by the spherical polar co-ordinates (p,θ,ϕ) of the foot of the perpendicular from the origin to the plane, the joint probability density function (p.d.f.) for θ and ϕ corresponding to an isotropic direction for the plane is

$$f(\theta,\phi) = \frac{1}{2\pi} \sin \theta \,. \qquad 0 \leq \theta,\ \phi < \pi$$

Hence an inhomogeneous Poisson point process of intensity $\left(\frac{\rho \sin \theta}{2\pi}\right)$ on the parameter space $(0 \leq \theta,\ \phi < \pi,\ -\infty < p < \infty)$ produces a random distribution of planes which tessellate $\mathbb{E}^3$ into convex polyhedra. See Miles [1972] for details on this Poisson plane process and Matheron [1975], Miles [1974] for the extension to the polytopal tessellation of $\mathbb{E}^d$ generated by random $(d - 1)$ dimensional hyperplanes. Miles has also considered modifications of these Poisson processes, involving anisotropic distributions for orientation and the thickening of lines and planes into strips and slabs (Miles [1964, 1972]). There has also been some work on the properties and characterization of more general line and hyperplane processes (Davidson [1974], Krickeberg [1973], Kallenberg [1976], Papangelou [1972]).

(d) Line Segment Processes

As with the line and plane processes above, we can specify a random process (field) of segments by a point process on the parameter space for these geometric elements, in this case (x,y,ϕ), where (x,y) are the co-ordinates of the midpoint of the segment and ϕ its angle with a fixed direction $(-\infty < x,y < \infty,\ 0 \leq \phi < \pi)$.

By an ingenious categorization of a random tessellation as a special case of random fields of line segments, Ambartzumian [1970] has proved that the vertices of 'regular' homogeneous isotropic random tessellations can only be of the 'T' and 'X' types, under the condition that the marked point process $\{a_i,\theta_i\}$ of intersection points a_i of an arbitrary line L with the tessellation (with accompanying angles θ_i) satisfies certain independence assumptions. (The θ_i must be mutually independent and independent of the a_i). A consequence of this theorem is that a random tessellation with no 'T' vertices is a mixture of Poisson line processes (see also Davidson [1970]). Further work by Ambartzumian [1974] using the process of intersection points $\{a_i,\theta_i\}$ with an arbitrary line yields the Laplace transform of the side length distribution and relationships between moments for cell characteristics such as area and perimeter and the moments for I, the interval length for $\{a_i,\theta_i\}$. These results are stereological in nature. See section 1.3 for an alternative derivation of some of these moment relationships and some additional results.

Category (ii) - Indirect Partitioning Induced by a Superposed Random Framework

The majority of tessellations in this category use a point process defined on the space as the basic framework from which to build the tessellation.

(a) Voronoi and Generalized Voronoi Tessellations

A point process of particles is defined on X. We imagine symmetric growth of cells in all directions from the particles as nuclei, with growth terminating when cell boundaries meet. The region associated with each particle is the set of points which have it as the closest particle. A natural generalization is to consider the regions where n particles are the closest n. These tessellations are studied in detail in following chapters.

(b) Johnson-Mehl Tessellation

In this tessellation cells are again formed by isotropic growth, but the particles now appear over time (instead of all being present at $t = 0$ as in the Voronoi case). The standard Johnson-Mehl tessellation, with a homogeneous Poisson birth process for particles (probability of birth in volume dV during time dt is $\alpha dVdt$) is considered by Meijering [1953]. A generalized form with birth process $\alpha(t)dVdt$, inhomogeneous in t, is considered by Miles [1972]. This tessellation has non-convex cells with hyperbolic boundaries, but all cells are star shaped relative to their nucleus.

We can also extend the Johnson-Mehl model by allowing anisotropic growth or different growth speeds. However these modifications are not really tractable, although some use has been made of this generation technique with the qualification that growth does not stop when cell boundaries meet. Thus cells can be composed of disconnected regions (Fischer and Miles [1973]).

(c) Gilbert's Radiating Segments Model

From each particle of a point process on X, a line segment grows at angle ϕ_i to a fixed direction (ϕ_i uniform on $[0,\pi]$ and independent) and at a constant rate in both directions from the generating particle. Growth terminates when a segment meets another segment. A convex polygonal tessellation of the plane results. Gilbert [1967] has used this as a model for the growth of needle-shaped crystals.

Relevant to Category (ii) methods of defining random tessellations is an analysis of the partitioning of the circular zones of influence associated with plants on a lattice (Gates et al. [1979]). The authors show that fairly general and natural assumptions about the partition sets associated with each plant lead to a very explicit form for the boundary curve between these sets, which includes the Voronoi and Johnson-Mehl boundaries as special cases. Thus the properties we naturally require if we wish to attribute a physical meaning to a tessellation cell in some practical competition context are shown to have a powerful limiting effect on the nature of the tessellation.

This completes the list for Category (ii). The above tessellations are the only models which have received significant mathematical attention. These models are few in number and their generating mechanisms are even more limited. New generation mechanisms, hopefully motivated by a better understanding of practical tessellation phenomena, are certainly needed before tessellation modelling can be of practical significance.

1.2 Ergodic Theory for Homogeneous Random Tessellations

For the purposes of this section we make the formal

Definition

Let (Ω, S, P) be a probability space. A *random tessellation* Ψ, is a random variable which maps Ω into the set of aggregates of convex polygons which tessellate the plane.

Let $T^a \underline{x} = \underline{x} + a$, $\underline{x} \in \mathbb{E}^2$. A random tessellation is *homogeneous* if T^a is measure preserving i.e. $P(T^a A) = P(A)$, $\forall A \in S$, and *ergodic* if T^a is ergodic i.e. $A = T^a A \Rightarrow P(A) = 0$ or 1.

A cell *characteristic* of a cell of Ψ is a scalar, determined by the cell, which is translation invariant e.g. N, the number of sides (or vertices); A, the area; S, the perimeter and I, the inradius. Let $Z = (Z_1, Z_2, \ldots, Z_m)$ be a vector description of a Ψ cell, where the Z_i are cell characteristics.

For (almost) all realizations ω of Ψ we have an infinite aggregate of polygons, and we are naturally interested in the distribution of polygon characteristics for a typical representative of this aggregate. We cannot obtain these distributions by selecting, for example, the polygon which contains the origin, which is not typical but in fact 'area-weighted' in an analogous manner to the length weighting of the interval containing the origin in a strictly stationary linear point process.

A natural way to proceed is to consider the (random) empirical distribution function $F_{Z,r}(z)$ of Z for cells contained in the disk Q(r) and its limit as $r \to \infty$. Miles [1961], in his as yet unpublished PhD Thesis has shown that

$$F_{Z,r}(z) \xrightarrow{a.s.} F_Z(z) \quad , \tag{2.1}$$

a (constant) distribution function, as $r \to \infty$, by an application of Weiner's multiparameter ergodic theorem [1939], provided Ψ is homogeneous and ergodic. Weiner's Theorem states that under these assumptions, for a random variable X with $E|X| < \infty$,

$$\underset{a.s.}{\lim_{r\to\infty}} \frac{1}{\pi r^2} \int_{Q(r)} X(T^{-a}\omega)da \quad , \tag{2.2}$$

exists and equals E(X). This equality of a 'space average' over a single physical realization with a 'time average' over all realizations, was motivated by statistical mechanics. Ergodicity is the minimal requirement for such equality. However it can be verified by proving a (stronger) mixing condition that realizations of Ψ in different regions tend to independence as the separation of the regions increases.

The critical step in establishing (2.1) using (2.2) is the representation of $F_{Z,r}(z)$ as the integral of an appropriately defined X. For example, if $F_{A,r}(a)$ is the empirical d.f. for the area A of cells in Q(r) then

$$F_{A,r}(a) \equiv \frac{\text{number of cells in } Q(r) \text{ with } A \leq a}{\text{number of cells in } Q(r)}$$

$$= \frac{\frac{1}{\pi r^2}\int_{Q(r)} A(t,\omega,x)dt}{\frac{1}{\pi r^2}\int_{Q(r)} A(t,\omega)dt} \quad ,$$

where $A(t,\omega) = (\text{area of cell containing } t)^{-1}$ and $A(t,\omega,x)$ takes the same value for cells with area less than x, and is zero otherwise. For a detailed exposition of ergodic theory applied to homogeneous planar tessellations see Cowan [1978].

All tessellations considered in this thesis are homogeneous and ergodic. Hence all cell characteristics have well-defined ergodic limiting distributions which can be interpreted as the distribution of these characteristics for a cell of Ψ picked in such a way that each cell has an equal chance of being chosen; such a cell will be referred to as a *typical* or *uniform random* cell of Ψ.

Using the same theory we can show that any homogeneous ergodic point process has a well-defined particle density ρ where

$$\rho \underset{a.s.}{=} \lim_{r\to\infty} \frac{N(r)}{\pi r^2} ,$$

and $N(r)$ is the number of particles in $Q(r)$.

1.3 Moment Calculations for Random Tessellations

In general the full ergodic distributions for important polygon characteristics are beyond theoretical treatment, and for most of the well-known random tessellations the only theoretical results relate to low-order moments and cross-moments for some characteristics (notably A (area); S (perimeter) and N (number of sides)), as well as some probabilities $\{p_n\}$ from the discrete distribution for N, for small n values.

We note that even though the ergodic distribution for a polygon characteristic may exist (the moment condition in Weiner's theorem essentially puts restrictions on the smallness of polygons) this does not guarantee the existence of the moments of this characteristic, which requires restrictions on the largeness of polygons (see Cowan [1978]).

A moment calculation depends on a representation of the quantity of interest. Sometimes this representation will be obvious; sometimes it will be obtained by a trick of some sort. Obtaining the most convenient representation, or at least a workable one, is a task which often depends on special features of the particular tessellation - the theory of random tessellations lacks a body of routinely applicable 'methods'. However we can classify moment calculations into various types.

(i) Ergodic Theory Method

The empirical means over Q(r) for a cell characteristic Z_i, tend to the mean of Z_i relative to the limiting ergodic distribution $F_{Z_i}(z)$ (Miles [1970]). For example, Miles uses this technique to calculate E(A), E(S) and E(N) for generalized Voronoi cells (see section 3.1 and Miles [1970]).

(ii) Indicator Function Method

We can calculate the mean of a random area by representing it as an integral of its indicator function (Robbins [1944]). Examples of this technique occur in sections 3.2 and 4.4. As an example, for a general homogeneous isotropic tessellation Ψ, we have the expression

$$\begin{aligned} E(A) &= E\left(\int I_A(\underline{x})d\underline{x}\right) \\ &= \int EI_A(\underline{x})d\underline{x} \\ &= \int P(\underline{x} \in Q)d\underline{x} \\ &= 2\pi\int_0^\infty rP((r,0) \in Q)dr \quad , \end{aligned} \tag{3.1}$$

for the mean area of a typical cell Q. Analogous to this technique are the representations

$$S(\omega) = \int S(d\underline{x}) \tag{3.2a}$$

$$S(\omega) = \int_0^\infty S(r,dr) \quad , \tag{3.2b}$$

which can be used for the calculation of the first moment of the perimeter. (3.2b) is essentially Meijering's representation, which he used to calculate the first moments of S and N for two and three-dimensional Voronoi cells (see section 2.3).

(iii) Goudsmit's Method

Goudsmit obtained the mean square area for a typical polygon from a Poisson line process by calculating the probability that two random points are contained in the same polygon in two different ways (Goudsmit [1945]).

This technique was extended to general dimensional Poisson hyperslab processes by Miles [1961]. Richards [1964] generalizes the technique to obtain a variety of averages for a Poisson line process by averaging an arbitrary function of the distance between two random points, constrained to lie within a single polygon. Kendall (see Miles [1964]) obtained $E(A^3)$ for a Poisson line process by considering three random points instead of just two.

In fact the technique, and Richard's generalization, is applicable to general homogeneous isotropic tessellations, and enables us to relate the moments of several polygon characteristics to the moments of certain interval distributions for a linear transect of the process. In this way we duplicate (and extend) certain results of

Ambartzumian [1974]. These results are essentially stereological in nature, and are intimately linked with integral geometry.

Definition

Let L be an arbitrary linear transect of a homogeneous isotropic tessellation Ψ. The 'events' on L are the intersection points of L with cell boundaries of Ψ. Since Ψ is homogeneous, I, the inter-event distance, has a well-defined *stationary* ergodic distribution. So does J, the distance from an arbitrary point on L to the next 'event'.

Theorem 1

Let Ψ be a homogeneous isotropic random tessellation, and let $G_a(x)$ denote the distribution function of J, G(x) the distribution function of I. Then

$$E\left(\iint_{Q\times Q} f(|\underline{x} - \underline{y}|)d\underline{x}d\underline{y}\right) = 2\pi E(A) \int_0^\infty xf(x)(1 - G_a(x))dx \quad ,$$

where f is an arbitrary function of the distance $|\underline{x} - \underline{y}|$ between points $\underline{x}$ and $\underline{y}$, and the integral is taken over the interior of a typical polygon Q.

Proof

Let $$D = E\left(\iint_{Q\times Q} f(|\underline{x} - \underline{y}|)d\underline{x}d\underline{y}\right)$$

$$= E\left(\iint f(|\underline{x} - \underline{y}|)I(\underline{x})I(\underline{y})d\underline{x}d\underline{y}\right) \quad ,$$

where $I(\underline{x})$ is the indicator function of Q i.e.

$$I(\underline{x}) = \begin{cases} 1 & \underline{x} \in Q \\ 0 & \underline{x} \notin Q \end{cases}$$

Hence

$$D = \iint f(|\underline{x} - \underline{y}|)E(I(\underline{x})I(\underline{y}))d\underline{x}d\underline{y}$$

Now

$$\begin{aligned} E(I(\underline{x})I(\underline{y})) &= P(\underline{x} \text{ and } \underline{y} \in Q) \\ &= P(\underline{y} \in Q|\underline{x} \in Q)P(\underline{x} \in Q) \\ &= (1 - G_a(c))P((r_1,0) \in Q) \ , \end{aligned}$$

where c is the distance between $\underline{x}$ and $\underline{y}$, and (r_1,θ_1), (r_2,θ_2) are the polar co-ordinates of $\underline{x}$ and $\underline{y}$ (see Figure 1). Note that $P((r_1,\theta_1) \in Q) = P((r_1,0) \in Q)$ by isotropy of Ψ.

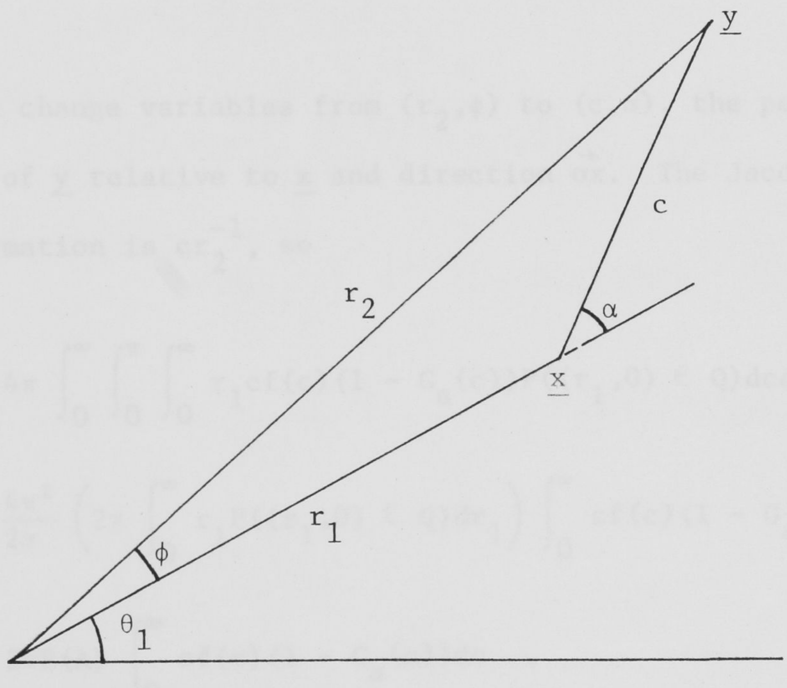

Figure 1

Changing to polar co-ordinates gives

$$D = \iiiint f(c)(1 - G_a(c))P((r_1,0) \in Q)r_1r_2 \ dr_1dr_2d\theta_1d\theta_2 \ .$$

Note that c is a function only of $\phi = |\theta_2 - \theta_1|$, and hence D is of the form

$$\int_0^{2\pi}\int_0^{2\pi} F(|\theta_2 - \theta_1|)d\theta_1 d\theta_2 \quad ,$$

where F has the property that $F(\phi) = F(2\pi - \phi)$. In this case we have the useful formula,

$$\int_0^{2\pi}\int_0^{2\pi} F(|\theta_2 - \theta_1|)d\theta_1 d\theta_2 = 4\pi \int_0^{\pi} F(\phi)d\phi \qquad (3.3)$$

Hence

$$D = 4\pi \int_0^{\infty}\int_0^{\pi}\int_0^{\infty} r_1 r_2 f(c)(1 - G_a(c))P((r_1,0) \in Q)dr_2 d\phi dr_1$$

Fixing r_1, we change variables from (r_2,ϕ) to (c,α), the polar co-ordinates of $\underline{y}$ relative to $\underline{x}$ and direction $\vec{ox}$. The Jacobian of this transformation is cr_2^{-1}, so

$$D = 4\pi \int_0^{\infty}\int_0^{\pi}\int_0^{\infty} r_1 c f(c)(1 - G_a(c))P((r_1,0) \in Q)dc d\alpha dr_1$$

$$= \frac{4\pi^2}{2\pi}\left(2\pi \int_0^{\infty} r_1 P((r_1,0) \in Q)dr_1\right)\int_0^{\infty} cf(c)(1 - G_a(c))dc$$

$$= 2\pi E(A)\int_0^{\infty} cf(c)(1 - G_a(c))dc \quad ,$$

using (3.1), which completes the proof.

Applications of Theorem 1

We can obtain a variety of averages from this theorem by appropriate choices of the function f. Consider $f(x) = x^n$ for example. Then

$$E\left(\iint_{Q\times Q} |\underline{x} - \underline{y}|^n d\underline{x}d\underline{y}\right) = 2\pi E(A) \int_0^\infty x^{n+1}(1 - G_a(x))dx$$

$$= \frac{2\pi E(A)}{(n + 2)} \left[(n + 2) \int_0^\infty x^{n+1}(1 - G_a(x)dx\right]$$

$$= \frac{2\pi E(A)E(J^{n+2})}{(n + 2)} \quad , \quad n = -1,0,1,.. \qquad (3.4)$$

We can also express (3.4) in terms of the moments for I, the more usual inter-event distribution. We note that if I has mean λ^{-1} say, then we have the following relationship between $G_a(x)$ and $G(x)$ (see Lewis [1972] p 354).

$$G_a(x) = 1 - \lambda \int_x^\infty (1 - G(u))du \; .$$

Hence
$$E(J^n) = n \int_0^\infty x^{n-1}[1 - G_a(x)]dx$$

$$= n\lambda \int_0^\infty \int_x^\infty x^{n-1}(1 - G(u))dudx$$

$$= \frac{\lambda}{(n + 1)} \left[(n + 1) \int_0^\infty u^n(1 - G(u))du\right]$$

$$= \frac{\lambda}{(n + 1)} E(I^{n+1}) \; , \qquad n = 1,2,.. \qquad (3.5)$$

We also note the relation

$$E(A) = E(S)E(I)/\pi = E(S)/\lambda\pi \quad , \qquad (3.6)$$

which holds for general homogeneous isotropic tessellations (see Ambartzumian [1974], where the divisor of π is omitted).

Combining (3.4), (3.5) and (3.6) yields

$$E\left(\iint_{Q\times Q} |\underline{x} - \underline{y}|^n d\underline{x}d\underline{y}\right) = \frac{2E(S)E(I^{n+3})}{(n+2)(n+3)}, \quad n = -1,0,1,.. \tag{3.7}$$

In particular, for n = -1,0,1 and 2 we have

$$\begin{aligned} E(\Phi) &= E(S)E(I^2) \\ E(A^2) &= E(S)E(I^3)/3 \\ E(A^2R) &= E(S)E(I^4)/6 \\ E(AM) &= E(S)E(I^5)/10 \ , \end{aligned} \tag{3.8}$$

where R denotes the mean separation of two random points in a typical polygon, A is its area, M its moment of inertia about its centre of gravity and Φ is its "Newtonian self-energy" (see Richards [1964], for calculation of these moments in the Poisson line process case).

Use is made of (3.4) and (3.8) in sections 4.5 and 6.2, where the moments of J are used to calculate the variance of the area of V_n cells.

(iv) Weighting Methods

We have defined a 'typical cell' of a random tessellation and mentioned that the cell containing the origin is 'area-weighted'. From the mean area of an 'area-weighted' cell we can obtain the second moment of the area of a typical cell (see section 4.4 and (4.4.4)). We can also weight cells in various ways. Choosing a uniform random vertex and then choosing (uniformly) from the cells which meet at that vertex gives an [N]-weighted cell, provided an equal number of sides join at each vertex. Superimposing an independent Poisson line process and choosing cells which are hit by m lines gives an $[e^{-S}S^m]$-weighted cell. Similarly, considering the sub-aggregate of n-gons of a Poisson line process intersected by $m = i + 2j$ hitting lines we again obtain an $[e^{-S}S^m]$-weighted cell; the subclass of these cells where the hitting lines contain j pairs intersecting inside the cell forms an $[e^{-S}S^iA^j]$-weighted aggregate.

Miles [1973] uses these results to calculate higher moments for the Poisson line process.

Devising various methods for choosing polygons and utilizing the weighted aggregates which result is a major but relatively undeveloped technique for obtaining higher moments. For example, consider the following two methods of choosing an 'adjacent polygon pair':- i.e. a pair of adjacent polygons with a common side.

<u>Method 1</u> Choose a uniform random side and take the pair of polygons which have this side as a common side - this is a uniform random 'polygon pair'.

<u>Method 2</u> Choose a uniform random cell. Then choose (uniformly) a side of that cell, and take the polygon pair with this side as their common side.

Now consider a side s shared by two polygons with side numbers N_1 and N_2. Under Method 2,

$$P(\text{s is chosen}) \propto \frac{1}{N_1} + \frac{1}{N_2} = \frac{N_1 + N_2}{N_1 N_2} .$$

Hence s, and the polygon pair associated with s, is $\left[\frac{N_1 + N_2}{N_1 N_2}\right]$-weighted. If $\underline{Z}$ is any characteristic of the polygon pair, then

$$f_2(N_1,N_2,\underline{Z}) \propto \frac{N_1 + N_2}{N_1N_2} f_1(N_1,N_2,\underline{Z}) \quad ,$$

where f_i is the joint density of N_1, N_2 and $\underline{Z}$ under method i. Write E_i for expectation relative to f_i. Then

$$f_2(N_1,N_2) = \frac{k(N_1 + N_2)}{N_1N_2} f_1(N_1,N_2) \quad , \qquad (3.9)$$

where
$$k^{-1} = E_1\left(\frac{N_1 + N_2}{N_1N_2}\right)$$

$$= E_1\left(\frac{1}{N_1}\right) + E_1\left(\frac{1}{N_2}\right)$$

$$= 2E_1\left(\frac{1}{N_1}\right) \quad .$$

To calculate $E_1\left(\frac{1}{N_1}\right)$, we note that each individual polygon associated with a uniform random side is [N]-weighted. If g and f are the densities of N for [N]-weighted and uniform random cells respectively, then

$$g(N) = \frac{Nf(N)}{E_f(N)} \quad ,$$

and hence

$$E_g(N) = \frac{E_f(N^2)}{E_f(N)}$$

$$E_g\left(\frac{1}{N}\right) = \frac{1}{E_f(N)} \quad ,$$

where E_f and E_g represent expectations with respect to f and g. Hence

$$E_1\left(\frac{1}{N_1}\right) = \frac{1}{E_f(N_1)}$$

and
$$k = \tfrac{1}{2}E_f(N_1) \quad .$$

Multiplying both sides of (3.9) by N_1N_2 and summing gives the interesting relationship

$$E_2(N_1N_2) = k(E_1(N_1) + E_1(N_2))$$

$$= 2kE_1(N_1)$$

$$= E_f(N_1^{\ 2}) \quad .$$

Hence for a Poisson line process, the 'adjacent' moment $E_2(N_1N_2)$ is $(\pi^2 + 24)/2 = 16.93$, predictably smaller, but not substantially, than $E_1(N_1N_2) = 10 + {}^{3\pi^2}/4 = 17.40$ (see Miles [1973] sections 8 and 9).

For a Voronoi tessellation (see Chapter 2),

$$E_2(N_1N_2) \mathrel{\overline{\sim}} 37.8 \quad ,$$

which is the simulation estimate of $E_f(N^2)$ given by Hinde and Miles [1980]. However, the value of $E_2(N_2) = k\left(1 + E_f\left(\frac{N_1}{N_2}\right)\right)$ is an open problem for both tessellations.

Weighting arguments are essential to arguments used in sections 4.3 and 4.4 for the calculation of certain moments and probabilities.

CHAPTER 2

THE VORONOI TESSELLATION

2.1 Introduction - Basic Geometry

This chapter is concerned with the Voronoi (or Dirichlet) tessellation, which was first considered in the 19^{th} century (Dirichlet [1850]), and which has played an increasingly important role in attempts to model tessellated phenomena in a wide range of subjects.

The tessellation is generated by a process of particles distributed on a space upon which a distance function is defined (a general metric space could be used). We make the following assumptions about the particle process -

(i) spatial homogeneity

(ii) countable particle set (a.s.)

(iii) no multiple particles i.e. particles which are co-incident (a.s.)

(iv) a.s. particles are in 'general position' e.g. no three particles are co-linear, no four particles lie on the same circle.

<u>Definition</u> A particle process in d-dimensions satisfying (i) - (iv) will be referred to as a π_d type process.

Label the particles of a π_d type process $\omega_1, \omega_2, \ldots$ and define $K_{ij} = \{\underline{x} : |\underline{x} - \omega_i| \leq |\underline{x} - \omega_j|, \underline{x} \in X\}$, the half-space of points nearer to ω_i than ω_j. Consider an arbitrary particle ω_i. The Voronoi cell of ω_i, $[\omega_i]$, consists of all those points $\underline{x}$ with ω_i as the nearest particle. An example of a Voronoi tessellation for a small number of particles is given in Figure 1. Obviously,

$$[\omega_i] = \bigcap_{j:j\neq i} K_{ij} \tag{1.1}$$

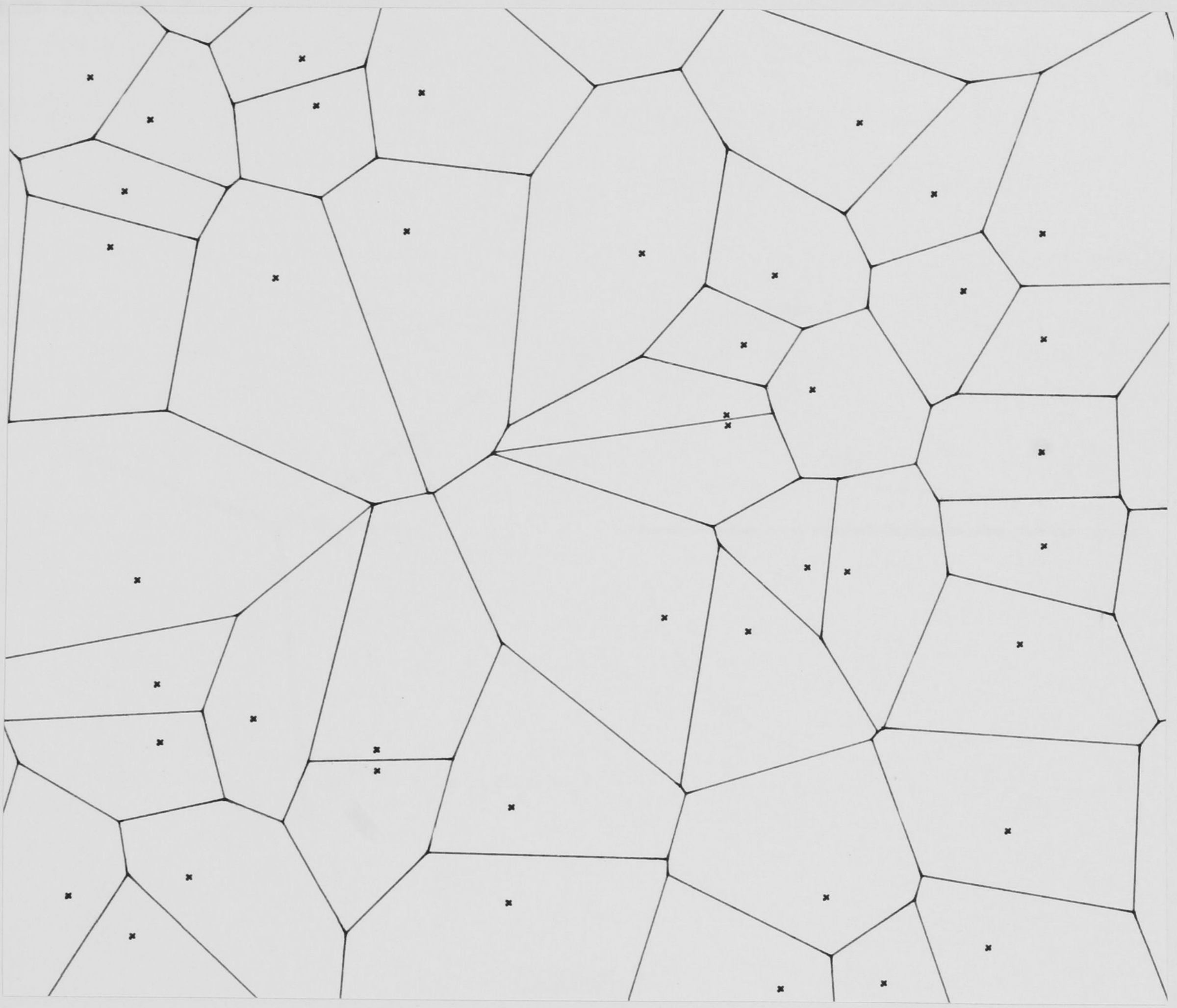

Figure 1

Definition

$V \equiv \{[\omega_i] : \omega_i$ varies over all particles of a π_d type process$\}$,

is a Voronoi tessellation of the space upon which π_d is defined.

If the generating particle process π_2 is defined on the plane $\mathbb{E}^2$ then, from (1.1), each $[\omega_i]$ is a convex polygon, and V is thus a convex polygonal tessellation of $\mathbb{E}^2$. Apart from the null set of polygon boundaries, every point of $\mathbb{E}^2$ belongs to one, and only one $[\omega_i]$. Consideration of these boundary points shows that they are of the two types shown in Figure 2 - either a vertex of exactly three cells or in the dividing edge between two adjacent cells - as is clear from Figure 1.

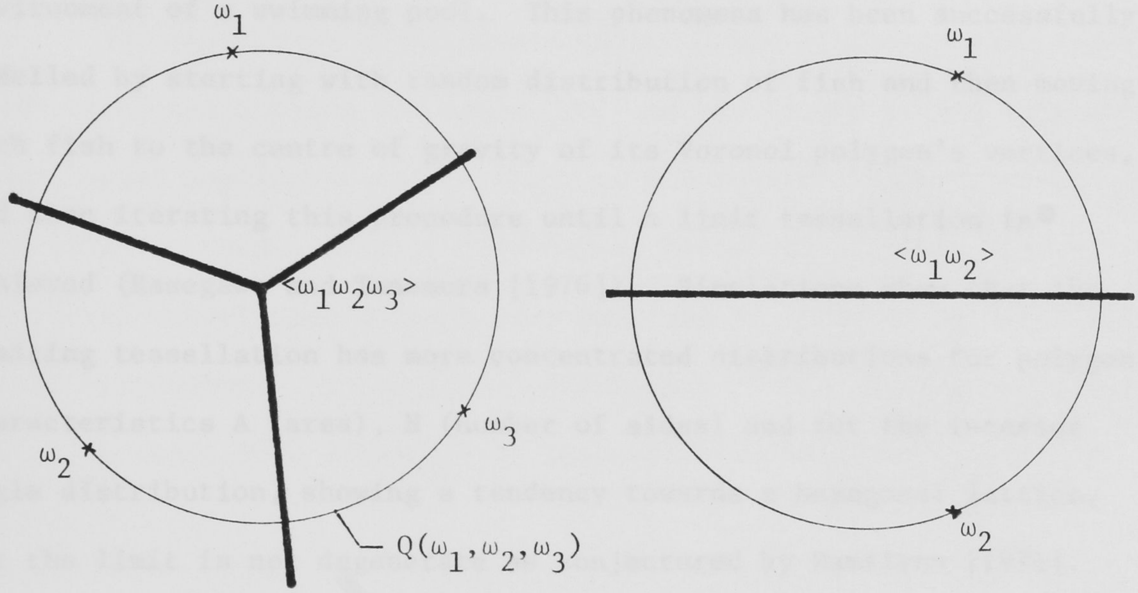

Figure 2

We write $<\omega_1\omega_2>$ for the perpendicular bisector of particles ω_1, ω_2 and $<\omega_1\omega_2\omega_3>$ for the circumcentre of ω_1, ω_2 and ω_3. $Q(\omega_1,\omega_2,\omega_3)$ is the circumdisk associated with the vertex $<\omega_1\omega_2\omega_3>$ (see Figure 2).

2.2 Applications of the Voronoi Tessellation

The Voronoi tessellation has been re-invented in numerous fields as a natural way of tessellating a space occupied by a collection of entities competing in some manner for territory, hence the alternative descriptions of the construct as a Dirichlet or

Thiessen tessellation.

In many cases the tessellation is an idealized or simplified way of dividing the space; however there are some remarkable practical examples of visible territory division conforming to the Voronoi model. For example, mouthbreeder fish, 'Tilapia mossambica', which define their territory by spitting sand at their neighbours, have produced a Voronoi tessellation formed with sand parapets in the uniform environment of a swimming pool. This phenomena has been successfully modelled by starting with random distribution of fish and then moving each fish to the centre of gravity of its Voronoi polygon's vertices, and then iterating this procedure until a limit tessellation is achieved (Hasegawa and Tanemura [1976]). Simulations show that the limiting tessellation has more concentrated distributions for polygon characteristics A (area), N (number of sides) and for the interior angle distribution, showing a tendency towards a hexagonal lattice, but the limit is not degenerate as conjectured by Hamilton [1971]. The iterative modification is based on the assumption that, although the territory will tend to be divided in a Voronoi manner, the animals will also wish to maximize their distance from their neighbours. A similar method was used to model the territories of pectral sandpipers, 'Celidris Melanotos', although in this case animals were introduced over time, instead of simultaneously at the beginning, with the constraint that a new animal could not be added within a certain distance of established animals (Hasegawa and Tanemura [1977a]). Related to this model is a method of 'areal random packing', where a particle can only be added if the Voronoi cells of the resulting tessellation are all above an appropriate proportion (1/total no. of particles) of the total area being tessellated (Hasegawa and Tanemura [1978]). Other evidence of visible Voronoi division is found in the arrangement of the endothelial cells of the cornea (Sato [1978]), and the epithelial cells of the gall bladder (Hudspeth [1975]).

In three dimensions, polyhedral Voronoi cells are the natural model for crystals formed by spherically symmetric growth with the particles as nuclei (Meijering [1953]). They have also been used to classify the nature of nuclei in a geometrical model for the crystallization of super-cooled liquids (Tanemura et al. [1977]), and in the modelling of the liquid state itself (Bernal [1959]).

The assumption of simultaneous emergence of plants with equal growth rates competiting for space, soil nutrients and light, make the Voronoi model applicable to the study of plant competition (Maynard Smith [1974]; Mead [1971]). Fischer and Miles [1973] study such a territorial competition between crop and weed as affected by different spatial arrangements of the crop. Relaxation of the equal growth rate assumption leads to a Johnson-Mehl type tessellation with hyperbolic division lines.

Particles generating a Voronoi tessellation are said to be contiguous if their Voronoi cells are adjacent. Constructing the line segments joining all contiguous particle pairs yields the triangular Delaunay tessellation, which, in a sense, is the dual graph to the Voronoi tessellation. Figure 3 shows both the Voronoi and Delaunay tessellations for a small number of particles. All Ergodic distributions for the Delaunay tessellation are essentially known (Miles [1970]). This triangulation has been used to test the randomness of arrangements of towns as against a regular hexagonal arrangement (central place theory), by use of the known distributions for the area and angles of a Delaunay triangle (Mardia et al. [1978]). Other geographical uses of Voronoi and Delaunay tessellations are noted in Rhynsburger [1973] and Boots [1974].

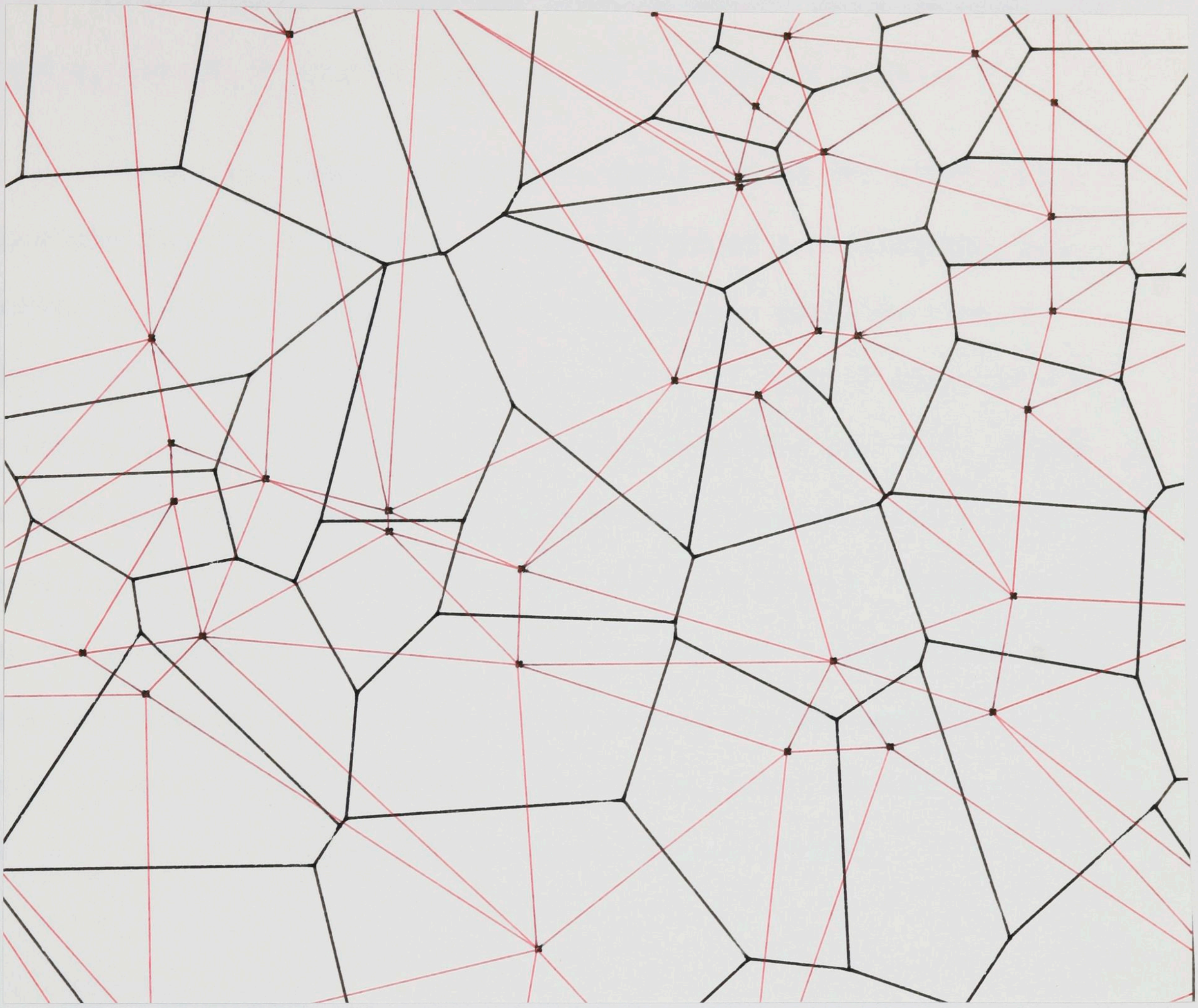

Figure 3

Hamilton [1971] considered that animal movement was influenced by the resulting effect on the size of the animal's Voronoi cell relative to its associated herd. In view of the simulation work of Hasegawa and Tanemura, effects on the tessellation due to particle relocations are of some interest, although not readily amenable to theoretical treatment. Hasegawa and Tanemura [1977b], note that movement of one particle, in a regular lattice of particles, towards the nearest neighbour may increase its Voronoi cell size. The mean area and number of sides of the Voronoi cell of a single moving particle in certain regular tessellations are considered by Cruz Orive [1979]. Also of interest here is the result of Sibson [1980a], that the nucleus ω, of a Vornoi cell is at the centre of gravity of weights T_i, placed at each of the particles ω_i contiguous to ω. These weights are just the areas of the V_2 cells generated by ω and ω_i i.e. T_i = area of $[\omega\omega_i]$ in the notation of section 3.1.

Green and Sibson [1978] have developed an efficient computer algorithm for the calculation of planar Voronoi tessellations (see Chapter 5). They suggest that the tessellation could be used as a computational aid in distance based methods of spatial analysis e.g. by decreasing the time taken for nearest neighbour searches. Green has modelled the spread of infection on an irregular lattice using the tessellation (personal comm.). See also Besag [1974]. Sibson points out the possibility of uses in curve fitting and interpolation. The Delaunay triangulation uniquely possesses an optimal equiangularity property which makes it suitable for use in finite element methods for the solution of differential equations (Sibson [1980b]).

2.3 Voronoi Theory

Despite the wide variety of practical applications for the Voronoi tessellation, relatively few papers have explored the theoretical properties of V.

Meijering [1953] considered two models of crystal growth - the cell model, which was a Voronoi tessellation based on Poisson distributed particles, and the related Johnson-Mehl model, where the nuclei of growing crystals appear at different times. For the two-dimensional case he obtained the mean number of vertices (sides), the mean perimeter and the mean area; for the three-dimensional case the mean number of edges, vertices and faces, and the mean surface area and volume. These values are summarized in Table 1, where ρ is the density of the Poisson generating process.

Table 1

	Quantity	Expectation
Two-dimensional Voronoi		
	number of sides	6
	perimeter	$4\,\rho^{-\frac{1}{2}}$
	area	ρ^{-1}
Three-dimensional Voronoi		
	number of vertices	27.07
	number of edges	40.61
	number of faces	15.54
	edge length	$17.50\,\rho^{-1/3}$
	surface area	$5.821\,\rho^{-2/3}$
	volume	ρ^{-1}

Gilbert [1962] calculated the variance of the area A for two- and three-dimensional versions of V, and obtained upper and lower bounds on the distribution function F(a) of A indicating that $-\log(1 - F(a))$ is $O(a)$. Gilbert's arguments are discussed and extended to the generalized Voronoi case in section 4.4.

We can choose a uniform random member of V by choosing a uniform random particle of the generating process, since each V cell contains exactly one particle 'nucleus'. By homogeneity, and the complete independence of $\mathbb{P}$ in disjoint sets, we can assume that our uniform random particle is at the origin, and construct its Voronoi cell with respect to Poisson particles $\mathbb{E}^2 - \{\underline{0}\}$. Since $\mathbb{E}^2 - \{\underline{0}\}$ and $\{\underline{0}\}$ are disjoint sets, the stochastic construction of $\mathbb{P}$ in $\mathbb{E}^2 - \{\underline{0}\}$ is not influenced by the assumption of a particle at $\{\underline{0}\}$. We write $[\omega_0]$ for the typical Voronoi cell of ω_0 generated by $\mathbb{P} \cup \{\omega_0\}$ with ω_0 assumed placed at the origin.

As an example of the use of this construction of a typical polygon, consider the mean area A of $[\omega_0]$ (see Figure 4).

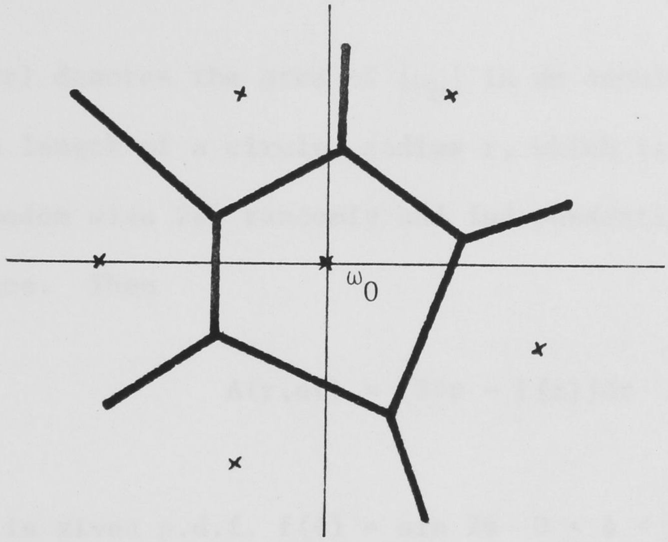

Figure 4

Using Robbins [1944] technique, we use the representation

$$A = \int I(\underline{x})d\underline{x} \quad ,$$

where $I(\underline{x})$ is the indicator function of $[\omega_0]$. Hence

$$\begin{aligned} E(A) &= \int P(\underline{x} \in [\omega_0])d\underline{x} \\ &= 2\pi \int_0^\infty r.P(r \in [\omega_0])dr \\ &= 2\pi \int_0^\infty r\exp\{-\rho\pi r^2\}dr = \rho^{-1} \quad . \end{aligned}$$

By comparison, Meijering's technique of integrating over radial distance can also be applied to the calculation of the mean area for a Voronoi cell. This approach reveals an interesting analogy with the coverage of a circle by a special class of random arcs. In this case we use the representation

$$A = \int_0^\infty A(r,dr) \quad ,$$

where $A(r,dr)$ denotes the area of $[\omega_0]$ in an annulus $(r,r + dr)$. Let $L(r)$ be the length of a circle, radius r, which is covered by N_1 random arcs, of random size 2ϕ, randomly and independently placed on the circumference. Then

$$A(r,dr) = [2\pi r - L(r)]dr \quad ,$$

provided ϕ is given p.d.f. $f(\phi) = \sin 2\phi \quad 0 < \phi < \pi/2$, and $N_1 \sim$ Poisson, with mean $4\rho\pi r^2$ (see Figure 5).

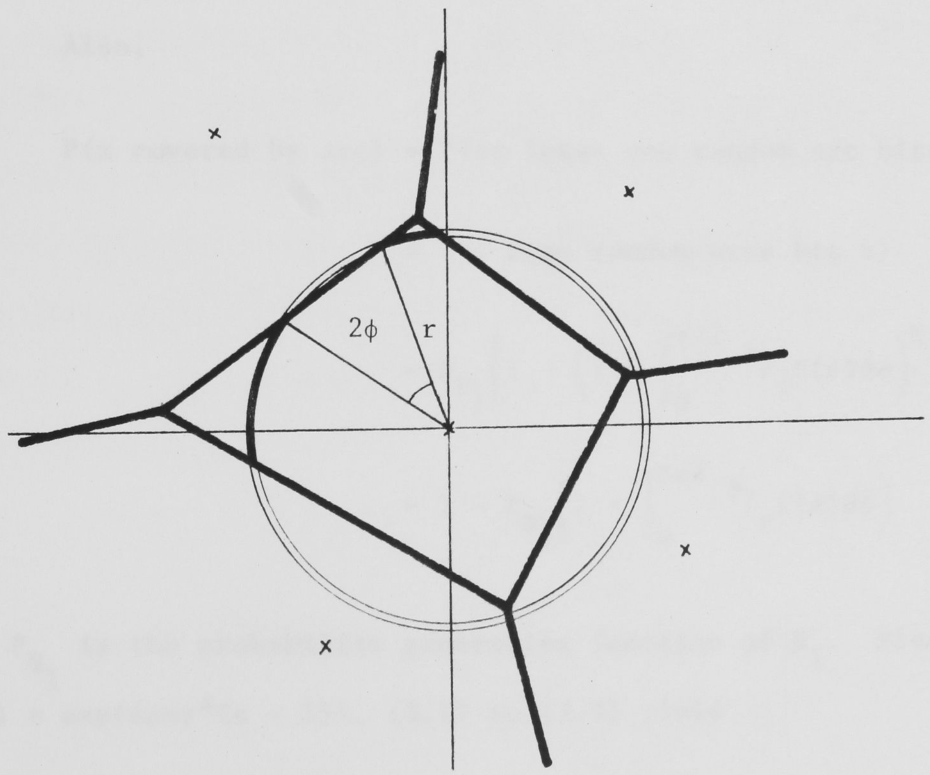

Figure 5

Hence

$$E(A) = \int_0^\infty E(2\pi r - L(r))dr \ . \qquad (3.1)$$

Now

$$L(r) = \int_0^{2\pi r} I(x)dx \quad ,$$

where x is a point on the circumference of Q(r) and

$$I(x) = \begin{cases} 1 & \text{x covered by an arc} \\ 0 & \text{otherwise} \end{cases} \ .$$

So $$E(L(r)) = \int_0^{2\pi r} P(\text{x covered by arc})dx$$

$$= 2\pi r . P(\text{x covered by arc}) \ . \qquad (3.2)$$

Also,

$$P(\text{x covered by arc}) = P(\text{at least one random arc hits x})$$

$$= 1 - P(\text{no random arcs hit x})$$

$$= E_{N_1}\left[1 - \left(1 - \int_0^{\pi/2} {}^{\phi}/_{\pi} f(\phi)d\phi\right)^{N_1}\right]$$

$$= 1 - P_{N_1}\left(1 - \int_0^{\pi/2} {}^{\phi}/_{\pi} f(\phi)d\phi\right) \ , \qquad (3.3)$$

where P_{N_1} is the probability generating function of N_1. Since $P_{N_1}(s) = \exp\{4\rho\pi r^2(s - 1)\}$, (3.1) to (3.3) yield

$$E(A) = \int_0^\infty [2\pi r - 2\pi r(1 - \exp\{- \rho\pi r^2\})]dr = \rho^{-1} \ .$$

Extending this argument to the second moment we have

$$A^2 = \int_0^\infty \int_0^\infty A(r_1, dr_1) A(r_2, dr_2)$$

$$E(A^2) = \int_0^\infty \int_0^\infty E[(2\pi r_1 - L(r_1))(2\pi r_2 - L(r_2))] dr_1 dr_2 ,$$

illustrating the connection between the covariance of coverage on concentric circles and the second moment of the area. In the next section we utilize our construction of a typical polygon to write down some theoretical expressions for cells of $\mathcal{V}$.

2.4 Ergodic Theory for $\mathcal{V}$

Consider a uniform random cell $T \equiv [\omega_0]$ of $\mathcal{V}$, generated by $\mathbb{P} \cup \{\omega_0\}$. Figure 6 illustrates the geometric structure around such a cell. ω_0 is the nucleus of T, which is the intersection of N half-planes (N = 5 in Figure 6). The sides of T are portions of perpendicular bisectors B_i between ω_0 and ω_i, $i = 1,2,..,N$. Each vertex of T is the circumcentre of ω_0 and two of the ω_i. V, the union of the circumdisks associated with each vertex must be empty of particles except for ω_0 in its interior and $\omega_1, \omega_2, .., \omega_N$ on its boundary. Let $|V|$ be the area of V.

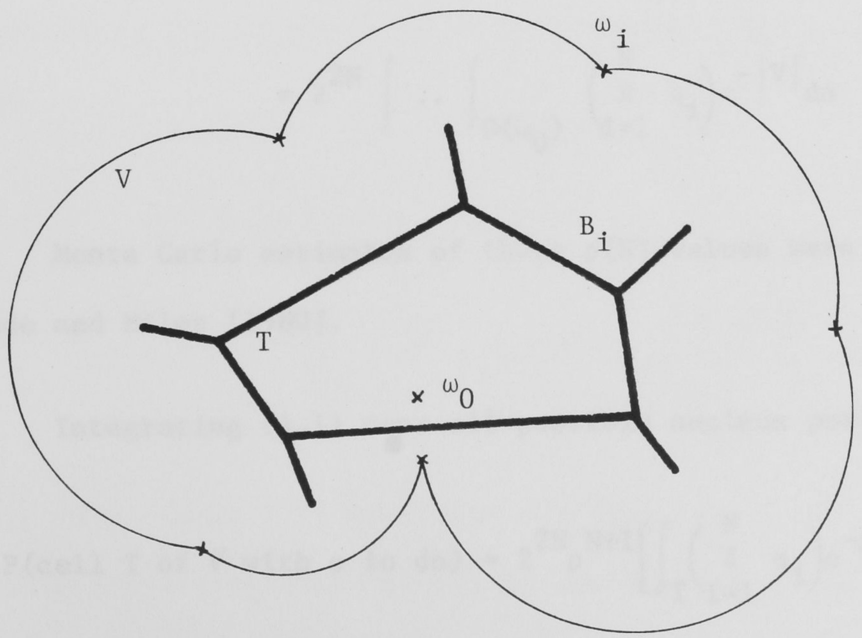

Figure 6

Parametrize B_i by the polar co-ordinates of the foot of the perpendicular from $\underline{0}$, (p_i, θ_i), and let q_i be the perpendicular distance from ω_0 to B_i, $i = 1,2,..N$. Let $\alpha = (p_1, \theta_1, .., p_N, \theta_N)$, and define

$$D(\omega_0) = \{\alpha : B_1, ..B_N \text{ determine a convex N-gon} \ni \omega_0\} .$$

Then

$$P(\text{there is a particle in } d\omega_0 \text{ and } T \equiv [\omega_0] \text{ has N sides with } \alpha \in d\alpha)$$

$$= \rho d\omega_0 P(\text{there is a particle in each of N distinct area elements, of areas } 4q_i dp_i d\theta_i \text{ and no other particles in V})$$

$$= \rho d\omega_0 \left(\prod_{i=1}^{N} 4\rho q_i dp_i d\theta_i\right) e^{-\rho|V|}$$

$$= 2^{2N} \rho^{N+1} \left(\prod_{i=1}^{N} q_i\right) e^{-\rho|V|} d\alpha d\omega_0 \quad . \tag{4.1}$$

Integrating over all possible shapes for T, and setting $\rho = 1$, w.l.o.g.,

$$p(N) \equiv P(T \text{ has N sides} | \text{particle at } \omega_0)$$

$$= 2^{2N} \int .. \int_{D(\omega_0)} \left(\prod_{i=1}^{N} q_i\right) e^{-|V|} d\alpha \quad .$$

Monte Carlo estimates of these p(N) values were calculated by Hinde and Miles [1980].

Integrating (4.1) over all possible nucleus positions gives

$$P(\text{cell T of } V \text{ with } \alpha \text{ in } d\alpha) = 2^{2N} \rho^{N+1} \left[\iint_T \left(\prod_{i=1}^{N} q_i\right) e^{-\rho|V|} d\omega_0\right] d\alpha \ . \tag{4.2}$$

Alternatively, for fixed nucleus ω_0 with $[\omega_0]$ an N-gon, (4.1) implies the density

$$f(\alpha \,|\, \text{particle at } \omega_0,\ [\omega_0] \text{ an N-gon}) \propto \left(\prod_{i=1}^{N} q_i\right) e^{-\rho|V|}, \quad \alpha \in D(\omega_0)\ .$$

Also from (4.1) we have

$$f(\omega_0 \,|\, \text{there is a cell } T \text{ of } \mathcal{V} \text{ with sides } \alpha) \propto \left(\prod_{i=1}^{N} q_i\right) e^{-\rho|V|}, \quad \omega_0 \in T\ , \tag{4.3}$$

which shows that the nucleus is not uniformly distributed, and has small probability density near the edges of T, where $|V|$ is large.

These relationships can be re-expressed in terms of the alternative parametrization of T, $\nu = (\nu_1,..,\nu_N)$, where $\nu_i = B_i \cap B_{i+1}$ is the i^{th} vertex of T ($B_{N+1} \equiv B_1$), by use of the Jacobian relation (Miles [1970]),

$$\left(\prod_{i=1}^{N} L_i\right) d\alpha = \left(\prod_{i=1}^{N} |\sin \phi_i|\right) d\nu\ , \tag{4.4}$$

where L_i are the side lengths of T and ϕ_i the changes in direction at each vertex as the perimeter of T is traversed. For example (4.2) becomes

P(there is a cell T of $\mathcal{V}$ with ν in $d\nu$)

$$= 2^{2N}\rho^{N+1}\left\{\int_T \left(\prod_{i=1}^{N} q_i\right) e^{-\rho|V|} d\omega_0\right\} \prod_{i=1}^{N}\left(\frac{|\sin \phi_i|}{L_i}\right) d\nu\ .$$

From Figure 6 we note that A = area of T < $|V|$. However we can obtain the distribution of $|V|$ by application of the complementary theorem for homogeneous Poisson processes (see Miles [1971] and Miles

[1970], Theorem 5.1, for the specialization to the planar case). This states that the distribution of any area associated with n particles chosen from a Poisson process by a homothetic invariant map, and m-filled by particles of that process, has distribution $\Gamma_1(m + n - 1,\rho)$, where ρ is the density of the process (see (3.5.4)). A mapping ϕ from sets of n particles from $\mathbb{P}$ into sets in $\mathbb{E}^2$ is homothetic invariant if translation and rescaling of the particles results in the same translation and rescaling of the image set. Examples of such mappings are the circumcircle of three particles, the minimal disk for n particles (the disk of minimum radius covering all n particles) and the convex hull of the particles.

If we choose the mapping ϕ defined on the N + 1 particles $\omega_0,\omega_1,..,\omega_N$, as

$$\phi(\omega_0,\omega_1,..,\omega_N) = \begin{cases} |V| & \text{if } \omega_0 \text{ is only particle inside} \\ & \text{convex hull of the } \omega_i \\ 0 & \text{otherwise} \end{cases} ,$$

then if V is empty, $|V| \sim \Gamma_1(N + 1 + 0 - 1,\rho)$ i.e. $\Gamma_1(N,\rho)$.

Hence, if $F_n(a)$ and $F(a)$ are the distribution functions for the area of a uniform random n-gon of V and a uniform random cell of V respectively, then

$$F_n(a) \geqslant \sum_{i=n}^{\infty} e^{-\rho a}(\rho a)^i/i! = P(M \geqslant n) \quad ,$$

where M $\sim$ Poisson with mean ρa, and

$$F(a) \geqslant \sum_{n=3}^{\infty} \sum_{i=n}^{\infty} P(M = i)p(n) = E(P(M \geqslant N)) \quad ,$$

where N is the number of sides of a typical cell with probability distribution $\{p(n)\}$. Also, since (4.3) suggests that the nucleus of T will be centrally located, A will be approximately $|V|/4$ for large N, and hence the area distribution for N-gons when N is large will be approximately $\Gamma_1(N,4\rho)$.

The results in this section represent joint work between R.E. Miles and the author.

CHAPTER 3

GENERALIZED VORONOI TESSELLATIONS

3.1 V_n - Basic Geometry

In this chapter we introduce the random tessellations V_n, $n = 2,3,\ldots$, which form the main topic of study in this thesis.

The V_n tessellations are a natural generalization of the Voronoi tessellation , which can be written as V_1. All points in a V_1 cell have the same closest particle; all points in a V_n cell have the same n closest particles. These particles are referred to as the *proximity* particles of the cell. If a V_n cell T has proximity particles $\omega_1,\omega_2,\ldots,\omega_n$ we write $T \equiv [\omega_1\ldots\omega_n]$.

In full generality we can define V_n relative to a d-dimensional point process π_d (see section 2.1). In fact, the assumption of particles in general position can be waived, and some examples of V_n's based on a degenerate square grid of particles are given, but most of the theory deals with processes of type π_2, and more particularly, planar Poisson processes. We note that multiplicity of particles in the generating process must be excluded.

The geometry of V_n is complicated and hard to visualize. The geometrical viewpoint must be chosen to suit the problem to be solved - hence we look at the vertex structure, the construction of individual polygons, the associated point processes on arbitrary linear transects and on arbitrary perpendicular bisectors of particle pairs, and the relationships between superpositions of V_n's for consecutive n values.

The computation of V_n's is covered in Chapter 5. As an introduction here however, Figure 1 shows plots of V_1, V_2, V_3 and V_1 and V_2 superposed - $V_{1,2}$. These plots are based on a random distribution of particles. In Figure 2, various V_n for a square grid of particles are illustrated. These plots are invaluable to an understanding of the geometry which follows.

Consider the arbitrary n-set of particles $\omega_1, \omega_2, \ldots, \omega_n$ chosen from a π_d type process defined on a space X. For the V_n cell $[\omega_1\omega_2\ldots\omega_n]$ to be non-empty requires that there be at least one point of X with $\omega_1, \ldots, \omega_n$ as the nearest n particles. If we label the remaining particles $\omega_{n+1}, \omega_{n+2}, \ldots$, this is equivalent to insisting that each ω_i, $1 \leqslant i \leqslant n$ is closer to the point then any ω_j, $j \geqslant n+1$. Hence, if $K_{ij} = \{\underline{x} : |\underline{x} - \omega_i| \leqslant |\underline{x} - \omega_j|, \underline{x} \in X\}$, we have the important representation

$$[\omega_1\omega_2\ldots\omega_n] = \bigcap_{i=1}^{n} \bigcap_{j\geqslant n+1} K_{ij} \tag{1.1}$$

Definition

$$V_n \equiv \left\{[\omega_1\omega_2\ldots\omega_n] : \omega_1, \ldots, \omega_n \text{ vary over all possible n-sets from } \pi_d \text{ type process}\right\},$$

is called a generalized Voronoi tessellation of the space X on which π_d is defined.

If X is the plane, then (1.1) shows that each $[\omega_1\ldots\omega_n]$ is a convex polygon. Since, apart from the null set of polygon boundaries, every point of $\mathbb{E}^2$ belongs to one and only one $[\omega_1\ldots\omega_n]$, V_n is a convex polygonal *tessellation* of the plane, as is clear from Figures 1 and 2. In fact, the higher V_n's appear to have exactly the same topological structure as V. However there are some important geometrical differences, as we see as soon as we start to investigate the different types of points in the polygon boundaries.

If a point $\underline{x}$ has a well-defined set of n closest particles then it will be contained in the V_n cell with those particles as its proximity particles. Precisely, a point has n well-defined nearest particles iff a circle can be drawn, centered at $\underline{x}$, which contains exactly n particles in its interior. A little thought reveals that points of $\mathbf{E}^2$ fall into one of four types relative to a V_n tessellation, which are illustrated in Table 1.

Table 1

Particle configuration around $\underline{x}$ — **$\underline{x}$'s place in V_n boundary**

(i)

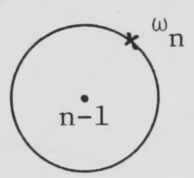

$\underline{x}$ is inside V_n cell $[\omega_1 \ldots \omega_n]$

(ii)

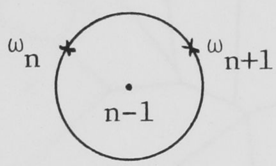

$\underline{x}$ is on the edge between two V_n cells $[\omega_1 .. \omega_{n-1}\omega_n]$ and $[\omega_1 .. \omega_{n-1}\omega_{n+1}]$

(iii)

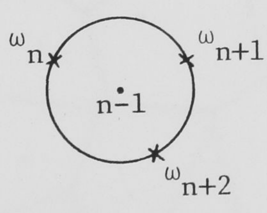

$\underline{x}$ is at the vertex of three V_n cells $[\omega_1\omega_2 .. \omega_{n-1}\omega_n]$, $[\omega_1\omega_2 .. \omega_{n-1}\omega_{n+1}]$, $[\omega_1\omega_2 .. \omega_{n-1}\omega_{n+2}]$

(iv)

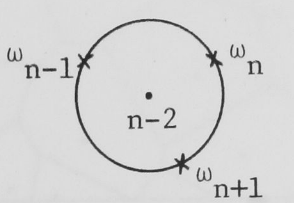

$\underline{x}$ is at the vertex of three V_n cells

$[\omega_1\omega_2 .. \omega_{n-2}\omega_{n-1}\omega_n]$

$[\omega_1\omega_2 .. \omega_{n-2}\omega_{n-1}\omega_{n+1}]$

$[\omega_1\omega_2 .. \omega_{n-2}\omega_n\omega_{n+1}]$

Each circle is centred at $\underline{x}$ and is labelled with the number of filling particles.

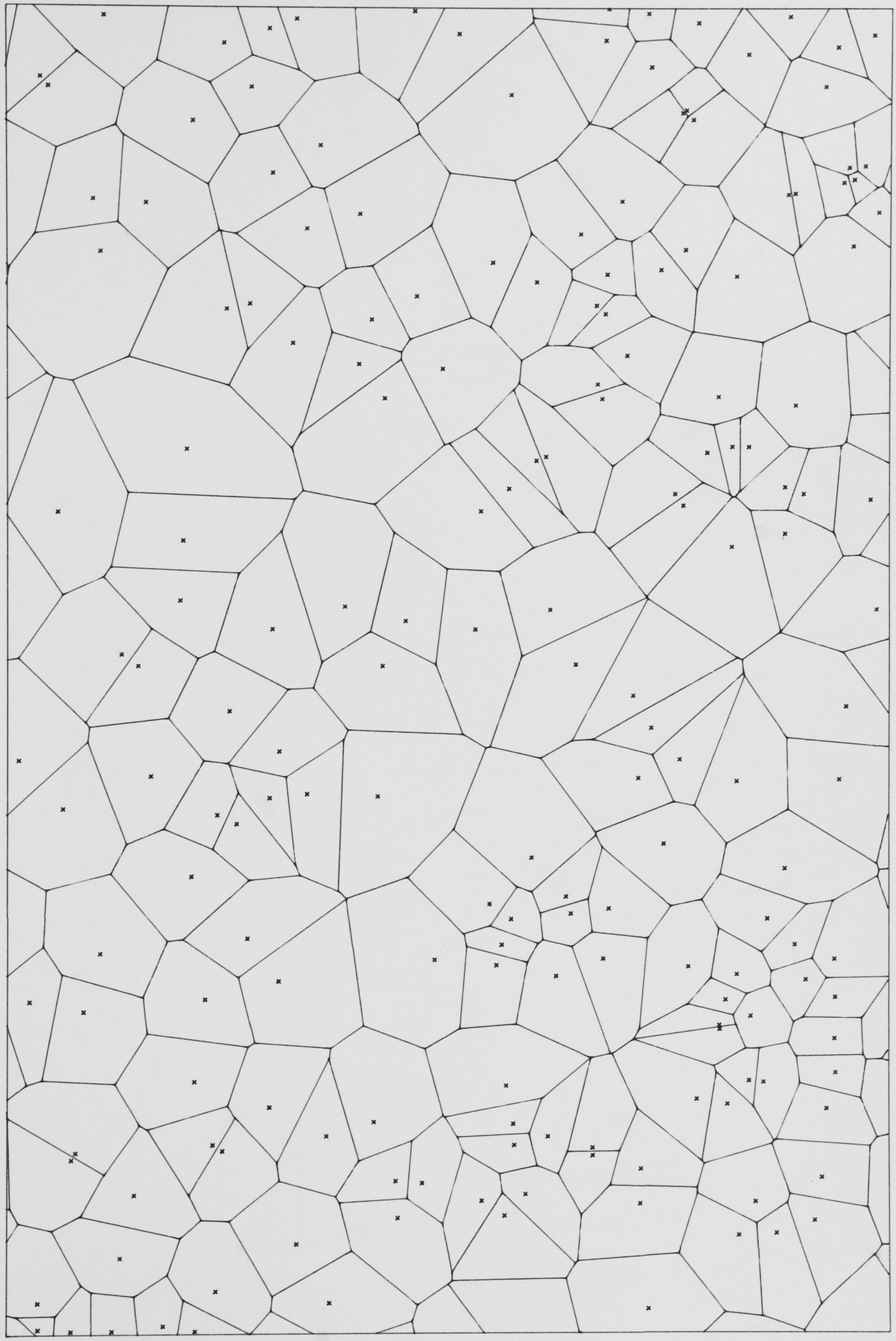

Figure 1 (i). V_1 *for a set of random particles.*
Each cell contains one particle or nucleus, shown by a cross.

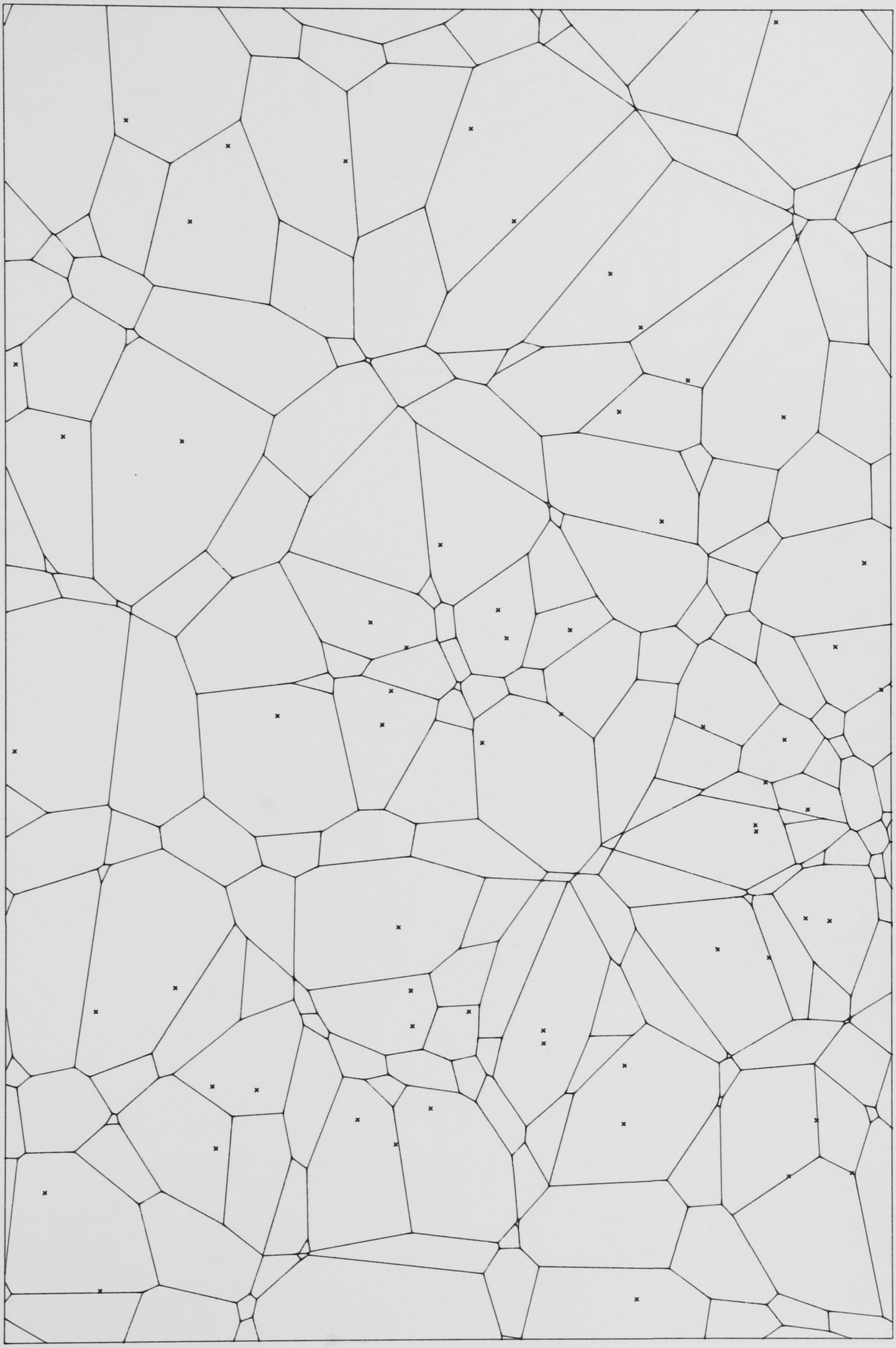

Figure 1 (ii). V_2 *for a set of random particles.*

Note that each cell contains none, one or two particles.

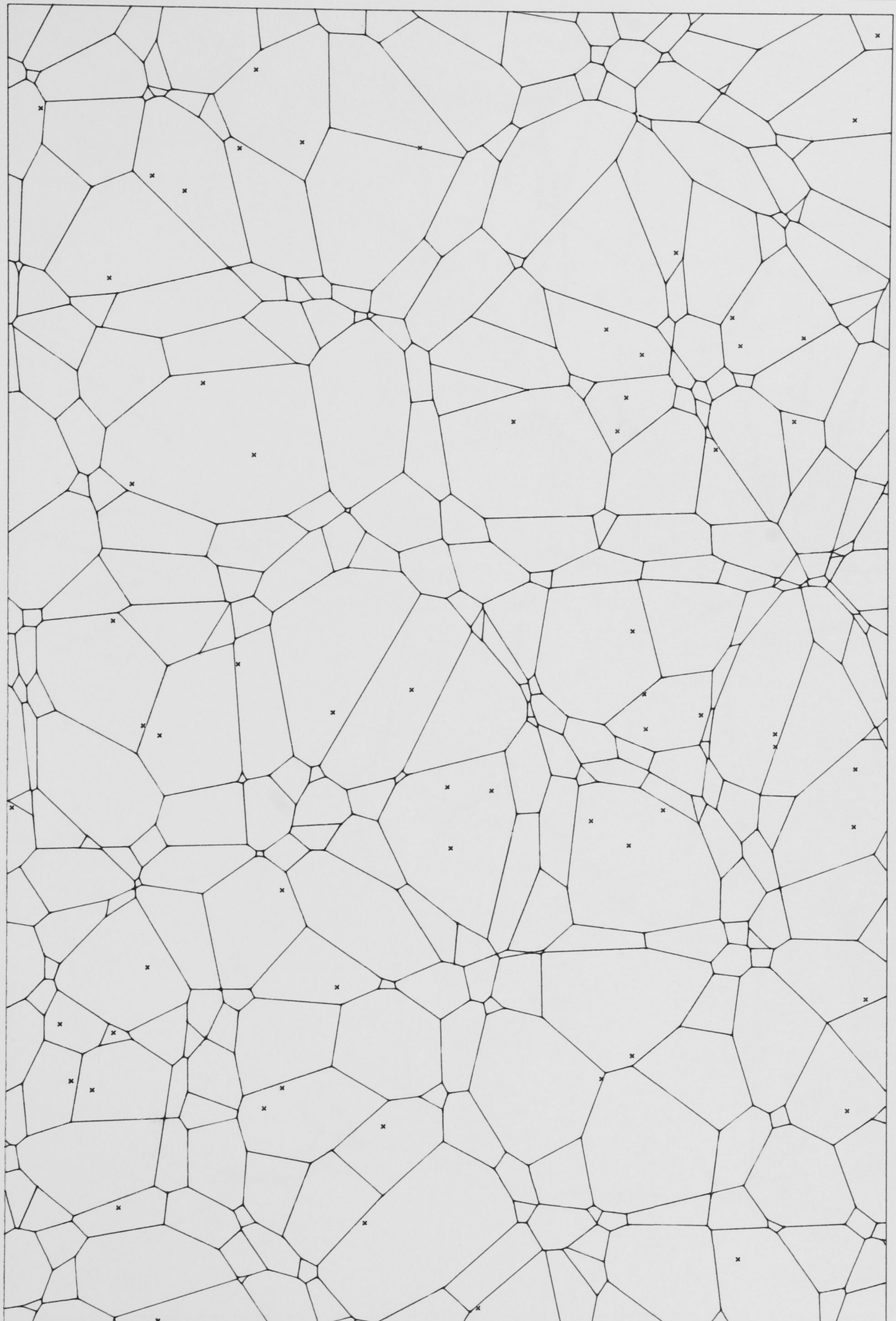

Figure 1 (iii). V_3 *for a set of random particles.*
Note that each cell can contain up to three particles.

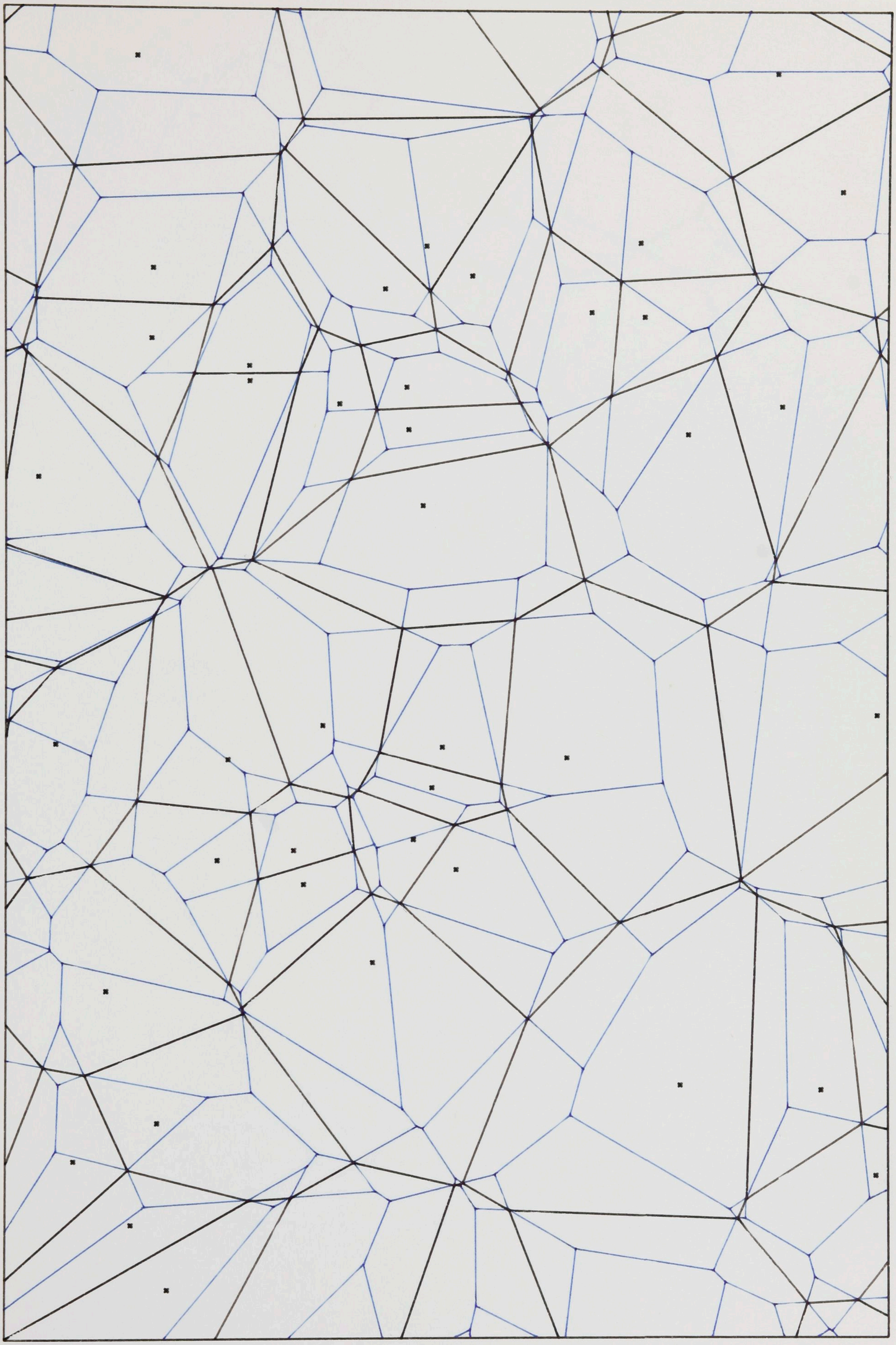

Figure 1 (iv). *Superposition of V_1 and V_2 for a set of random particles.* V_1 shown in black, V_2 in blue. Note the two vertex types in V_2 - (1,2) vertices where black and blue lines meet, (2,3) vertices where only blue lines meet.

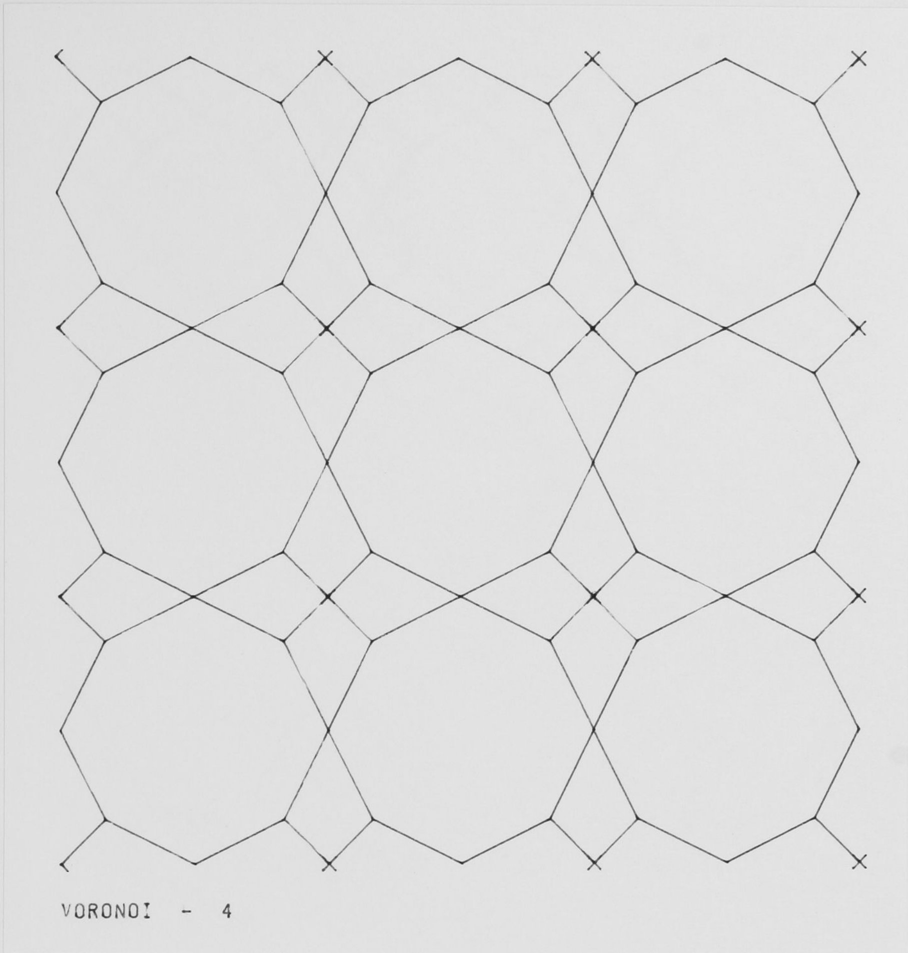

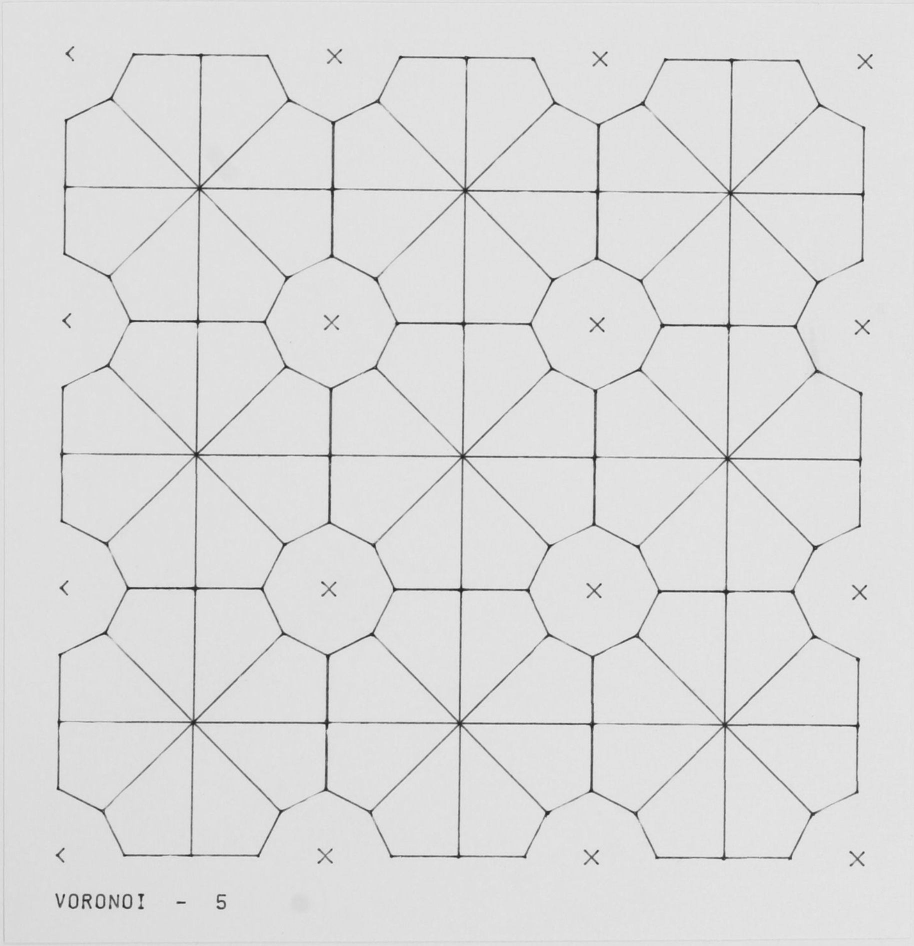

Figure 2 (i). V_n*'s based on a square grid of particles*
The particles are shown by crosses.

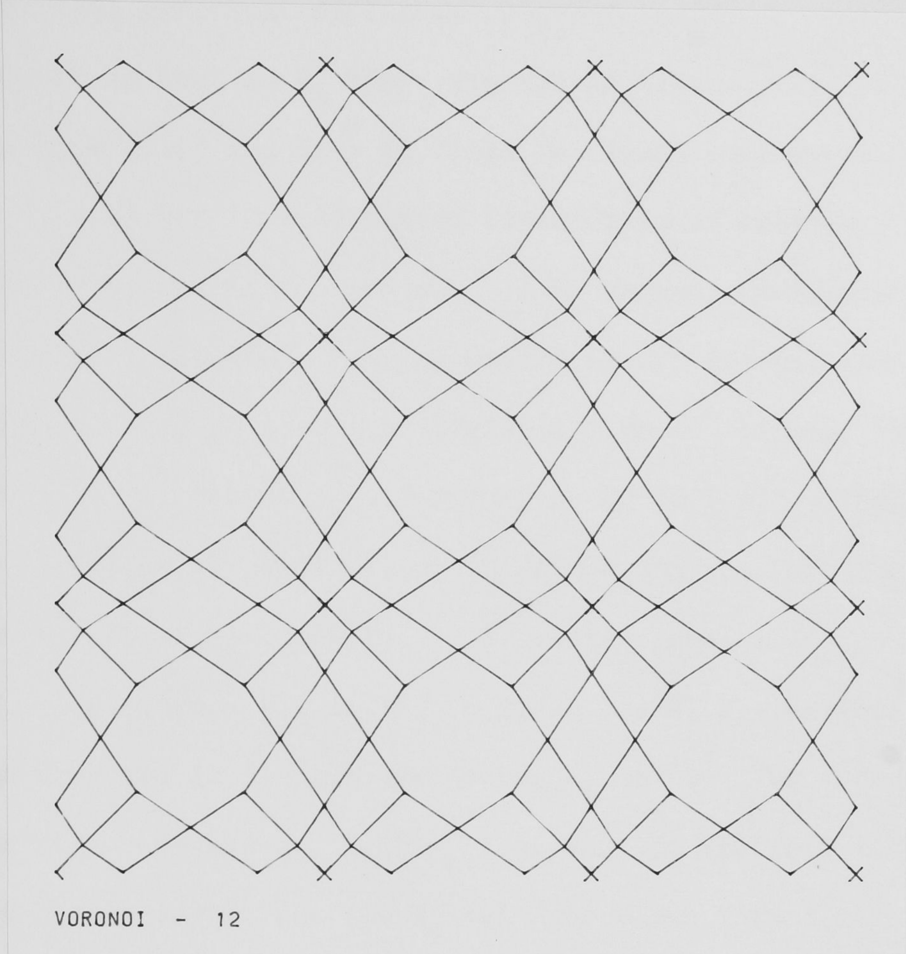

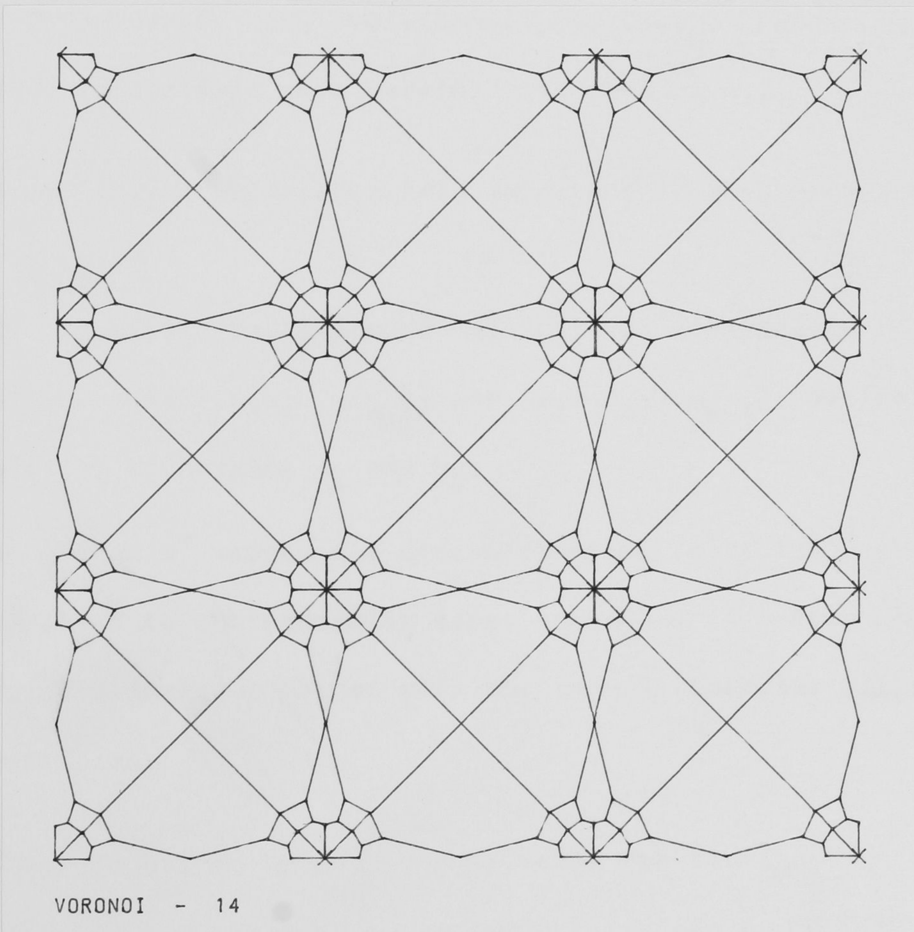

Figure 2 (ii). V_n*'s based on a square grid of particles*
The particles are shown by crosses.

The most important difference between V_1 and V_n $(n > 1)$ boundary points is that in V_n there are two different sorts of vertices, i.e. points type (iii) and (iv) in Table 1. These correspond to the centres of $(n - 1)$ and $(n - 2)$-filled circumdisks of triples of particles from the generating process. A V_n vertex corresponding to an $(n - 1)$-filled circumdisk will be called an n^+ vertex, that corresponding to an $(n - 2)$-filled circumdisk an n^- vertex. Since it is clear that an n^+ vertex is equivalent to an $(n + 1)^-$ vertex, both being $(n - 1)$-filled circumdisks, we sometimes use the more convenient notation $(n,n + 1)$ vertex. An $(n,n + 1)$ vertex appears in both V_n and V_{n+1}. For example, from V_{12} in Figure 1, V_2 has (1,2)-vertices shared with V_1 and isolated (2,3)-vertices inside V_1 cells. The situation is similar for higher n-values. Each V_{n+1} grows from the $(n,n + 1)$ vertices of V_n and partitions the V_n cells by a web formed by $(n + 1,n + 2)$-vertices. This relationship between successive V_n tessellations is analysed more carefully in section 4.2.

From Table 1 we note certain important local properties for

V_n

(i) the proximity particles of adjacent cells separated by $\langle\omega_1\omega_2\rangle$ and $[\omega_1\omega_3\omega_4\cdots\omega_{n-1}]$ and $[\omega_2\omega_3\omega_4\cdots\omega_{n-1}]$, differing only by exchanging ω_1 and ω_2;

(ii) around an n^+ vertex the circumferential particles enter singly into the proximity sets, around an n^- vertex they enter pairwise combined with the $(n - 2)$-interior filling particles.

The generalized Voronoi tessellation was first defined by Miles [1970], who used ergodic theory methods to calculate E(A), E(N) and E(S) for V_n $n = 1,2,3,\ldots$ where the generating point process was Poisson with density ρ. These values are

$$E(A) = \frac{1}{(2n-1)\rho}$$

$$E(N) = 6$$

$$E(S) = \frac{(2n)!}{(n!(n-1)!(2n-1)2^{2n-3}\rho^{\frac{1}{2}})} \sim \frac{4}{(\pi n \rho)^{\frac{1}{2}}} \quad .$$

3.2 n-Circuits and n-Areas in V_n

Before exploring further the local geometry of V_n, we introduce a global geometric construct which is interesting in itself, and is a useful tool for geometric arguments to follow.

Definition

Let ω be a particle of the point process generating V_n.

Let $P = \{P : P\text{'s proximity set contains } \omega,\ P \in V_n\}$.

Then the n-Area of ω is $A_{\omega,n} \equiv \bigcup_{P \in P} P$

and the n-Circuit of ω is $C_{\omega,n} \equiv \partial A_{\omega,n}$.

$A_{\omega,n}$ is simply the collection of all V_n cells with ω in their proximity set - see Figure 3 for an illustration of 2 and 3-Areas with their surrounding 2- and 3-circuits.

Lemma 1 The n-Area of ω contains ω, and is star-shaped relative to ω.

Proof First we show that

$$A_{\omega,n} = X \equiv \{\underline{y} : Q(\underline{y}, |\omega - \underline{y}|) \text{ contains} \leqslant n-1 \text{ particles}\}$$

Take $\underline{y} \in A_{\omega,n}$. Then there is a $P_n \in P$ such that $\underline{y} \in P_n$.

Figure 3 (i). *2-Circuit and 2-Area in* V_2

The particle ω is circled in blue, and its 2-circuit is shaded in yellow. Particles which are cell-contiguous with ω (see section 3.3) are shaded in yellow; particles which are edge-contiguous with ω (but not cell-contiguous) are shaded in green.

Figure 3 (ii). *3-Circuit and 3-Area in* V_3

The particle ω is circled in blue, and its 3-Circuit is shaded in yellow. As in Figure 3 (i), cell-contiguous particles are shaded yellow, and particles which are edge-contiguous, but not cell-contiguous are shaded in green.

The incomplete portion of the 3-circuit from A to B (lower right) is shown in greater detail in Figure 3 (iii).

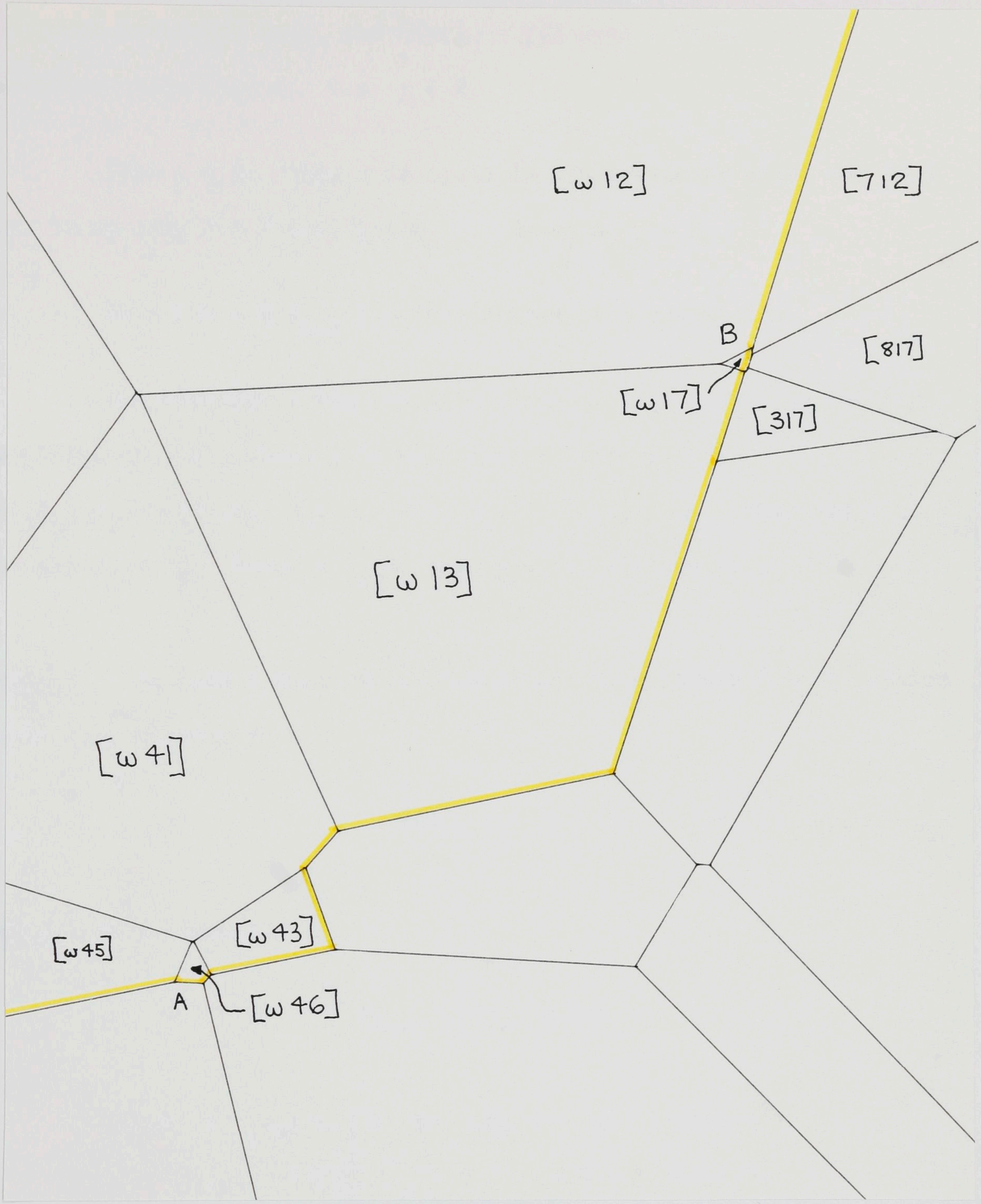

Figure 3 (iii). Completion of 3-Circuit from Figure 3 (ii)

This plot completes the 3-circuit of ω between points A and B. It clearly shows two pentagons which are too small to appear on the smaller scale plot. To clarify Figure 3 (ii), certain cells are labelled with their proximity sets, using the numbering of particles on Figure 3 (ii).

Therefore ω is contained in $\underline{y}$'s proximity n-set i.e. in the set of the n closest particles to $\underline{y}$, and $Q(y,|\omega - \underline{y}|)$ must contain $\leqslant n - 1$ particles other than ω. i.e. $\underline{y} \in X$.

Take $\underline{y} \in X$. Then ω is again in $\underline{y}$'s proximity n-set and so $\underline{y}$ must be in some $P \in \mathcal{P}$ i.e. $\underline{y} \in A_{\omega,n}$. Hence $A_{\omega,n} = X$.

As $\omega \in X$, $\omega \in A_{\omega,n}$ i.e. the n-Area of ω contains ω.

Now consider a ray emanating from ω, with points on the ray specified by $\underline{y}(d)$, where d is the distance from ω. As $Q(y(d_1),d_1) \supset Q(y(d_2),d_2)$ for $d_1 > d_2$, if $y(d_1) \in A_{\omega,n}$ then $y(d_2) \in A_{\omega,n}$ for all $d_2 < d_1$. Hence $A_{\omega,n}$ is star-shaped relative to ω.

<u>Lemma 2</u> The mean n-Area for a typical particle chosen from a Poisson generating process $\mathbb{P}$ is

$$E(A_{\omega,n}) = n\rho^{-1} \qquad n = 1,2,\ldots$$

<u>Proof</u> From Lemma 1,

$$A_{\omega,n} = \int I_{\omega,n}(\underline{x})d\underline{x} \ ,$$

$$\text{where} \quad I_{\omega,n}(\underline{x}) = \begin{cases} 1 & \text{if } Q(\underline{x},|\omega - \underline{x}|) \text{ contains} \\ & \qquad \leqslant n-1 \text{ particles} \\ 0 & \text{ow.} \end{cases}$$

Hence $$E(A_{\omega,n}) = \iint P(Q(\underline{x},|\omega - \underline{x}|) \text{ contains } \leqslant n - 1 \text{ particles})\, d\underline{x}$$

$$= 2\pi \int_0^\infty P(\text{circle radius } r \text{ has } \leqslant (n-1) \text{ particles in it})\, rdr$$

$$= 2\pi \int_0^\infty \sum_{k=0}^{n-1} \frac{(\rho\pi r^2)^k e^{-\rho\pi r^2}}{k!}\, rdr$$

$$= 2\pi \sum_{k=0}^{n-1} \int_0^\infty \frac{1}{2\rho\pi} . f(r;2k+2,\rho\pi)dr ,$$

where f is the density function for a random variable with distribution $\Gamma_2(2k + 2,\rho\pi)$. (see (5.4).)

Hence
$$E(A_{\omega,n}) = \sum_{k=0}^{n-1} \frac{1}{\rho} = n\rho^{-1} .$$

As a check on Lemma 2 we note that the 1-Area of a particle is simply its Voronoi cell, with mean area ρ^{-1}, and the 1-circuit is the boundary of the cell.

The 1-Areas therefore form a tessellation or 1-covering of the plane, i.e. the Voronoi tessellation V. In an analogous way the n-Areas form an n-covering of the plane, for, ignoring the null set of boundary points, each point $\underline{x} \in \mathbb{E}^2$ has n particles $\omega_1 .. \omega_n$ in its proximity n-set and hence lies in each $A_{\omega_i,n}$, i = 1,2,...n. Obviously

$$[\omega_1 \omega_2 .. \omega_n] = \bigcap_{i=1}^{n} A_{\omega_i,n} .$$

<u>Lemma 3</u>

The mean number $E(N_{\omega,n})$ of V_n cells is an n-Area when the generating process is $\mathbb{P}$ is

$$E(N_{\omega,n}) = n(2n - 1) \qquad n = 1,2,...$$

<u>Proof</u>
$$E(N_{\omega,n}) = \frac{E(A_{\omega,n})}{E(A_n)}$$

$$= \frac{(2n - 1)n\rho}{\rho}$$

$$= n(2n - 1) ,$$

independent of ρ.

Some values of $E(N_{\omega,n})$ are listed in Table 2.

Table 2

n	$E(N_{\omega,n})$
1	1
2	6
3	15
8	120
300	179,700

Since $A_{\omega,1}$ is the Voronoi cell of ω, $N_{\omega,1} \equiv 1$, so obviously $E(N_{\omega,1}) = 1$.

An examination of V_{12} (Figure 1) suggests that ω and ω_i generate a V_2 cell iff they have a V_1 segment on their perpendicular bisector. Hence

$$N_{\omega,2} = N , \tag{2.1}$$

where N is the number of sides of the Voronoi cell for ω. Lemma 3 therefore verifies that $E(N) = 6$ for V_1. In the next section we prove (2.1) in the context of a general analysis of particle contiguities using n-Areas. The only other point of interest in Table 2 is to note the rapid increase in $E(N_{\omega,n})$.

3.3 Particle Contiguity in V_1 and V_n

In V_1 we naturally define two particles to be contiguous if they generate adjacent V_1 cells, or, equivalently, if they have a V_1 segment on their perpendicular bisector.

In V_n we apparently have several choices for the definition of pairwise contiguity:-

(i) cell-contiguity; ω_1 and ω_2 both appear in the proximity set of at least one V_n cell. We write $[\omega_1\omega_2 \to n]$

(ii) edge-contiguity; $\langle\omega_1\omega_2\rangle \cap \mathcal{L}_n \neq \phi$, where $\mathcal{L}_n$ is the aggregate of sides of members of V_n, i.e. $\langle\omega_1\omega_2\rangle$ contains a segment belonging to the boundary of V_n. We write $\langle\omega_1\omega_2 \to n\rangle$

(iii) extended-cell contiguity - at least one of ω_1 and ω_2 appear in the proximity sets of adjacent V_n cells.

<u>Lemma 4</u> $[\omega_1\omega_2 \to n]$ iff $\langle\omega_1\omega_2 \to n - 1\rangle$ $n = 2,3,\ldots$

<u>Proof</u> By definitions of cell and edge contiguity,

$$[\omega_1\omega_2 \to n] \Leftrightarrow \text{int } A_{\omega_1,n} \cap \text{int } A_{\omega_2,n} \neq \phi$$

$$\langle\omega_1\omega_2 \to n - 1\rangle \Leftrightarrow A_{\omega_1,n-1} \cap A_{\omega_2,n-1} \neq \phi,$$

where int $A_{\omega,n}$ is the interior of the n-Area.

Assume $\langle\omega_1\omega_2 \to n - 1\rangle$. Consider $\underline{x} \in \langle\omega_1\omega_2\rangle \cap \mathcal{L}_{n-1}$. Then $Q(\underline{x},|\underline{x} - \omega_1|)$ is $(n - 2)$-filled with particles $\omega_3,\omega_4,\ldots\omega_n$ say, so $\underline{x} \in [\omega_1\ldots\omega_n]$ i.e. $[\omega_1\omega_2 \to n]$.

Assume $[\omega_1\omega_2 \to n]$. Then there exists $\underline{x}$ such that $Q_1 = Q(\underline{x}, \max[|\underline{x} - \omega_1|,|\underline{x} - \omega_2|])$ is at most $(n - 2)$-filled, excluding ω_1 and ω_2. Construct the line L (see Figure 4), joining $\underline{x}$ to whichever of ω_1 or ω_2 is on the boundary of Q_1, and let $\underline{y} \equiv L \cap \langle\omega_1\omega_2\rangle$.

Then $Q(\underline{y},|\underline{y} - \omega_1|)$ is at most $(n - 2)$-filled, and hence $\underline{y} \in \mathcal{L}_i$ for some i, $1 \leqslant i \leqslant n - 1$. But if $\langle\omega_1\omega_2\rangle$ contains a V_i segment, it must contain V_j segments, for all $j > i$ (see section 5.2). Therefore $\langle\omega_1\omega_2 \to n - 1\rangle$. This completes the lemma.

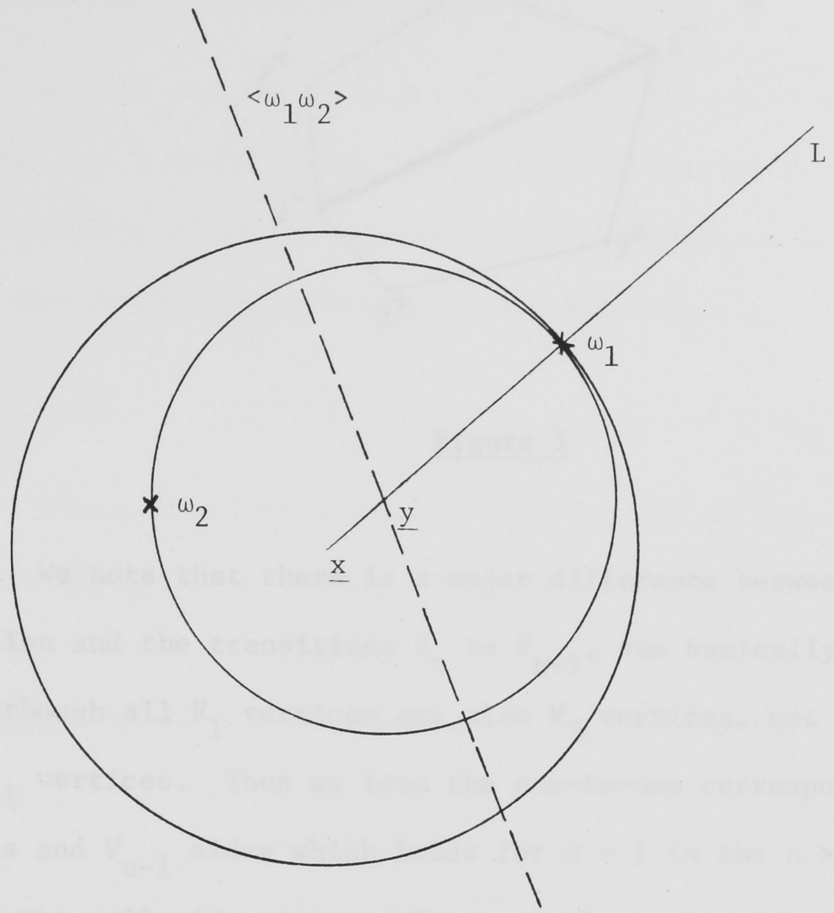

Figure 4

Lemma 5 There is a one-to-one correspondence between V_1 sides and V_2 cells - each V_2 cell contains exactly one V_1 side.

Proof Consider a non-empty V_2 cell $[\omega_1\omega_2]$. By Lemma 4, $<\omega_1\omega_2>$ must contain a V_1 segment, which is contained in the V_2 cell since if $\underline{x} \in V_1$ segment then $Q(\underline{x}, |\underline{x} - \omega_1|)$ is empty, and ω_1 and ω_2 are the closest two particles. No V_2 cell can contain two V_1 segments on $<\omega_1\omega_2>$ and $<\omega_3\omega_4>$ since each segment would determine two particles which are the closest two leading to a contradiction unless $\omega_1 \equiv \omega_3$ and $\omega_2 \equiv \omega_4$ which is impossible since no perpendicular bisector can contain more than one V_1 segment. (see section 5.2.)

From Lemma 5, all V_2 cells are as illustrated in Figure 5 partitioned into two sections by a single V_1 segment. Hence a V_2 N-gon has two 2^- vertices and $(N - 2)$ 2^+ vertices (see also Figure 1).

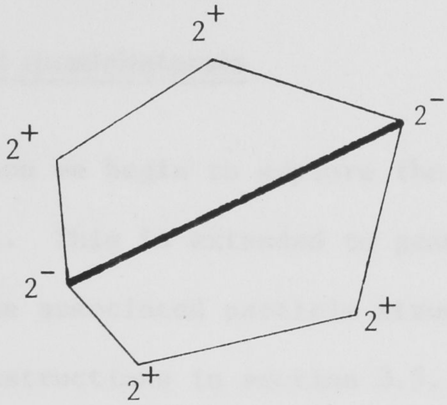

Figure 5

We note that there is a major difference between the V_1 to V_2 transition and the transitions V_n to V_{n+1}, due basically to the fact that although all V_1 vertices are also V_2 vertices, not all V_n vertices are V_{n+1} vertices. Thus we lose the one-to-one correspondence between V_n cells and V_{n-1} sides which holds for $n = 1$ in the $n > 1$ case. However the cell-side correspondence can be replaced by a combination cell-side and cell-vertex correspondence which is used to calculate mean cell areas for general homogeneous tessellations. (see section 4.1.)

Extended cell contiguity is equivalent to edge-contiguity. For if ω_1 and ω_2 are extended-cell contiguous with more than one of ω_1 or ω_2 in adjacent cells, they are cell-contiguous and hence edge-contiguous. If only one of the pair appears in each adjacent cell, the separating V_n segment must appear on $\langle\omega_1\omega_2\rangle$ and again we have edge contiguity. The reverse implication is obvious.

In 4.6 we make use of the geometric lemmas here, together with the stochastic constructions for V_n vertices given in 3.5 to derive some distributions related to pairwise contiguous particles.

3.4 $\mathcal{V}_n$ - triangles and quadrilaterals

In this section we begin to explore the total geometry around a $\mathcal{V}_n$ N-gon for N small. This is extended to general N in section 3.6. An understanding of the associated particle structure is also necessary for the stochastic constructions in section 3.5.

Triangles

Triangles occur in $\mathcal{V}_1$, but as a perusal of Figure 1 indicates, none occur in $\mathcal{V}_n$ for $n > 1$.

Lemma 6 There are a.s no triangles in $\mathcal{V}_n$, $n = 2,3\ldots$

Proof

Assume there is a triangle $T \in \mathcal{V}_n$.

As adjacent vertices of T must have two circumferential particles in common we can label its vertices and sides as shown on Figure 6. $\langle\Omega_0\Omega_1\rangle$ is the perpendicular bisector of particles Ω_0 and Ω_1, $\langle\Omega_0\Omega_1\Omega_2\rangle_j$ is a j-filled $\mathcal{V}_n$ vertex with circumferential particles Ω_0, Ω_1 and Ω_2.

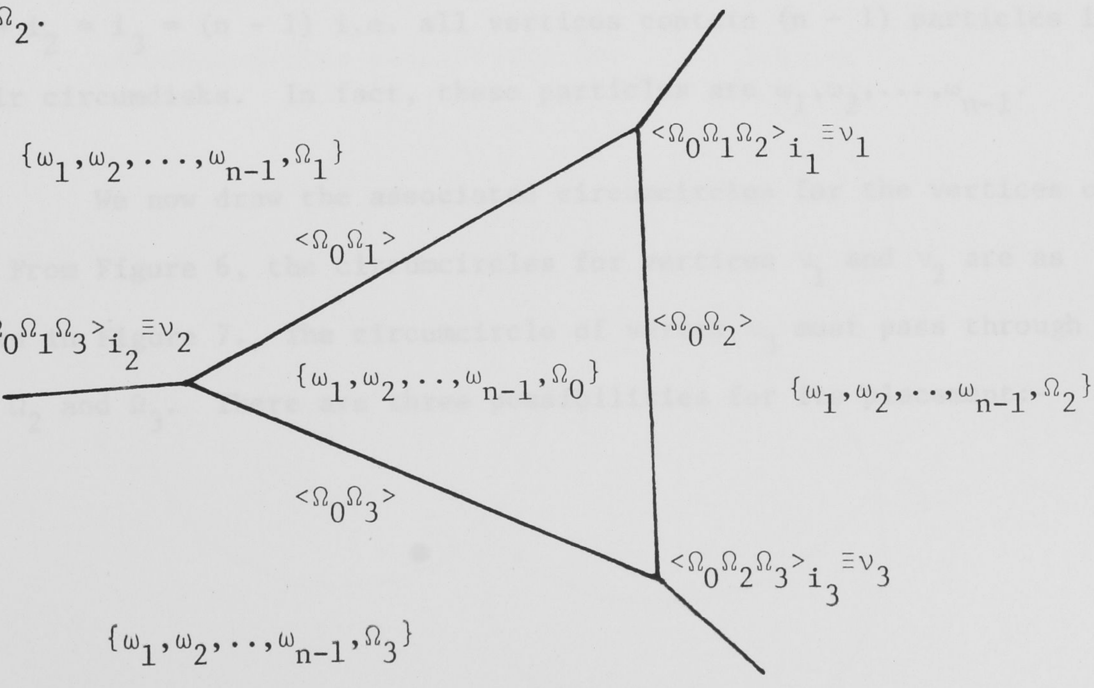

Figure 6

If $P_n \equiv [\omega_1,\ldots,\omega_n]$ shares a boundary $<\omega_n\omega_{n+1}>$ with R_n then the proximity set of R_n is $\{\omega_1,\ldots,\omega_{n-1},\omega_{n+1}\}$. As Ω_0 appears in all sides of T, it is either in T's proximity set, or the proximity sets of all three adjacent regions.

If $\Omega_0 \in T$, then it must appear in T's proximity set.

Assume $\Omega_0 \notin T$, and that Ω_0 is not in T's proximity set i.e. Ω_0 must then appear in the proximity sets of all three adjacent regions.

Draw a ray from Ω_0 which hits the interior of T. This ray intersects $A_{\Omega_0,n}$ in at least two disjoint line segments, violating the star-shaped property of $A_{\Omega_0,n}$ about Ω_0. Therefore Ω_0 must be in T's proximity set for any position of Ω_0.

As the sides of T are segments on $<\Omega_0\Omega_i>$, $i = 1,2,3$, Ω_i cannot be in T's proximity set for $i = 1,2,3$. Hence $T \equiv [\Omega_0,\omega_1,\ldots,\omega_{n-1}]$ with no $\omega_i \equiv \Omega_1$, Ω_2 or Ω_3, $i = 1,2,\ldots,n-1$. From T's proximity set we can obtain the proximity sets of all adjacent regions (see Figure 6). The V_n vertex type is determined by the proximity sets of the three cells surrounding the vertex. For T, $i_1 = i_2 = i_3 = (n-1)$ i.e. all vertices contain $(n-1)$ particles in their circumdisks. In fact, these particles are $\omega_1,\omega_2,\ldots,\omega_{n-1}$.

We now draw the associated circumcircles for the vertices of T. From Figure 6, the circumcircles for vertices ν_1 and ν_2 are as shown in Figure 7. The circumcircle of vertex ν_3 must pass through Ω_0, Ω_2 and Ω_3. There are three possibilities for its placement:-

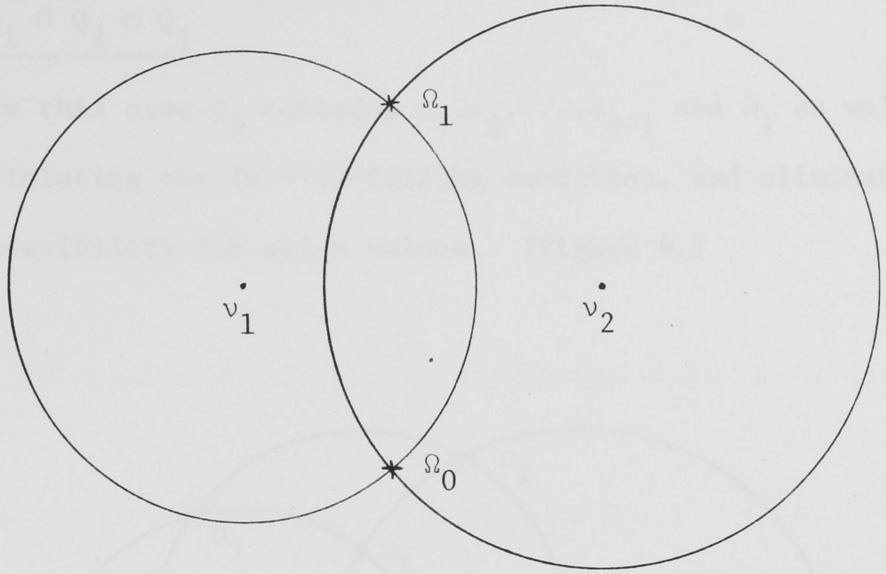

Figure 7

Write Q_i for the open circumdisk of vertex ν_i.

(i) $\bigcap_{i=1}^{3} Q_i = \phi$. As all Q_i must contain the particles $\omega_1, \omega_2, \ldots, \omega_{n-1}$, this possibility is eliminated, unless n = 1.

(ii) $\bigcap_{i=1}^{3} Q_i \subset \bigcap_{i=1}^{2} Q_i$. As in (i) above $\bigcap_{i=1}^{3} Q_i$ must contain $\omega_1, \ldots, \omega_{n-1}$. However, in this case Ω_2 or Ω_3 or both must be on $\delta\left(\bigcap_{i=1}^{2} Q_i\right)$ and hence in Q_1 or Q_2. (See Figure 8.) Therefore either Q_1 or Q_2 or both contain (n - 1) + 1 particles, violating the condition that all Q_i are (n - 1)-filled. This eliminates this possibility for all values of n.

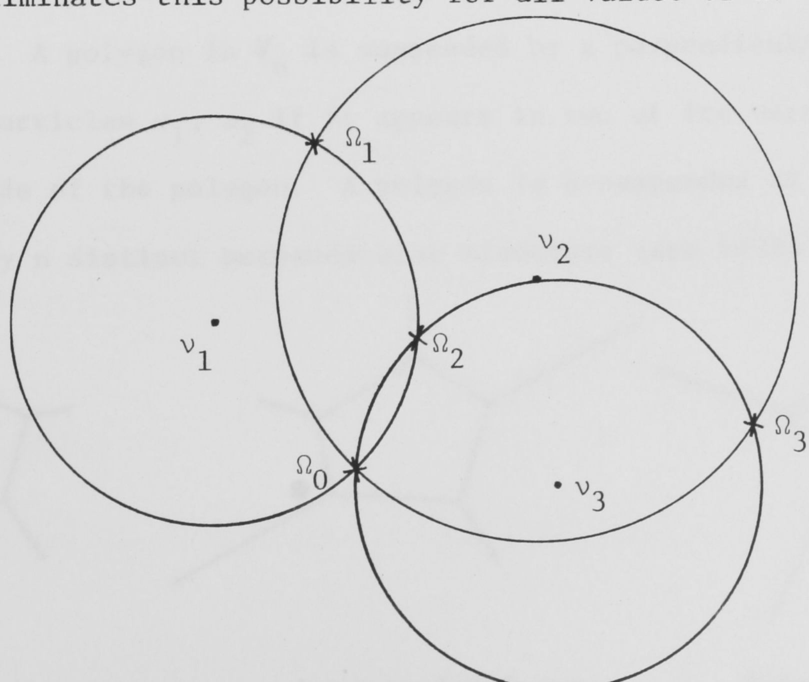

Figure 8

(iii) $Q_1 \cap Q_2 \subset Q_3$

In this case Q_3 contains $\omega_1, \omega_2, \ldots, \omega_{n-1}$ and Ω_1 as well, violating the (n - 1)-filling condition, and eliminating this possibility for all n values. (Figure 9.)

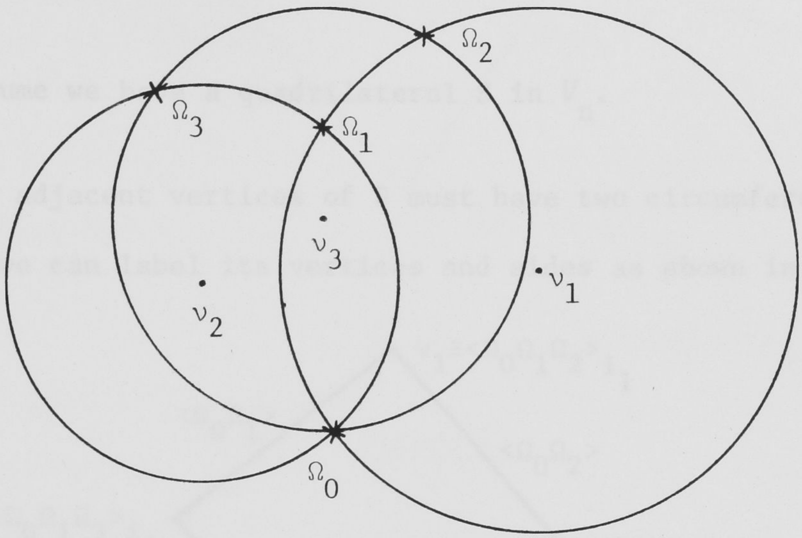

Figure 9

This completes the proof of the lemma.

Polygons in V_n

Definition A polygon in V_n is suspended by a perpendicular bisector $<\omega_1\omega_2>$ of particles ω_1, ω_2 if it appears in two of its vertices, but not as a side of the polygon. A polygon is n-suspended if it is suspended by n distinct perpendicular bisectors (see below).

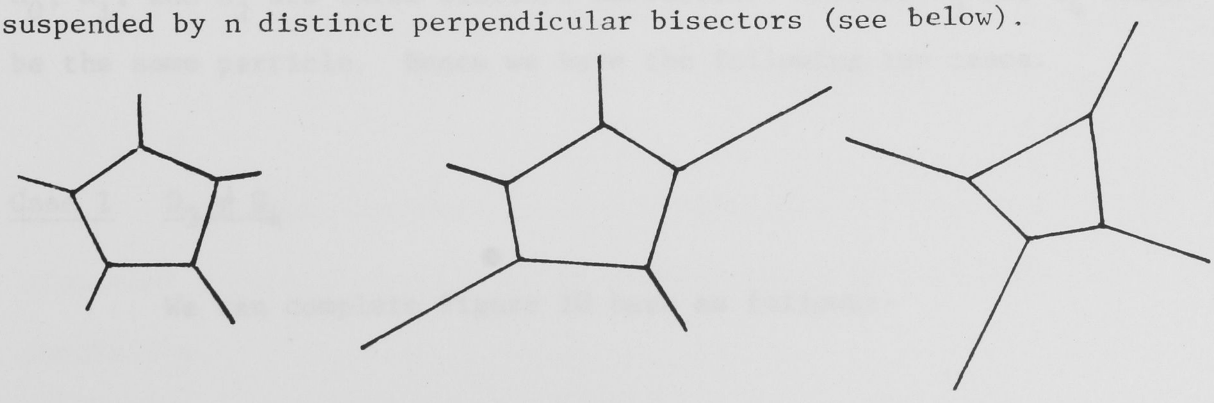

0-suspended 5-gon 1-suspended 5-gon 2-suspended 4-gon

As any $<\omega_1\omega_2>$ can contain at most one side of a member of V_1, all $P \in V_1$ are 0-suspended.

Simulation drawings of V_n realizations for $n > 1$ (see Figure 1) suggested the

<u>Lemma 7</u> All quadrilaterals in V_n are 2-suspended. $n = 2,3,4...$

<u>Proof</u> Assume we have a quadrilateral S in V_n.

As adjacent vertices of S must have two circumferential points in common, we can label its vertices and sides as shown in Figure 10

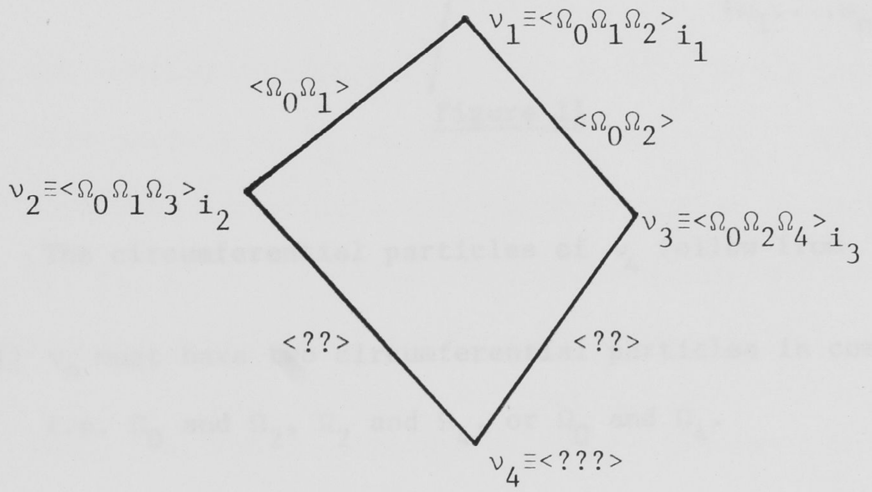

<u>Figure 10</u>

The assignment of circumferential particles on Figure 10 is unique, apart from permutations due to relabelling. The particles Ω_0, Ω_1, and Ω_2 are three distinct particles. However Ω_3 and Ω_4 could be the same particle. Hence we have the following two cases.

<u>Case 1</u> <u>$\Omega_3 \neq \Omega_4$</u>

We can complete Figure 10 here as follows:-

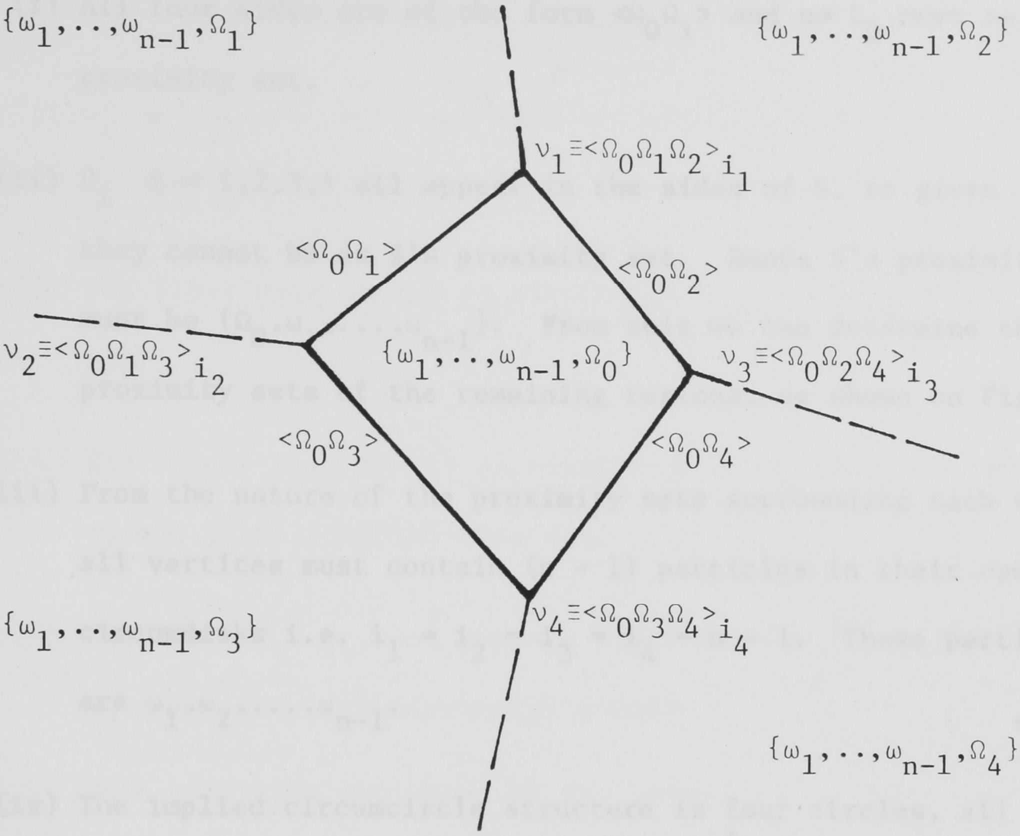

Figure 11

The circumferential particles of ν_4 follow from

(i) ν_4 must have two circumferential particles in common with ν_3 i.e. Ω_0 and Ω_2, Ω_2 and Ω_4, or Ω_0 and Ω_4.

(ii) the first pair in (i) is eliminated as this is shared by ν_3 with ν_1.

(iii) the second pair in (i) is eliminated as ν_4 must have two circumferential particles in common with ν_2 and $\Omega_4 \neq \Omega_3$.

(iv) this leaves Ω_0, Ω_4 and Ω_3 as ν_4's circumferential particles. Ω_3 has to be chosen to comply with requirement in (iii).

Analogous arguments to those used in the triangle case now show that a quadrilateral with vertex structure as in Figure 11 is impossible.

(i) All four sides are of the form $<\Omega_0\Omega_i>$ and so Ω_0 must be in S's proximity set.

(ii) Ω_i $i = 1,2,3,4$ all appear in the sides of S, so given (i) they cannot be in S's proximity set. Hence S's proximity set must be $\{\Omega_0,\omega_1,\ldots,\omega_{n-1}\}$. From this we can determine the proximity sets of the remaining regions, as shown on Figure 11.

(iii) From the nature of the proximity sets surrounding each vertex, all vertices must contain (n - 1) particles in their open circumdisks i.e. $i_1 = i_2 = i_3 = i_4 = n - 1$. These particles are $\omega_1,\omega_2,\ldots,\omega_{n-1}$.

(iv) The implied circumcircle structure is four circles, all intersecting at Ω_0, with $\omega_1\ldots\omega_{n-1} \in \bigcap_{i=1}^{4} Q_i$. However it is impossible to achieve this without putting at least one of Ω_1, Ω_2, Ω_3 or Ω_4 inside a Q_i, which means that not all Q_i can contain only (n - 1) particles, unless n = 1.

Hence the vertex structure in Figure 11 cannot correspond to a quadrilateral for n = 2,3... .

Case 2 $\Omega_3 = \Omega_4$

We complete Figure 10 as follows:-

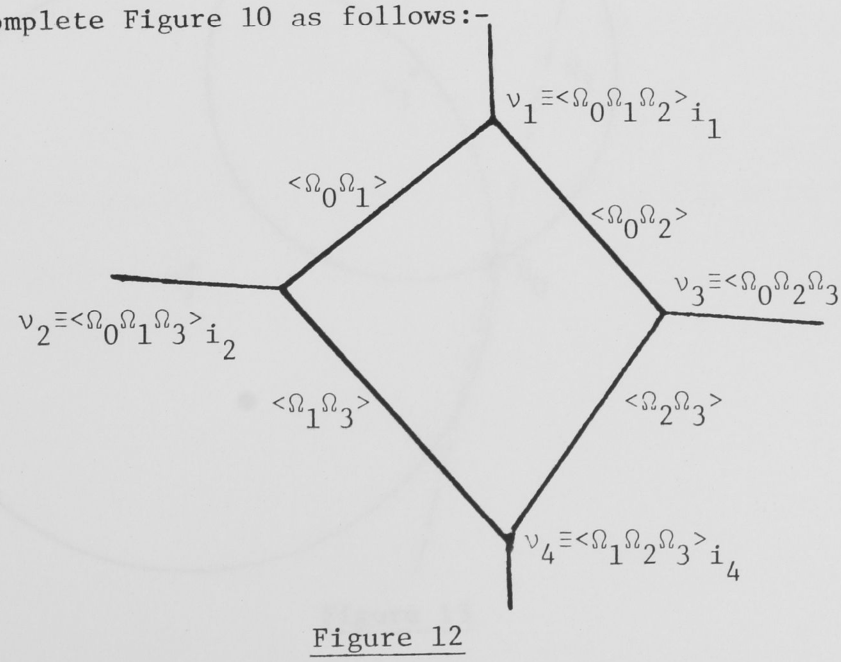

Figure 12

The circumferential structure of ν_4 follows from

(i) ν_4 and ν_3 must have two common circumferential particles - either $\Omega_0\Omega_2$, $\Omega_0\Omega_3$, or $\Omega_2\Omega_3$.

(ii) The first pair in (i) is eliminated as ν_3 and ν_1 share this pair.

(iii) The second pair in (i) is eliminated as ν_4 and ν_3 as well as ν_2 and ν_4 would share this pair.

(iv) Therefore Ω_2, Ω_3 must appear, together with Ω_1 so that ν_2 and ν_4 share two circumferential points.

This completes the proof of the lemma.

Quadrilaterals - associated point structure

We can use the vertex structure above to develop in more detail the point structure associated with a quadrilateral in V_n $n = 2,3,\ldots$, by looking at the circumdisks Q_i of the vertices ν_i (see Figure 13).

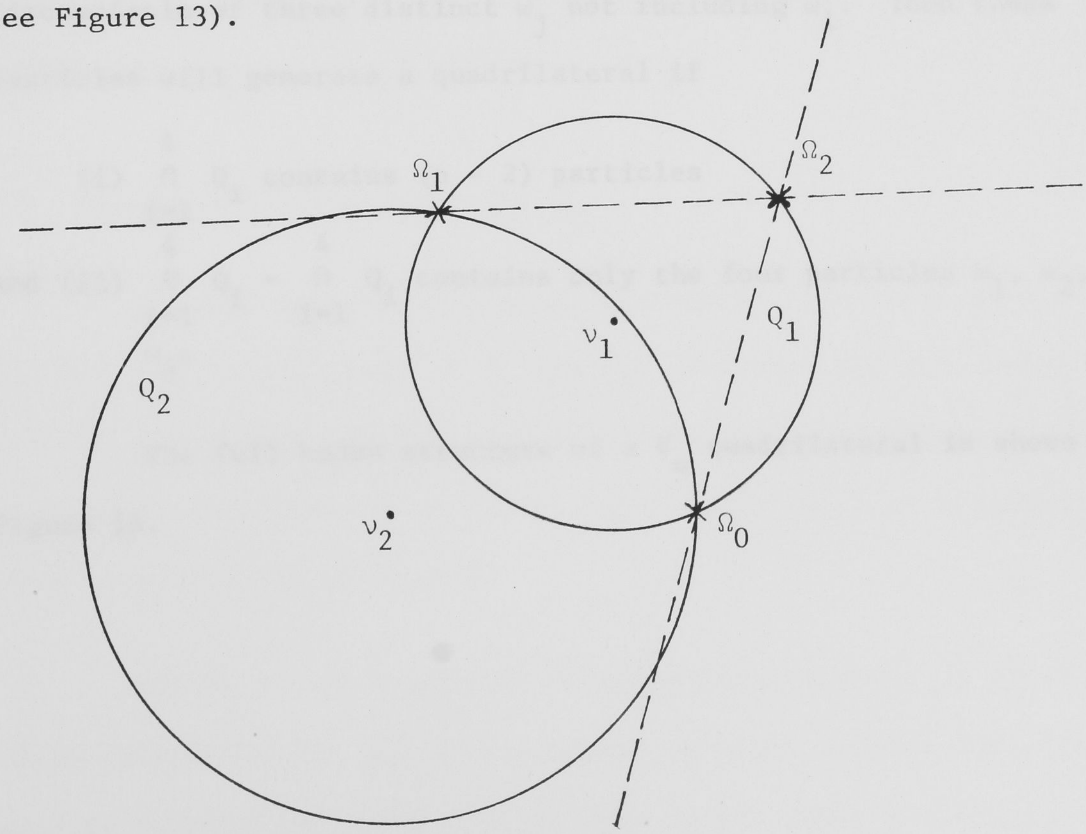

Figure 13

(i) Ω_0, Ω_1, and Ω_2 can be arbitrarily placed on the circumference of Q_1.

(ii) As $\bigcap_{i=1}^{3} Q_i \neq \phi$, and as ∂Q_3 must pass through Ω_0, Ω_3 must lie between the dotted lines in Figure 13. This is equivalent to requiring that the four circumferential points have a quadrilateral convex hull, as $\Omega_3 \notin Q_1$ as then $\bigcap_{i=1}^{4} Q_i$ would be void.

(iii) As Ω_3 and Ω_1 must both lie on the same side of the line joining $\Omega_0\Omega_2$, and $\Omega_3 \notin Q_1$, $\Omega_1 \in Q_3$.

(iv) As Ω_0 and Ω_3 must both lie on the same side of the line joining $\Omega_1\Omega_2$ and $\Omega_3 \notin Q_1$, $\Omega_0 \in Q_4$.

Hence we have the

Lemma 8 Quadrilaterals in V_n $(n = 2,3,\ldots)$ have the following associated point structure. Let $\omega_1,\ldots,\omega_4$ be four particles with a quadrilateral convex hull. Let Q_i be the disk bounded by the circumcircle of three distinct ω_j not including ω_i. Then these particles will generate a quadrilateral if

(i) $\bigcap_{i=1}^{4} Q_i$ contains $(n - 2)$ particles

and (ii) $\bigcup_{i=1}^{4} Q_i - \bigcap_{i=1}^{4} Q_i$ contains only the four particles ω_1, ω_2, ω_3, ω_4.

The full known structure of a V_n quadrilateral is shown in Figure 14.

Structure of Quadrilateral in $\mathcal{V}_n$ $n = 2,3,\ldots$

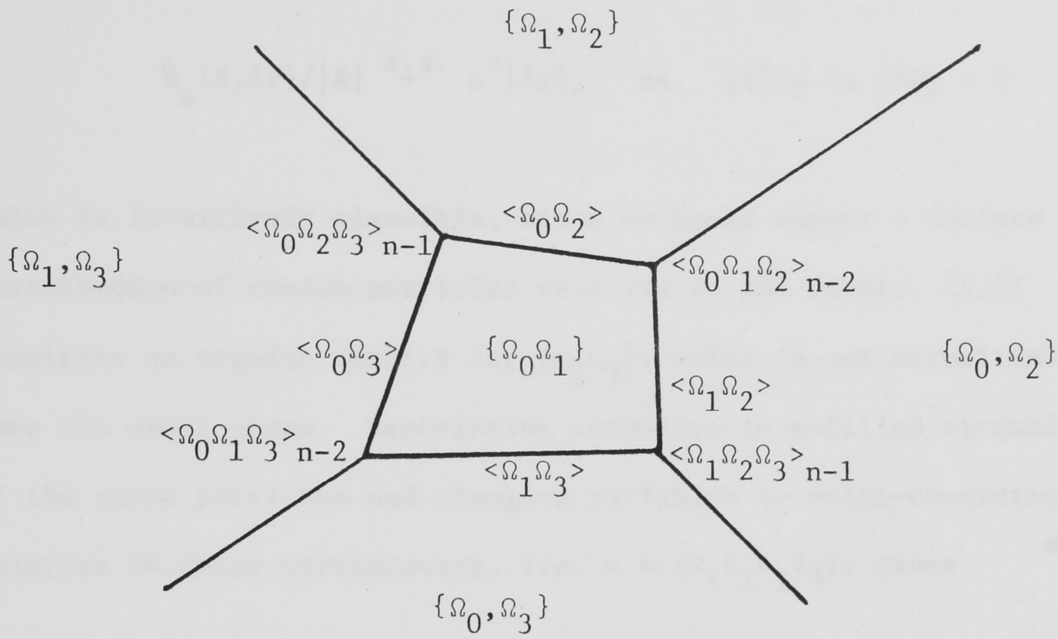

Figure 14

In Figure 14, each region is marked with part of its neighbouring n-set. The complete neighbouring n-set is the set marked plus $\{\omega_1,\ldots,\omega_{n-2}\}$ with no $\omega_i = \Omega_i$.

3.5 Stochastic Constructions for $\mathcal{V}_n$

In this section we present stochastic constructions for vertices, cells and sides of $\mathcal{V}_n$ for the case when the generating process is a planar Poisson process $\mathbb{P}$. These constructions are based on ergodic results of Miles [1970] relating to m-filled circumdisks of three particles chosen from $\mathbb{P}$.

Let $\dot{P}_3$ be the aggregate of all ordered triples of particles chosen from $\mathbb{P}$ and let $\dot{H}_3\{X,\delta\psi\}$ = number of these triples with first particle ω_1 in X and whose ψ value lies in $\delta\psi$, where $\psi = (\xi_2\eta_2\xi_3\eta_3)$

are the co-ordinates of ω_2 and ω_3 relative to ω_1.

Then Miles shows, [Equation 3.14, 1970], that

$$\dot{H}_n\{X,\delta\psi\}/|X| \xrightarrow{a.s.} \rho^n|\delta\psi|, \quad \text{as} \quad |X| \to \infty, \ |\delta\psi| \to 0 \qquad (5.1)$$

which is intuitively plausible, since we would expect a uniform distribution of random particles relative to the first. (5.1) specifies an ergodic density for $(\omega_2\omega_3)$, which is not normalizable over the whole plane. Restricting attention to m-filled circumdisks of the three particles and changing variables to polar-co-ordinates relative to their circumcentre, i.e. $\kappa = (R_1\theta_1\theta_2\theta_3)$, gives

$$H_3^{(m)}\{X,\delta\kappa\}/|X| \xrightarrow{a.s.} \frac{1}{6}\rho^3\{(\pi\rho)^m R^{2m+3} e^{-\pi\rho R^2}/m!\}|\sigma||\delta\kappa| \qquad (5.2)$$

where $H_3^{(m)}\{X,\delta\kappa\}$ denotes the number of m-filled circumdisks of three unordered particles from $\mathbb{P}$, all contained in X, and

$$\sigma = -4\sin\left(\frac{\theta_2-\theta_3}{2}\right)\sin\left(\frac{\theta_3-\theta_1}{2}\right)\sin\left(\frac{\theta_1-\theta_2}{2}\right). \qquad (5.3)$$

Hence

<u>Lemma 9</u>

A stochastic construction for a uniform random m-filled circumdisk of three particles chosen from $\mathbb{P}$

(i) Choose R, the circumdisk radius, with p.d.f. $f(r;\nu,\lambda)$ where $\nu = 2m+4$, $\lambda = \pi\rho$ i.e. $R \sim \Gamma_2(2m+4,\pi\rho)$. This distribution is a particular case of the gamma-type distributions defined by Miles [p 88, 1970]. If $Y \sim \Gamma_2(\nu_1\lambda)$, $Y^2 \sim \Gamma(\nu/2,\lambda)$. The p.d.f. for $\Gamma_2(\nu,\lambda)$ has the form

$$f(r;\nu,\lambda) = \frac{2\lambda^{\nu/2} r^{\nu-1}}{\Gamma(\nu/2)} \exp\{-\lambda r^2\}, \quad r \geq 0 \; . \qquad (5.4)$$

(ii) Choose $(\theta_1,\theta_2,\theta_3)$ in accordance with the joint density

$$f(\theta_1\theta_2\theta_3) = \frac{|\sigma|}{24\pi^2}, \; 0 \leq \theta_i < 2\pi \quad i = 1,2,3 \qquad (5.5)$$

Note that R and $(\theta_1\theta_2\theta_3)$ are independent by (5.2).

(iii) The m-filling particles are uniformly and independently distributed on the interior of the circumdisk.

Vertices in V_n are of two types, corresponding to (n − 1) and (n − 2) filled circumdisks of triples of particles from $\mathbb{P}$. Integrating (5.2) over R and $(\theta_1\theta_2\theta_3)$ gives

$$H_3^{(m)}\{X\}/|X| \overset{a.s.}{\to} 2\rho(m+1) \; , \qquad |X| \to \infty \; ,$$

where $H_3^{(m)}\{X\}$ is the number of m-filled circumdisks in X. Let $N_{\pm}(X)$ denote the number of vertices of V_n corresponding to i-filled circumdisks in X, i = n − 1, n − 2 i.e. the number of n^+ or n^- vertices in X. We are interested in a uniform random vertex of V_n.

$p_{\pm} \equiv$ P(uniform random V_n vertex corresponds to an i-filled circumdisk)

$$= \underset{|X|\to\infty}{\text{a.s. lim}} \frac{N_{\pm}(X)}{N_+(X) + N_-(X)}$$

$$= \underset{|X|\to\infty}{\text{a.s. lim}} \frac{H_3^{(i)}(X)}{H_3^{n-1}(X) + H_3^{n-2}(X)}$$

$$= \frac{i+1}{(2n-1)} \, , \qquad i = n-1, \, n-2 \; .$$

$p_{\pm}$ is the ergodic probability of the vertex being of a particular type. Note that for $n = 1$, $p_- = 0$, corresponding to the existence of only one vertex in V_1, namely empty circumdisks.

From the above, and lemma 9,

Lemma 10

Stochastic construction for uniform random V_n vertex

(i) choose vertex type $n^{\pm}$ with probability $p_{\pm}$.

(ii) $R_i \equiv$ the radius of the vertex $\sim \Gamma_2(2i + 4, \pi\rho)$, where $i = n - 1$ for n^+ vertex, $n - 2$ for n^- vertex.

(iii) $(\theta_1\theta_2\theta_3)$ are distributed in accordance with (5.5), and the i-filling particles are again uniformly and independently distributed on the circumdisk.

Lemma 11

Stochastic Constructions for uniform random V_n side and [N]-weighted V_n gon

Let $S(\ell)$ denote the square of side length ℓ with vertices $(\pm\frac{\ell}{2}, \pm\frac{\ell}{2})$.

(i) Since the density of the process ρ is simply a scale parameter, we are free to set it to any convenient arbitrary value, so we let $\rho = kn$, which normalizes the expected radius of the circumdisk of a V_n vertex to $(1/\sqrt{\pi k})$, for large n. [In a practical simulation k would be chosen to reduce the probability of the circumdisks associated with the constructed polygon's vertices extending outside $S(\ell)$.]

(ii) Construct a V_n vertex with circumdisk Q centered at the origin using Lemma 10 (see Figure 15), with circumferential particles ω_1, ω_2, ω_3.

(iii) Construct a realization of $\mathbb{P}$ in $S(1) - Q$.

(iv) Randomly choose one of the three V_n sides meeting at the origin, generated by circumferential particles ω_1 and ω_2 say.

(v) Move along $<\omega_1\omega_2>$, from the origin until we reach the first circumcentre $<\omega_1\omega_2\omega_k>$, where ω_k is any other particle. This circumcentre is the centre of another V_n vertex, which terminates the first side of the V_n gon. The initial direction of movement along $<\omega_1\omega_2>$ is determined by the vertex type; if the initial vertex is an n^+ vertex, movement is away from the third circumferential particle ω_3, since the vertex already contains the $(n - 1)$ particles required for a point in a V_n side (see Table 1). If the initial vertex is an n^- vertex, movement is towards ω_3. (i) - (v) amount to a stochastic construction for a uniform random side of V_n.

(vi) If $\omega_k \in Q$, the new V_n vertex is of type n^-, otherwise it is n^+.

(vii) Step (v) is now iterated for successive sides of the polygon. We choose the circumferential particles of each new vertex so that we turn 'right', around the polygon. If the new particle met on proceeding down the selected perpendicular bisector lies in the previous vertex's circumdisk, the new vertex is an n^- vertex, otherwise it is an n^+. (v) is repeated until we return to the origin vertex. This completes the construction provided all vertex circumdisks be wholly inside $S(1)$. If not, $\mathbb{P}$ is constructed in $S(2) - S(1)$, and the above procedure repeated, and so on for $S(3) - S(2)$, $S(4) - S(3)$, until the circumdisks are contained in the generating square.

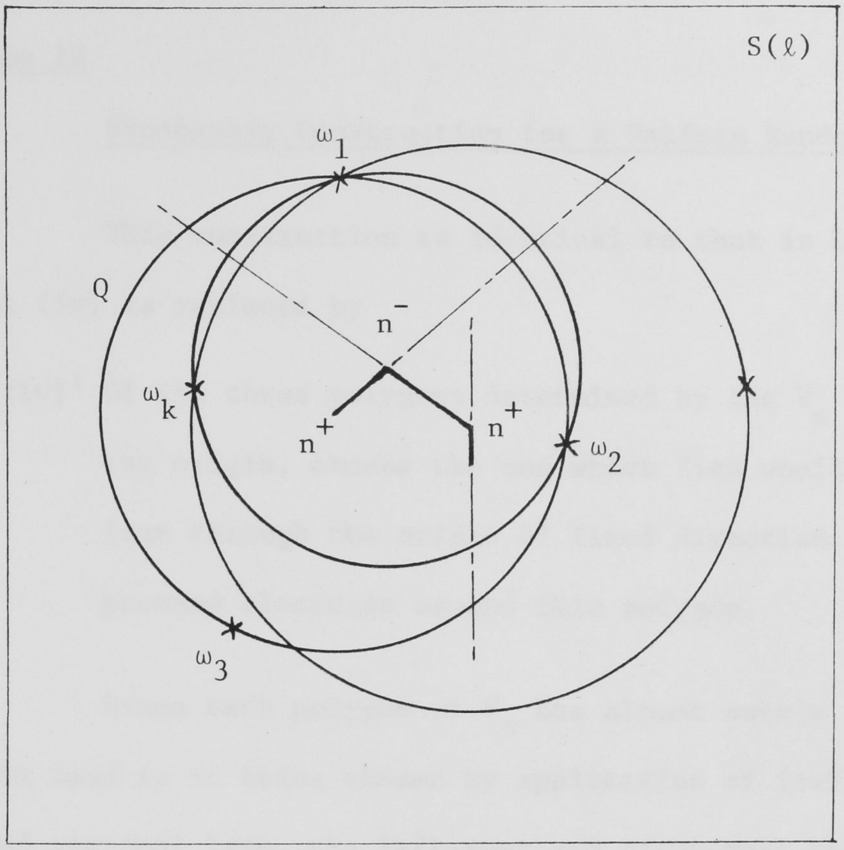

Figure 15

It should be clear from the geometry of Lemma 11 that if a V_n cell has vertices ν_i with associated circumdisks Q_i, $i = 1,2,\ldots,N$ then $\bigcup_{i=1}^{N} Q_i - \bigcap_{i=1}^{N} Q_i$ must be empty of particles and $\bigcap_{i=1}^{N} Q_i$ must contain N - 2 particles.

We note that lemma 11 yields an [N]-weighted V_n-gon, as the polygon generated is chosen by a random vertex. Hence, the probability of any polygon being chosen is directly proportional to N the number of sides. If $g(\underline{Z})$ is the density of a vector characteristic $\underline{Z}$ for such a polygon, and $f(\underline{Z})$ the density for a uniform random polygon, then

$$g(\underline{Z}) = \frac{E_f(N|\underline{Z})}{E_f(N)} f(\underline{Z}) .$$

However it is easy to modify lemma 11 to give

Lemma 12

Stochastic Construction for a Uniform Random V_n cell

This construction is identical to that in Lemma 11 except that (iv) is replaced by

(iv)' Of the three polygons determined by the V_n vertex centered on the origin, choose the one which lies wholly on one side of a line through the origin of fixed direction. We can then proceed clockwise around this polygon.

Since each polygon of V_n has almost surely two vertices which would lead to it being chosen by application of (iv)', e.g. for a fixed vertical line, the left-most and right-most vertices, we obtain a uniform random V_n gon by this procedure.

3.6 Geometry of V_n N-gons

The results in this section represent joint work between R.E. Miles and the author. We extend the theory developed in section 3.5 to detail the exact particle distribution around a V_n N-gon.

Lemma 13 Suppose $\omega_1, \omega_2, \ldots, \omega_n$ are particles of a Π_2 type process and $T = [\omega_1 \omega_2 \ldots \omega_n]$. Then

$$T = \bigcap_{i=1}^{n} T'(\omega_i) \quad ,$$

where $T'(\omega_i)$ is the V_1 cell corresponding to ω_i relative to the reduced particle aggregate $\Pi_2' = \Pi_2 - \{\omega_1 \omega_2 \ldots \omega_n\}$.

Proof. Is immediate on comparing (1.1) and (2.1.1). The second intersection in (1.1) represents, by (2.1.1), the V_1 cell of ω_i relative to all particles except $\omega_1, \omega_2, \ldots, \omega_n$.

Figure 16 illustrates a typical structure of a V_n cell $T = [\omega_1\omega_2 \cdot\cdot \omega_n]$ (with N = 7), viewed as the intersection of V_1 cells in accordance with lemma 13. The perimeter of T is composed of portions of individual $T'(\omega_i)$. (Three in Figure 16.) The other $T'(\omega_i)$ properly contain T in their interiors; for clarity these are not shown in the figure.

From Figure 16, we can characterize the two vertex types of V_n in yet another way. A vertex of T is either

(i) a vertex of $T'(\omega_i)$ for some i. This vertex is of the form $<\omega_i\Omega_1\Omega_2>$ where $\Omega_i \in \Pi_2'$, and we call it an outer vertex, or

(ii) an intersection point of $\partial T'(\omega_j)$ and $\partial T'(\omega_k)$ for some j, k. This vertex is of the form $<\omega_j\omega_k\Omega_1>$, $\Omega_1 \in \Pi_2'$ and we call this an inner vertex.

A comparison of Figure 16 and Table 1 and reference to geometric properties (i) and (ii) noted in section 3.1 will tie this vertex description in with previous ones. For convenience, Table 3 lists the alternative names for the V_n vertices.

Table 3

V_n vertex types

	Description	Names
(i)	(n - 2)-filled circumdisk of three particles	n^- vertex; (n - 1,n) vertex; inner vertex
(ii)	(n - 1)-filled circumdisk of three particles	n^+ vertex; (n,n + 1) vertex; outer vertex

We now classify the particles of Π_2 into four classes relative to T.

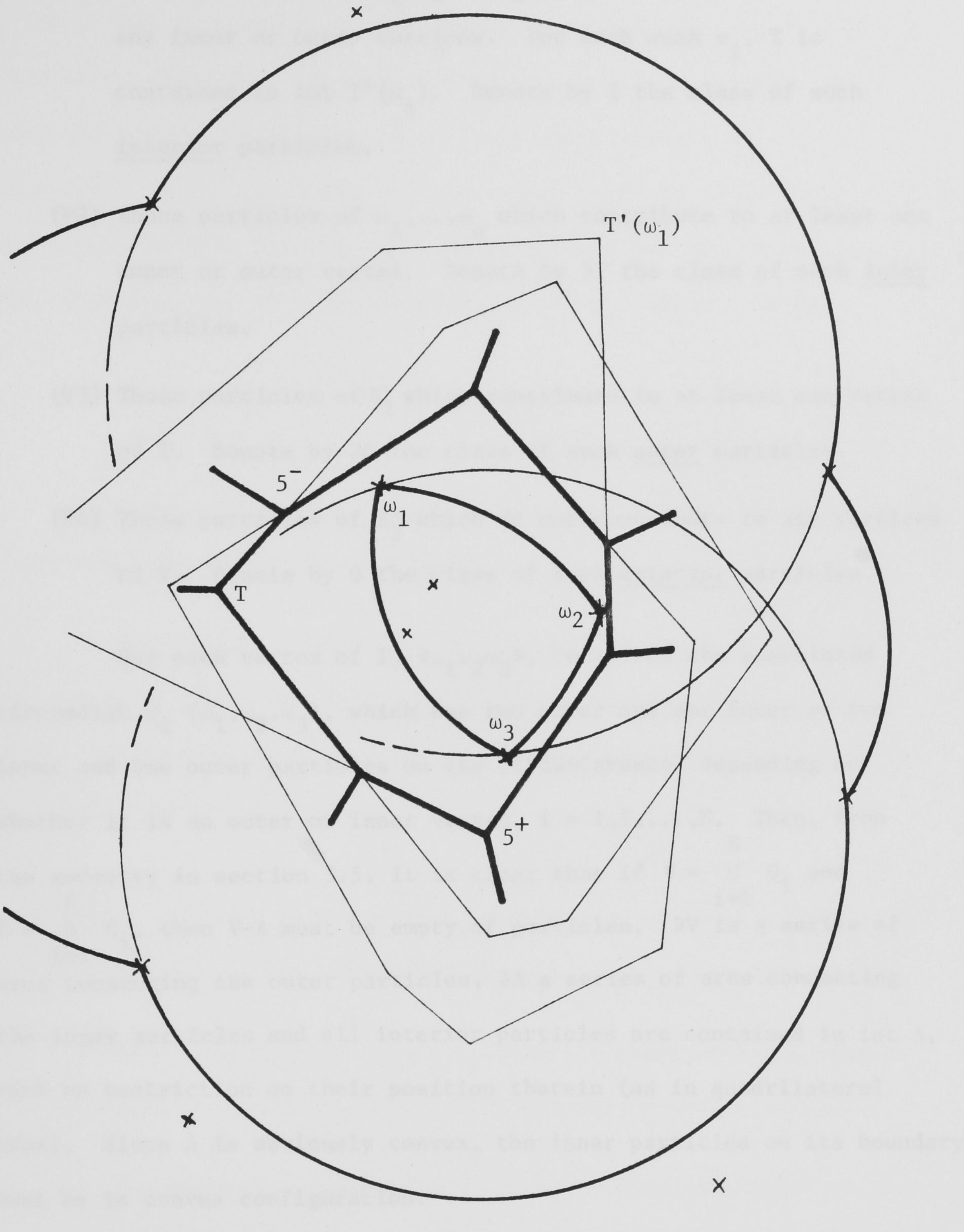

Geometric structure of a typical N-gon T of V_n. In this case n = 5, N = 7. T has two interior, three inner (ω_1, ω_2 and ω_3) and four outer particles, and is the intersection of the three $T'(\omega_i)$ shown, i = 1,2,3. Note the 5^+, 4-filled, outer and 5^-, 3-filled inner vertices of T.

<u>Figure 16</u>

(P1) Those particles of $\omega_1,\omega_2,..,\omega_n$ which do not contribute to any inner or outer vertices. For each such ω_i, T is contained in int $T'(\omega_i)$. Denote by I the class of such interior particles.

(P2) Those particles of $\omega_1,..,\omega_n$ which contribute to at least one inner or outer vertex. Denote by ∂I the class of such inner particles.

(P3) Those particles of Π_2' which contribute to at least one vertex of T. Denote by ∂O the class of such outer particles.

(P4) Those particles of Π_2' which do not contribute to any vertices of T. Denote by O the class of such exterior particles.

For each vertex of T, $<\omega_1\omega_2\omega_3>$, construct the associated circumdisk Q_i $(\omega_1,\omega_2,\omega_3)$, which has two outer and one inner or two inner and one outer particles on its circumference, depending on whether it is an outer or inner vertex, $i = 1,2,...,N$. Then, from the geometry in section 3.5, it is clear that if $V = \bigcup_{i=1}^{N} Q_i$ and $\Lambda = \bigcap_{i=1}^{N} Q_i$, then $V-\Lambda$ must be empty of particles. ∂V is a series of arcs connecting the outer particles, $\partial\Lambda$ a series of arcs connecting the inner particles and all interior particles are contained in int Λ, with no restriction on their position therein (as in quadrilateral case). Since Λ is obviously convex, the inner particles on its boundary must be in convex configuration.

Each side of T is part of the perpendicular bisector between an inner and outer particle, and as each outer/inner vertex is passed on a traversal of T's perimeter, a new outer/inner particle replaces one of the pair forming the previous side. Hence N = no of inner + no of outer particles, and the no of inner vertices = no of inner particles.

Since every V_n cell must contain a V_{n-1} segment, it must have at least two n^- vertices and therefore m = no of inner particles $\geqslant 2$. Similarly T must have at least two outer particles, for the outer particle replaces the inner particle in the proximity set of the adjacent V_n cell. If T had only one outer particle it would appear in the proximity sets for all cells surrounding T but not in T's proximity set, violating the star-shaped property of its n-Area. Hence

$$2 \leqslant m \leqslant \min\{n, N-2\} \quad . \tag{6.1}$$

Also, $N \geqslant 4$, verifying that there are no triangles in V_n. By comparison, triangles do occur in V_1.

The variable element in the above characterization is m, the number of inner particles or vertices, which is subject only to (6.1). Variations in m, and the arrangement of the vertices lead to different types of V_n cell.

<u>Definition</u> If T is an N-gon of V_n, let $\phi_i = +1[-1]$ if vertex ν_i is an outer (inner) vertex. Then $\phi = (\phi_1, \phi_2, \ldots, \phi_N)$ is the type of T.

Note from (7.1) that all V_n quadrilaterals are of a single type as shown in Figure 14, with two inner and two outer vertices.

The different types of pentagons can be investigated by starting with the unique quadrangle type and adding single particles, either inner or outer, at various locations within $V - \Lambda$. Figure 17 illustrates such augmentations. 5.[.5] in a region bounded by circular arcs indicates that the introduction of a new inner [outer] particle in that region produces a pentagon of $V_{n+1}[V_n]$. 4.[.4] indicates the similar introduction of a new particle leaves a new quadrangle of $V_{\leqslant n}[V_n]$, with a previous inner [outer] particle disappearing.

Pentagons thus have either two inner and three outer ($n \geqslant 2$) or three inner and two outer vertices ($n \geqslant 3$), which alternate between inner and outer, except that in the first (second) case there is a pair of adjacent outer (inner) vertices.

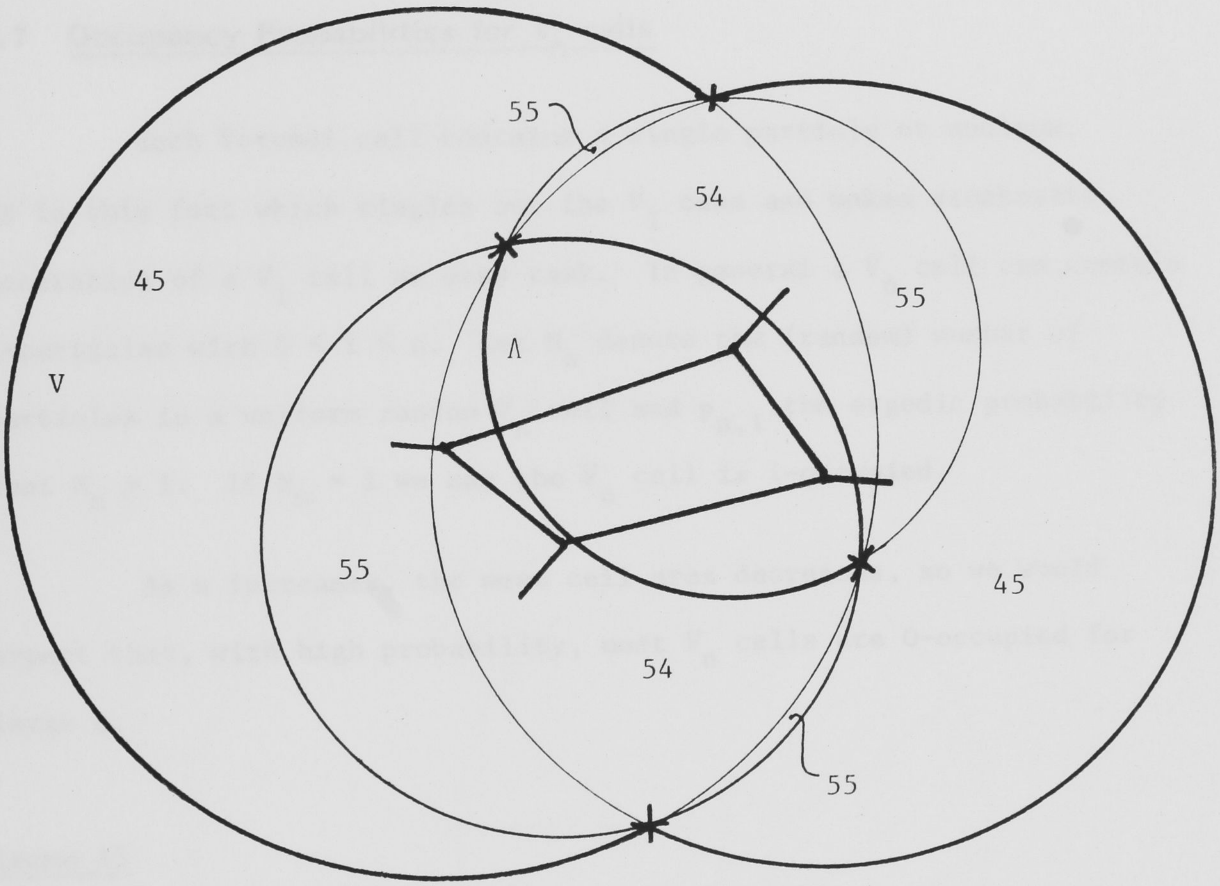

Figure 17

To summarize the structure of a V_n N-gon as detailed above, we have

Lemma 14

For a V_n N-gon with m inner vertices, $2 \leqslant m \leqslant \min\{n, N-2\}$, there are

(i) n-m interior particles in int Λ;

(ii) m inner particles in $\partial\Lambda$ in convex configuration;

(iii) no particles in int$(V - \Lambda)$;

(iv) N-m outer particles in ∂V; and

(v) no restriction on particles outside V.

3.7 Occupancy Probabilities for V_n cells

Each Voronoi cell contains a single particle or nucleus. It is this fact which singles out the V_1 case and makes stochastic generation of a V_1 cell an easy task. In general a V_n cell can contain i-particles with $0 \leqslant i \leqslant n$. Let N_n denote the (random) number of particles in a uniform random V_n cell and $p_{n,i}$ the ergodic probability that $N_n = i$. If $N_n = i$ we say the V_n cell is i-occupied.

As n increases, the mean cell area decreases, so we would expect that, with high probability, most V_n cells are 0-occupied for large n.

Lemma 15

$$\lim_{n\to\infty} p_{n,0} = 1 .$$

Proof

$$E(N_n) = \lim_{\text{a.s.}\,|X|\to\infty} \sum_{i=0}^{n} \frac{iN_i(X)}{N(X)} ,$$

where $N_i(X)$ = number of i-occupied V_n cells in X and $N(X)$ = total number of V_n cells in X. Obviously $\sum iN_i(X) = N_p(X)$ = total number of particles in X.

Hence
$$E(N_n) = \lim \frac{N_p(X)/|X|}{N(X)/|X|}$$

$$= \frac{\rho}{1/E(A_n)} = \frac{1}{2n-1} \quad .$$

Therefore
$$\sum_{i=1}^{n} p_{n,i} < \sum_{i=1}^{n} i p_{n,i} = E(N_n) = \frac{1}{(2n-1)} \quad .$$

So $p_{n,0} \to 1$ as $n \to \infty$.

In fact $p_{n,0}$ tends fairly rapidly to one, as we see in investigating the occupancy probabilities for a V_2-gon. From Figure 18, it is clear that two particles are contained in the same V_2 cell iff they each have each other as their nearest neighbour. We call such particles symmetric nearest neighbours.

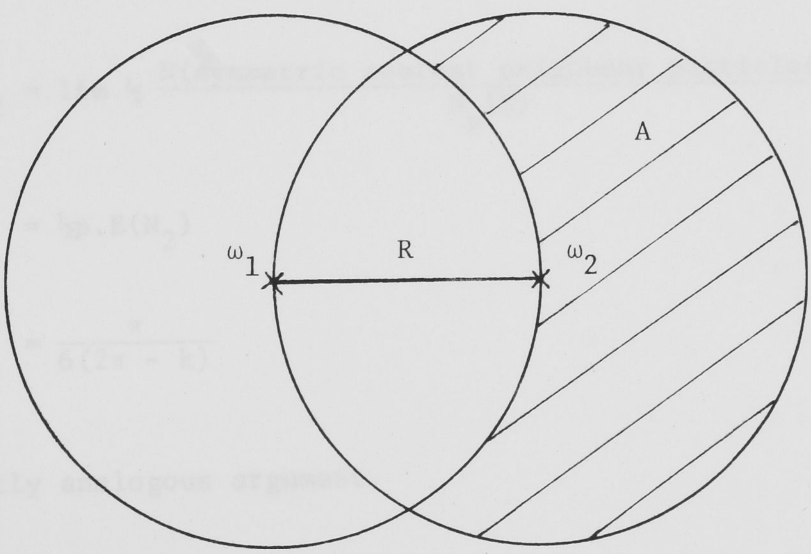

Figure 18

Take an arbitrary particle ω_1 and let R be the distance to its nearest neighbour ω_2 with p.d.f. $h(R) = 2\rho\pi R \exp\{-\rho\pi R^2\}$, for a $\mathbb{P}$ generating process.

Then $p = P(\omega_1$ and ω_2 are symmetric nearest neighbours)

$$= \int_0^\infty P(\omega_1, \omega_2 \text{ symmetric nearest neighbours} | R) h(R) dR$$

$$= \int_0^\infty P(A \text{ empty} | R) h(R) dR ,$$

where A denotes the area shaded in Figure 1 and $A = (\pi - k)R^2$ with $k = \frac{1}{6}(4\pi - 3\sqrt{3})$.

Hence
$$p = \int_0^\infty \exp\{- \rho(\pi - k)R^2\} 2\rho\pi R \exp\{- \rho\pi R^2\} dR$$

$$= \frac{\pi}{(2\pi - k)} = 0.6215$$

Now consider
$$p_{2,2} = \lim_{|X| \to \infty} \frac{N_2(X)}{N(X)} .$$

As $N_2(X) = \frac{1}{2}N(\text{symmetric nearest neighbour particles})$,

$$p_{2,2} = \lim \tfrac{1}{2} \frac{N(\text{symmetric nearest neighbour particles})}{N_p(X)} . \frac{N_p(X)}{N(X)}$$

$$= \tfrac{1}{2} p . E(N_2)$$

$$= \frac{\pi}{6(2\pi - k)}$$

By an exactly analogous argument,

$N(V_2$ cells which are 1-occupied) = N(particles whose nearest neighbours are not symmetric nearest neighbours)

so
$$p_{2,1} = \frac{1}{3}\left(1 - \frac{\pi}{(2\pi - k)}\right) .$$

The occupancy probabilities for V_2 cells are summarized in Table 4. Note that $E(N_2) = \frac{1}{3}$ as expected from Lemma 14, and that 77% of V_2 cells are 0-occupied.

Table 4

i	0	1	2
$p_{2,i}$	$\frac{1}{6}\left(4 + \frac{\pi}{(2\pi - k)}\right)$	$\frac{1}{3}\left(1 - \frac{\pi}{2\pi - k}\right)$	$\frac{\pi}{6(2\pi - k)}$
	0.77	0.13	0.10

CHAPTER 4

GENERALIZED VORONOI TESSELLATIONS - NEW THEORY

4.1 Mean Areas of Generalized Voronoi Cells

In this section a deeper analysis of the geometry of the V_n tessellation, and, in particular, superpositions of successive V_n, lead to an extension of the known means $E(A_n)$ for the area A_n of typical V_n cells from the Poisson to the general homogeneous case.

In Lemma 3.5, we noted the one-to-one correspondence between V_1 sides and V_2 cells. Analysis of a superposition of plots of V_1, V_2 and V_3 suggested the following natural extension of this correspondence (see Figure 1). The computer generated plots were instrumental in suggesting the geometrically based proofs of this section. The cell/side correspondence is replaced by a cell/side, cell/vertex correspondence in the V_3 case.

Before establishing this new correspondence we introduce some new

Notation Since every V_n vertex is also a vertex in V_{n-1} or V_{n+1}, it is clear that adjacent to any V_n segment on a perpendicular bisector there will be segments of either V_{n-1} or V_{n+1}. We write

$$\mathcal{L}_n = \{s : s \text{ is a side of } P,\ P \in V_n\}$$

and $\mathcal{L}_n(\pm,\pm)$ for members of $\mathcal{L}_n$ with a $V_{\substack{n+1 \\ n-1}}$ segment on either side. For example, members of $\mathcal{L}_2$ are of two types, $\mathcal{L}_2(-,+)$ or $\mathcal{L}_2(+,+)$.

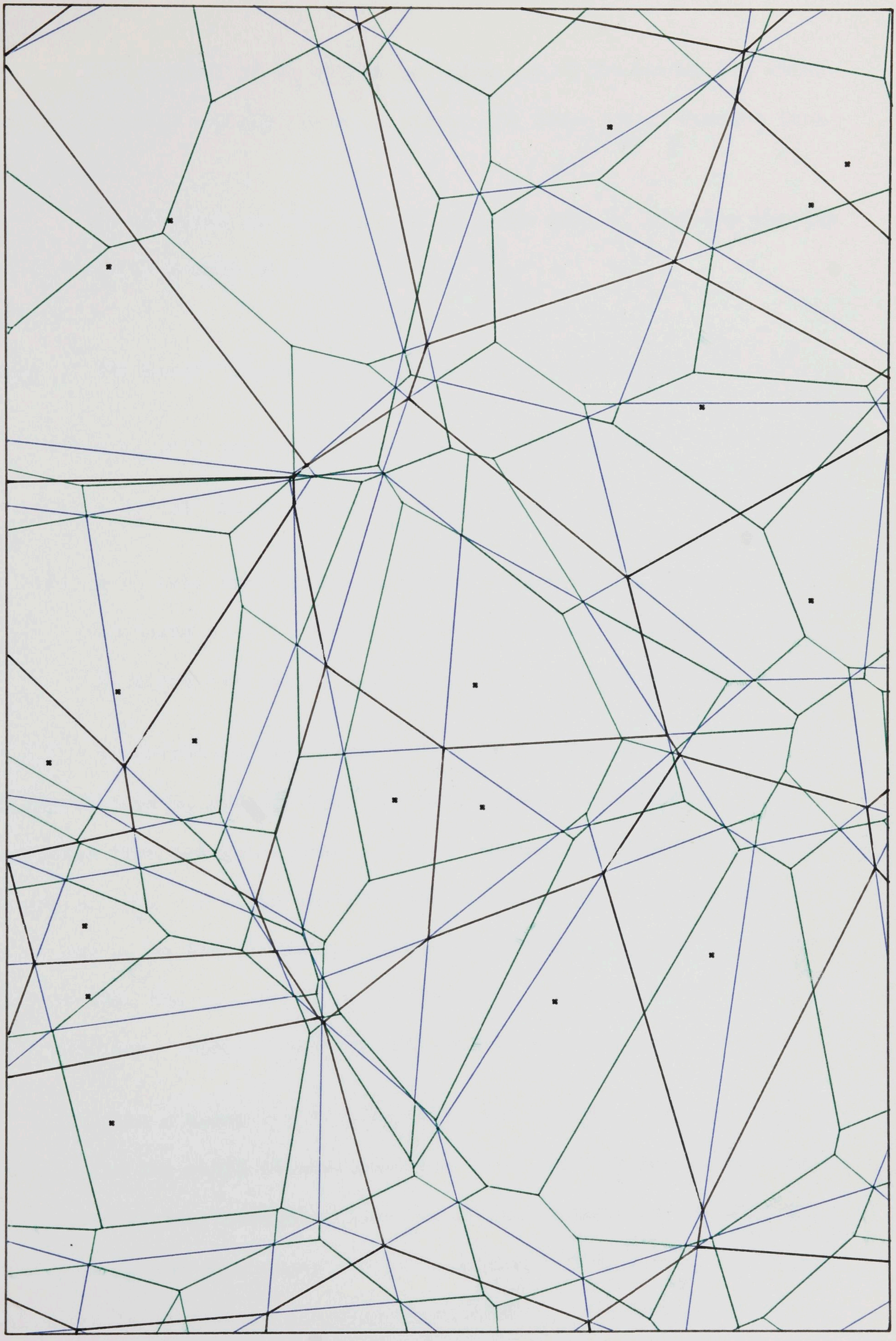

Figure 1. *Superposition of* V_1, V_2 *and* V_3 *for a set of random particles.* V_1 shown in black, V_2 in blue, V_3 in green.

Lemma 1

Each member of V_3 either contains one (1,2) vertex (in which case it contains exactly three V_2 sides, the three which emanate from that vertex)

or contains no (1,2) vertex in which case it contains exactly one V_2 side, a member of $\mathcal{L}_2(+,+)$.

Proof   The proof relies on three geometrical propositions

(i) a V_3 cell can contain at most one (1,2) vertex

(ii) a V_3 cell must contain at least one V_2 side

and

(iii) a V_3 cell can contain at most one side of V_2, unless it contains a (1,2) vertex, in which case it contains the three V_2 sides meeting at that vertex and no other V_2 sides.

To establish (i) assume a V_3 cell P contains two distinct (1,2) vertices ν_1 and ν_2, i.e. two zero-filled circumdisks of three particles from the generating process. Assume the particles generating ν_1 are ω_1, ω_2, ω_3. This implies that $P \equiv [\omega_1\omega_2\omega_3]$. ν_2 must have at least one ω_i on its circumference distinct from ω_1, ω_2 and ω_3. This implies that the V_3 cell is of the form $[\omega_i \ldots]$, which is a contradiction. Hence a V_3 cell can contain at most one (1,2) vertex.

(ii) Take a point $\underline{x} \in P$, a V_3 cell, and construct $Q(\underline{x}, |\underline{x} - \omega_3|)$, where ω_3 is the third closest particle to $\underline{x}$. Let ω_1 and ω_2 be first and second closest particles (see Figure 2). Construct the line L from $\underline{x}$ to ω_3 and move along L until reaching $L \cap \langle\omega_3\omega_1\rangle$ or $L \cap \langle\omega_2\omega_3\rangle$, whichever is closest to $\underline{x}$. Call this point $\underline{y}$. Assuming, w.l.o.g. that $\underline{y}$ is $L \cap \langle\omega_1\omega_3\rangle$, it is part of an $\mathcal{L}_2$ segment on $\langle\omega_1\omega_3\rangle$, since $Q(\underline{y}, |\omega_3 - \underline{y}|)$ is one-filled by ω_2. Since obviously $\underline{y} \in P$, every V_3 cell must contain at least one V_2 side.

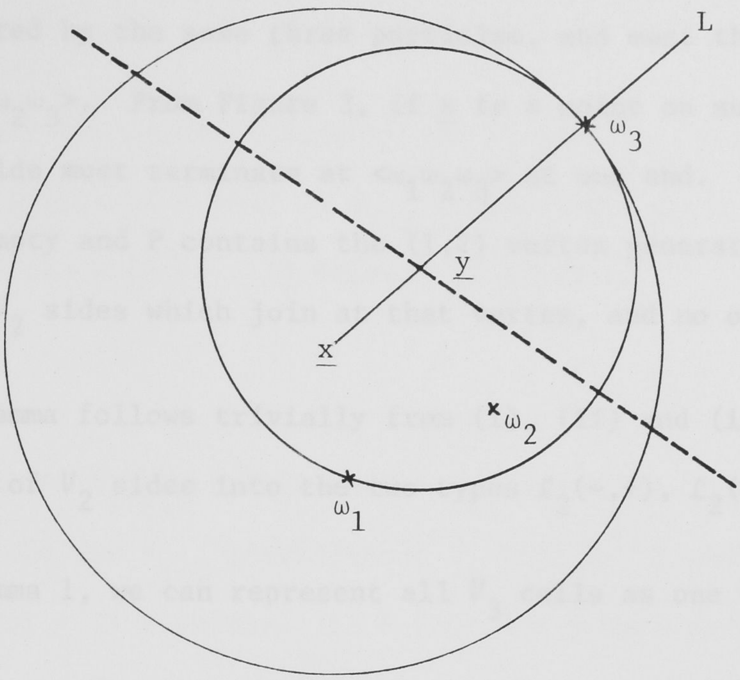

Figure 2

Finally to establish (iii), consider a V_2 side in a V_3 cell, P. Assume that the V_2 side is contained in $\langle\omega_1\omega_2\rangle$, and label the filling particle ω_3 (Figure 3).

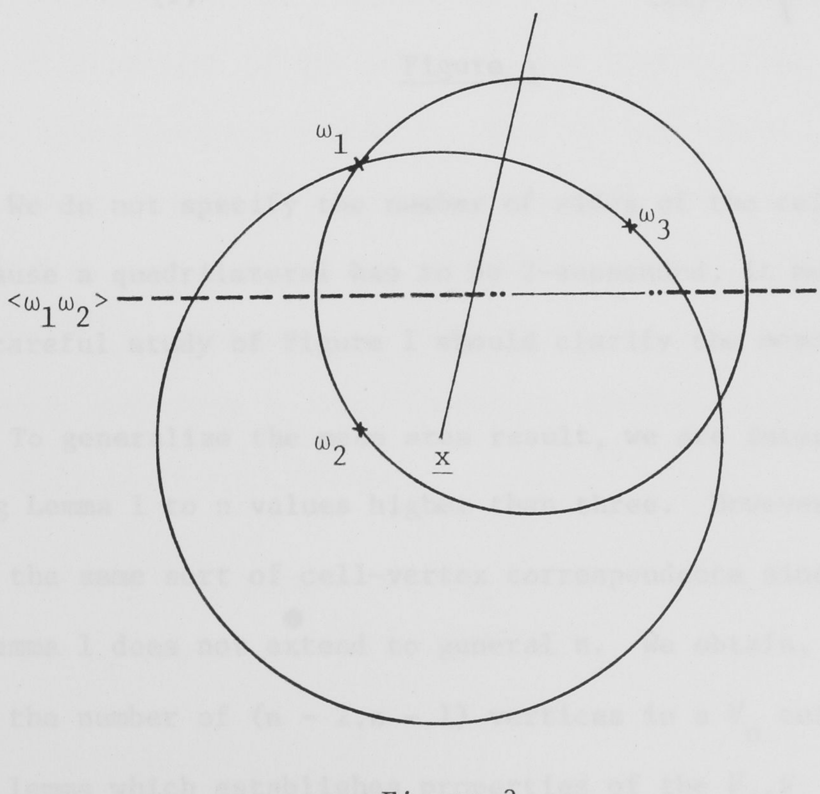

Figure 3

This implies $P \equiv [\omega_1\omega_2\omega_3]$, and hence any other V_2 side in P must be generated by the same three particles, and must therefore lie on $<\omega_1\omega_3>$ or $<\omega_2\omega_3>$. From Figure 3, if $\underline{x}$ is a point on such a V_2 side, then that V_2 side must terminate at $<\omega_1\omega_2\omega_3>$ at one end. Hence $Q(\omega_1\omega_2\omega_3)$ is empty and P contains the (1,2) vertex generated by $\omega_1\omega_2\omega_3$ and the three V_2 sides which join at that vertex, and no other sides.

The lemma follows trivially from (i), (ii) and (iii), and the classification of V_2 sides into the two types $\mathcal{L}_2(-,+)$, $\mathcal{L}_2(+,+)$.

By lemma 1, we can represent all V_3 cells as one of two types (see Figure 4).

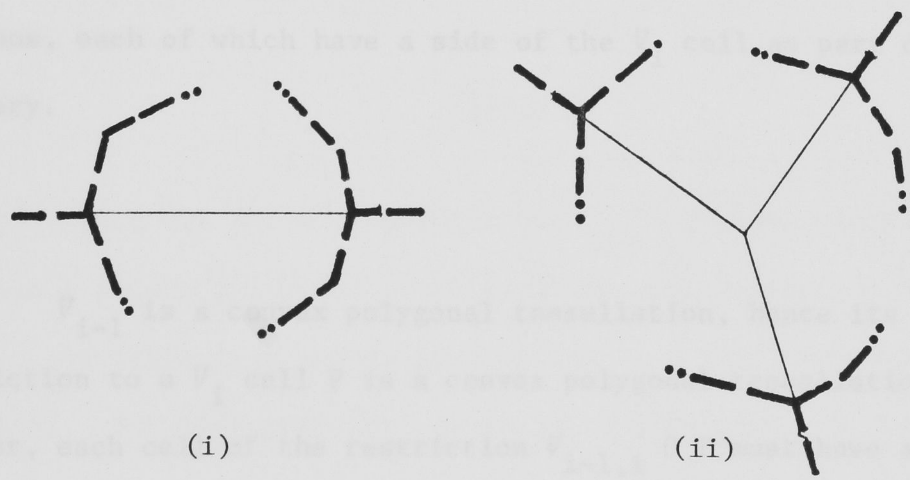

(i) (ii)

Figure 4

We do not specify the number of sides of the cells. But note that because a quadrilateral has to be 2-suspended, it must be of type (i). A careful study of Figure 1 should clarify the meaning of Lemma 1.

To generalize the mean area result, we are interested in extending Lemma 1 to n values higher than three. However we cannot maintain the same sort of cell-vertex correspondence since proposition (i) in Lemma 1 does not extend to general n. We obtain, instead, a bound on the number of (n - 2,n - 1) vertices in a V_n cell as part of the next lemma which establishes properties of the V_i, V_{i-1} superposition used in generalizing the result.

Definition

$$V_{i-1,i} \equiv \{P \cap Q : P \in V_i, Q \in V_{i-1}\} \quad i = 2,3,\ldots.$$

$V_{i-1,i}$ is simply the superposition of the V_i and V_{i-1} tessellations. Note that the points of a cell in $V_{i-1,i}$ have the same i nearest neighbours and the same (i - 1) nearest neighbours.

Lemma 2

Consider $V_{i-1,i} \cap P$ where $P \in V_i$, $i = 2,3,\ldots.$ i.e. we are interested in the way V_{i-1} partitions a V_i cell P. P contains at most (i - 2) (i - 2,i - 1) vertices. If P contains j such vertices, then it contains 2j + 1 V_{i-1} sides, which partition it into j + 2 convex polygons, each of which have a side of the V_i cell as part of their boundary.

Proof

V_{i-1} is a convex polygonal tessellation, hence its restriction to a V_i cell P is a convex polygonal tessellation of P. However, each cell of the restriction $V_{i-1,i} \cap P$ must have at least one side of P as part of its boundary, for otherwise we would have a V_{i-1} cell lying entirely inside P. This is impossible because every V_{i-1} cell must contain at least one side of V_i. To prove this take a point $\underline{x} \in R$, a V_{i-1} cell, and construct a line L joining $\underline{x}$ and ω_i, where $\omega_j = j^{th}$ closest particle to $\underline{x}$ $j = 1,2,\ldots i$ (see Figure 5). Move along L away from ω_i until capturing another particle ω at $\underline{y}$; $Q(\underline{y}, |y - \omega_i|)$ is (i - 1) filled.

Hence $\underline{y} \in \mathcal{L}_i$ segment on $<\omega\omega_i>$. Since $\underline{y} \in R$, R must contain at least one $\mathcal{L}_i$ segment.

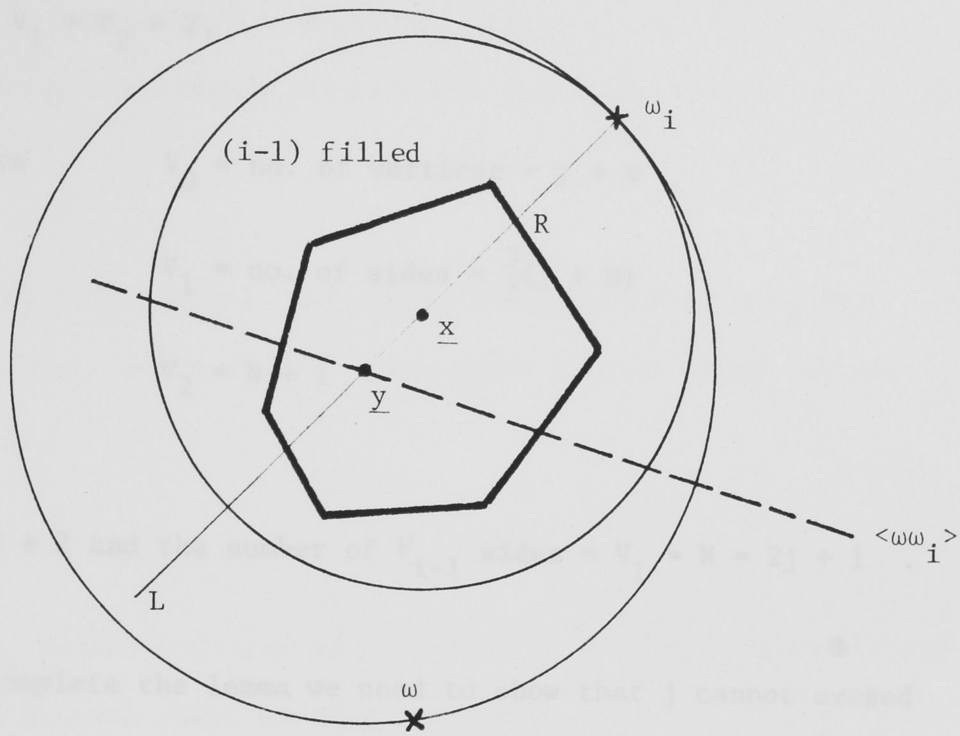

Figure 5

Given the above properties of V_{i-1}'s partitioning of P, we can form a planar polygonal graph with the same number of cells as $P \cap V_{i-1}$ by taking the convex hull of P's (i - 1,i) vertices (see Figure 6). For this polygonal graph three sides meet at each vertex. A planar version of Euler's polyhedral formula is applicable to this polygonal graph, provided we count the region external to the graph as a face. (For a proof see Ore [1963] p 99.)

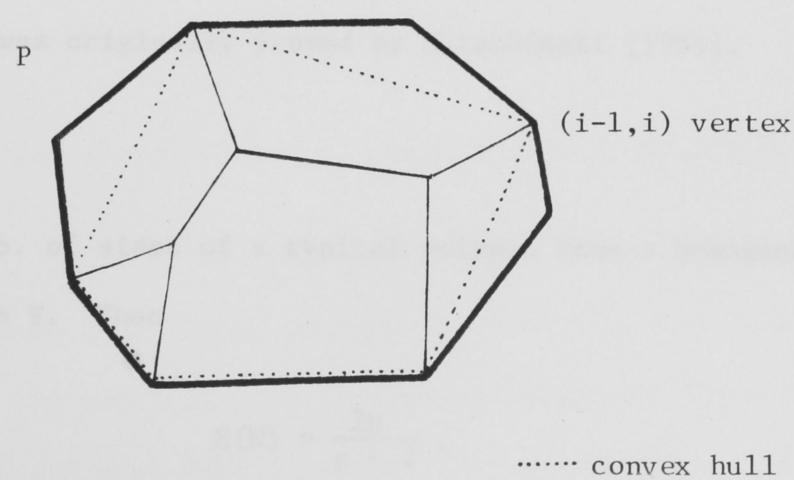

Figure 6

Assume that there are j (i - 2,i - 1) vertices in P and N sides on the convex hull. Applying Euler's formula to this figure we have $V_0 - V_1 + V_2 = 2$,

where V_0 = no. of vertices = j + N

V_1 = no. of sides = $\frac{3}{2}(j + N)$

$V_2 = N + 1$

and hence

$$N = j + 2 \text{ and the number of } \mathcal{V}_{i-1} \text{ sides} = V_1 = N = 2j + 1 .$$

To complete the lemma we need to show that j cannot exceed i - 2, or equivalently, that the number of cells which $\mathcal{V}_{i-1}$ partitions P into cannot exceed i. But each partitioning cell represents a region where one choice of (i - 1) particles from the set of P are the closest (i - 1). Hence there are a maximum of $\binom{i}{i-1} = i$ such cells.

Careful study of Figure 7, a computer-generated superposition of $\mathcal{V}_2$, $\mathcal{V}_3$ and $\mathcal{V}_4$ should illustrate Lemma 2 for the i = 4 case. $\mathcal{V}_4$ cells are partitioned by $\mathcal{V}_3$ into the topological types illustrated in Figure 8.

Before proving the main theorems of this section we need one more result which was originally proved by Matschinski [1954].

Lemma 3

Let N = no. of sides of a typical polygon from a homogeneous random tessellation Ψ. Then

$$E(N) = \frac{2\mu}{\mu - 2} ,$$

where μ = mean number of lines meeting at a typical vertex.

This is essentially a geometric result which follows from simple geometrical connections between the quantities involved in each mean.

Corollary $E(N) = 6$, for a V_n tessellation generated by a π_2 type process, $n = 1,2,..$, since for V_n three sides join at every vertex, and hence $\mu = 3$.

Theorem 1

Let A_n denote the area of a typical cell in a V_n tessellation generated by a general point process of type π_2.

Then

$$E(A_n) = [(2n - 1)\rho]^{-1}, \quad n = 1,2,3,$$

where ρ is the particle density for the π_2 process.

Proof

The proof for $n = 1$ is contained in the ergodic theory of section 1.2, where ρ, the particle density, is defined as

$$\underset{a.s.}{\lim}_{r\to\infty} \frac{N_r}{\pi r^2},$$

where N_r denotes the number of particles of π_2 in a circle radius r.

Lemma 3 shows that E (no. of sides) = 6 for V_n, $n = 1,2,3$. We note that since the particles are in general position, three sides meet at each vertex and each side is shared by just two cells. Using this information it is easy to sequentially obtain the densities listed in Table 1.

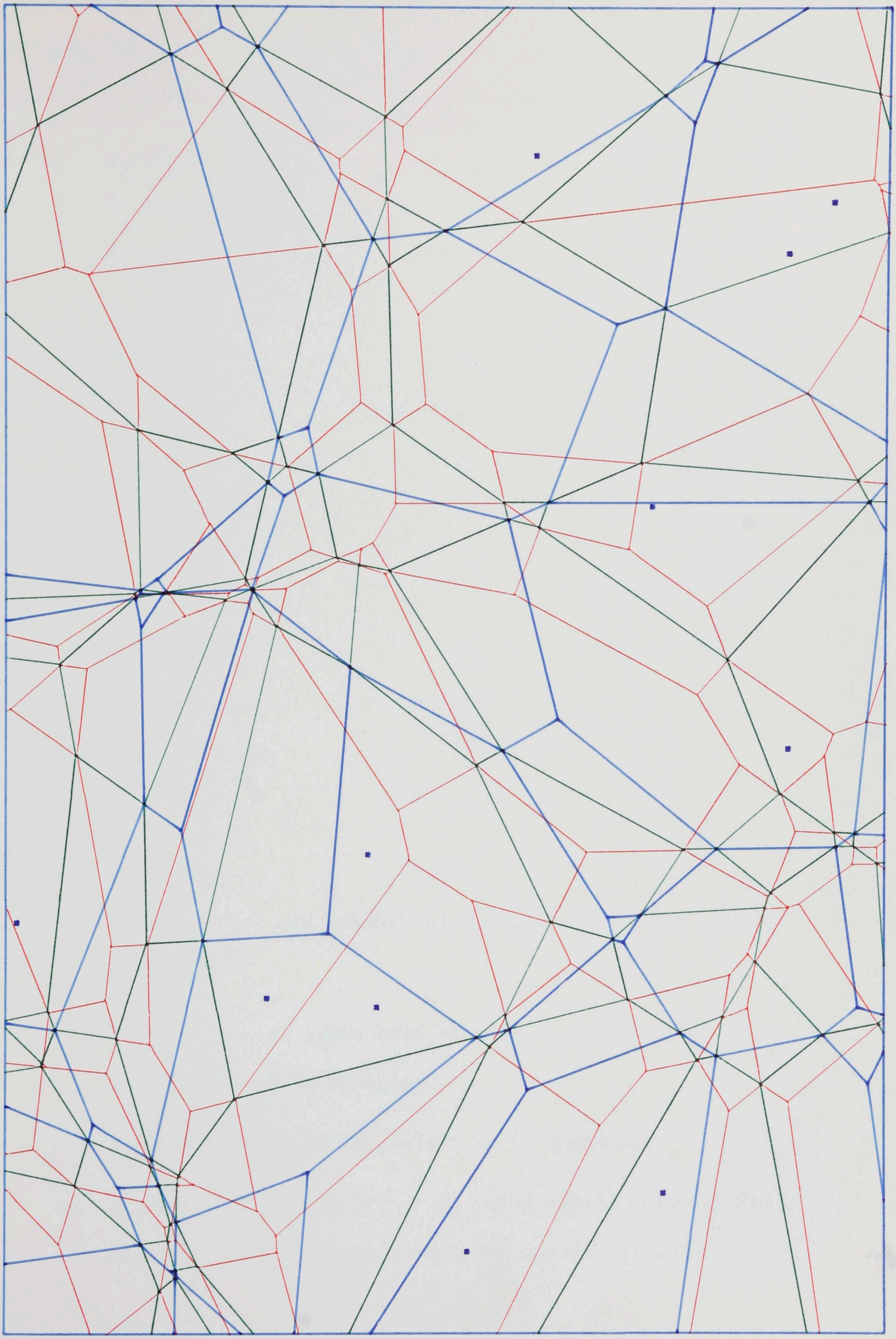

Figure 7. Superposition of V_2, V_3 and V_4 for a set of random particles.
V_2 shown in blue, V_3 in green, V_4 in red.

Table 1

Quantity	Density	Note
V_1 cells	ρ	
V_1 vertices	2ρ	
V_1 sides	3ρ	
V_2 cells	3ρ	(i)
V_2 vertices	6ρ	
V_2 sides	9ρ	
$\mathcal{L}_2(-,+)$ sides	6ρ	(ii)
$\mathcal{L}_2(+,+)$ sides	3ρ	
(1,2) vertices	2ρ	(iii)
(2,3) vertices	4ρ	
V_3 cells	5ρ	(iv)
V_3 vertices	10ρ	
(3,4) vertices	6ρ	

Notes on Table 1

(i) By Lemma 3.5, the density of V_2 cells equals the density of V_1 sides.

(ii) Since 3 $\mathcal{L}_2(-,+)$ sides meet at each V_1 vertex their density is 3 × density of V_1 vertices.

(iii) (1,2) vertices are equivalent to V_1 vertices.

(iv) By Lemma 1, the density of V_3 cells can be written as the density of (1,2) vertices and the density of $\mathcal{L}_2(+,+)$ sides.

Obviously from Table 1,

$$E(A_2) = \frac{1}{3\rho} \quad \text{and} \quad E(A_3) = \frac{1}{5\rho} .$$

This completes Theorem 1. In the next theorem we extend Theorem 1 to all n values, by utilizing Lemma 2.

Theorem 2

$$E(A_n) = [(2n - 1)\rho]^{-1} , \quad n = 4,5,6...$$

Proof

The proof is by induction. We first consider V_4 cells. Let $\sigma_4{}^i$ be the density of V_4 cells containing i (2,3) vertices, i = 0,1,2 (i ⩽ 2 by Lemma 2). (See Figure 8.)

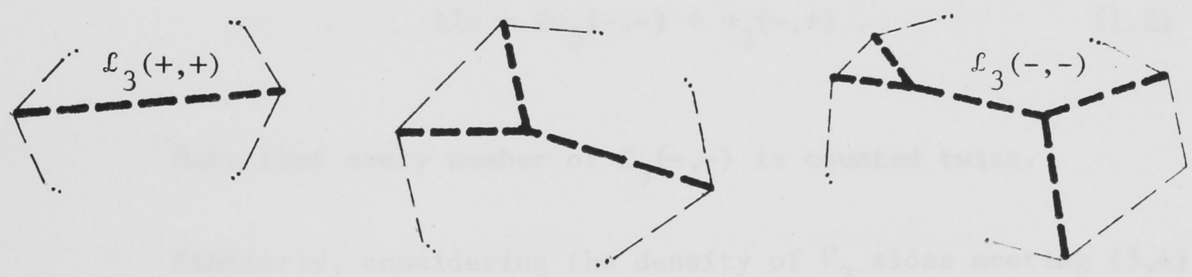

Figure 8

Since the density of (2,3) vertices is 4ρ from Table 1,

$$\sigma_4{}^1 + 2\sigma_4{}^2 = 4\rho .$$

Now V_3 sides are of three types $\mathcal{L}_3(-,-)$, one of which occurs in each (iii) type V_4 cell and nowhere else, $\mathcal{L}_3(+,+)$, one of which occurs in each (i) type V_4 cell and nowhere else, and $\mathcal{L}_3(-,+)$ (see Figure 8). We write $\sigma_j(\pm,\pm)$ for the density of $\mathcal{L}_j(\pm,\pm)$ sides. Hence

$$\left.\begin{aligned} \sigma_4{}^0 &= \sigma_3(+,+) \\ \sigma_4{}^2 &= \sigma_3(-,-) \end{aligned}\right\} \qquad (1.1)$$

So the total density of V_4 cells $\equiv \sigma_4$

$$= \sum_{i=0}^{2} \sigma_4{}^i$$

$$= \sigma_4{}^1 + 2\sigma_4{}^2 + [\sigma_3(+,+) - \sigma_3(-,-)]$$

$$= 4\rho + [\sigma_3(+,+) - \sigma_3(-,-)] \quad .$$

We now consider the density of V_3 sides which meet at (2,3) vertices. Since the density of (2,3) vertices is 4ρ from Table 1, and three V_3 sides join at each such vertex,

$$12\rho = 2\sigma_3(-,-) + \sigma_3(-,+) \quad . \tag{1.2}$$

Note that every member of $\mathcal{L}_3(-,-)$ is counted twice.

Similarly, considering the density of V_3 sides meeting (3,4) vertices, which have density 6ρ, we have

$$18 = \sigma_3(-,+) + 2\sigma_3(+,+) \quad . \tag{1.3}$$

Subtracting (1.3) - (1.2) gives

$$\sigma_3(+,+) - \sigma_3(-,-) = 3\rho \tag{1.4}$$

and hence

$$\sigma_4 = 7\rho$$

which verifies the theorem for n = 4.

For general n, we write σ_n for the density V_n cells, $\sigma(n,n + 1)$ for the density of $(n,n + 1)$ vertices, and $\sigma(n)$ for the density of V_n vertices.

Note from Table 1 that

$$\sigma(n, n + 1) = 2n\rho \tag{1.5}$$

holds for n = 1,2,3.

Now assume that the theorem holds for all n, with $1 \leq n \leq N - 1$, and that (1.5) holds for all n with $1 \leq n \leq N - 2$. (This has been established for N = 5.)

By this assumption, $\sigma_{N-1} = (2N - 3)\rho$, so $\sigma(N - 1) = 2(2N - 3)\rho$. Also by assumption, $\sigma(N - 2,N - 1) = 2(N - 2)\rho$, so

$$\sigma(N - 1,N) = [4N - 6 - (2N - 4)]\rho = 2(N - 1)\rho$$

So (1.5) holds for n = N - 1.

Let $\sigma_n^{\ i}$ denote the density of V_n cells containing i (n - 2,n - 1) vertices, $0 \leq i \leq n - 2$ (by lemma 2). Then

$$\sum_{i=0}^{N-2} i\sigma_N^{\ i} = \sigma(N - 2,N - 1) = 2(N - 2)\rho \ . \tag{1.6}$$

Using lemma 2 we can construct $V_{N-1,N}$ (see Figure 9). Again we have a one-to-one correspondence between $V_N^{\ 0}$ cells, containing 0 (N - 2,N - 1) vertices, and $\mathcal{L}_{N-1}(+,+)$ sides. Note that in each $V_N^{\ i}$ cell there are i - 1 $\mathcal{L}_{N-1}(-,-)$ sides, i = 1,2,...N-2.

Hence

$$\sigma_N^{\ 0} = \sigma_{N-1}(+,+) \tag{1.7}$$

$$\sum_{i=1}^{N-2} (i - 1)\sigma_N^{\ i} = \sigma_{N-1}(-,-) \tag{1.8}$$

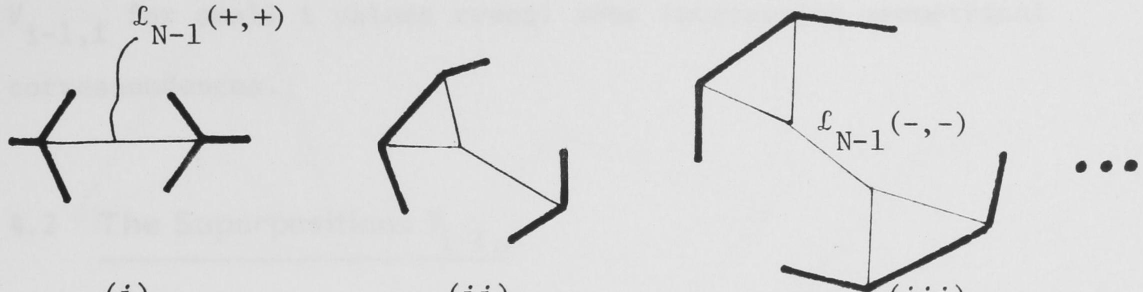

(i) (ii) (iii)

Figure 9

Now consider the density of V_N sides which meet $(N - 2, N - 1)$ vertices. By assumption, these vertices have density $2(N - 2)\rho$, so

$$6(N - 2)\rho = 2\sigma_{N-1}(-,-) + \sigma_{N-1}(-,+) . \tag{1.9}$$

The same argument applied to $(N - 1, N)$ vertices yields

$$6(N - 1)\rho = \sigma_{N-1}(-,+) + 2\sigma_{N-1}(+,+) \tag{1.10}$$

and subtraction yields

$$\sigma_{N-1}(+,+) - \sigma_{N-1}(-,-) = 3\rho . \tag{1.11}$$

Combining (1.6), (1.8) and (1.11) gives

$$\begin{aligned}
\sigma_N &= \sum_{i=0}^{N-2} \sigma_N^i \\
&= \sigma_N^0 + \sum_{i=0}^{N-2} i\sigma_N^i - \sum_{i=1}^{N-2} (i - 1)\sigma_N^i \\
&= 2(N - 2)\rho + [\sigma_{N-1}(+,+) - \sigma_{N-1}(-,-)] \\
&= (2N - 1)\rho
\end{aligned}$$

which completes the inductive proof.

In the next section a more careful look at the superpositions $V_{i-1,i}$ for small i values reveal some interesting geometrical correspondences.

4.2 The Superpositions $V_{i-1,i}$

We can analyse the superposition $V_{i-1,i}$ as a partitioning of V_i cells (as was done in Lemma 2) or as a partitioning of V_{i-1} cells. The nature of the partitioning is considerably different in the two cases. We illustrate this by considering $V_{i-1,i}$ for i = 2,3,4.

(i) $V_{1,2}$

Viewed as a partition of V_2 cells, this tessellation contains only one sort of cell - see Figure 1 and Figure 10.

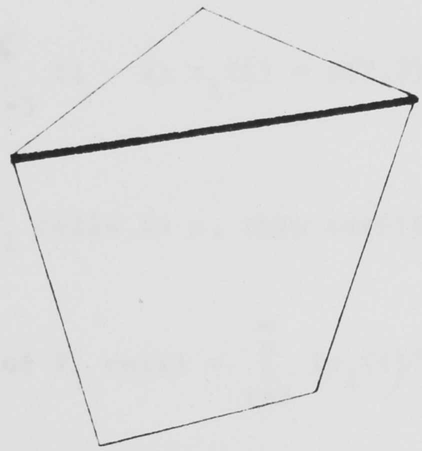

Figure 10

Viewed, however, as a partition of V_1 cells, study of Figure 1 shows that the cell types are as listed in Figure 11 for i-gons with i small.

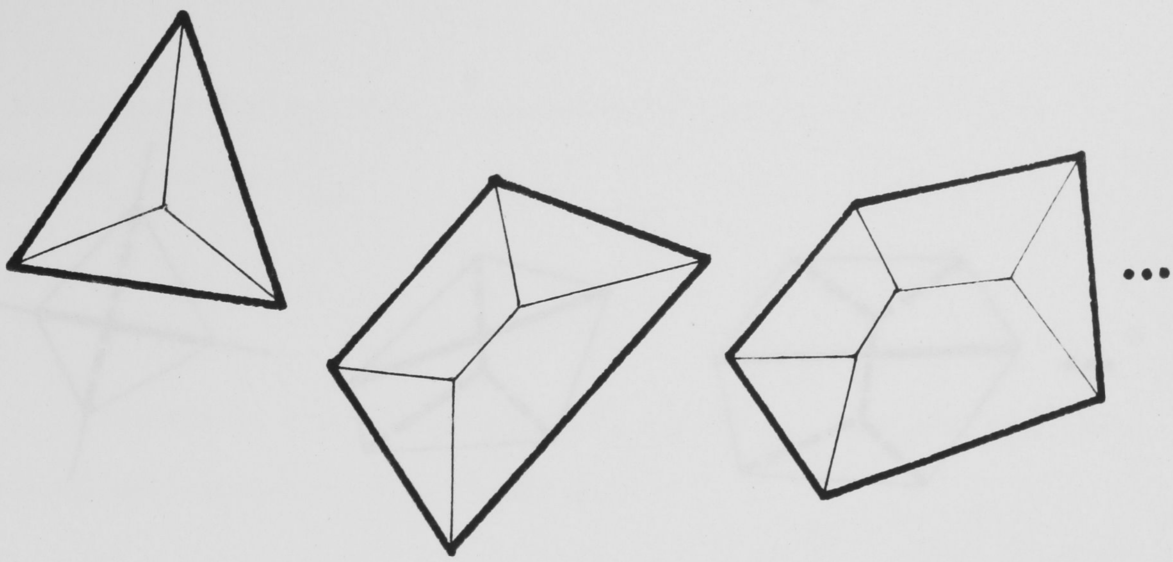

Figure 11

In fact V_2 divides a V_1 i-gon into i convex polygons and each V_1 i-gon contains i $\mathcal{L}_2(+,+)$ sides, (i - 3) $\mathcal{L}_2(+,+)$ sides and (i - 2) (2,3) vertices. Write $\sigma_N(i)$ for the density of i-gons in V_n. Then

$$\sum_{i=3}^{\infty} (i - 2)\, \sigma_1(i) = \sigma(2,3) = 4\rho \quad .$$

Since the density of V_1 cells is ρ, this verifies that

$$E(\text{no of sides of } V_1 \text{ cell}) = \sum_{i=3}^{\infty} i\sigma_1(i) \Big/ \sum_{i=3}^{\infty} \sigma_1(i) = \frac{6\rho}{\rho} = 6 \; .$$

(ii) $V_{2,3}$

Viewed as a partitioning of V_3 cells, $V_{2,3}$ contains the two sorts of cell illustrated in Figure 4.

Viewed as a partition of V_2 cells, study of Figure 1 shows that the cell types are as listed in Figure 12.

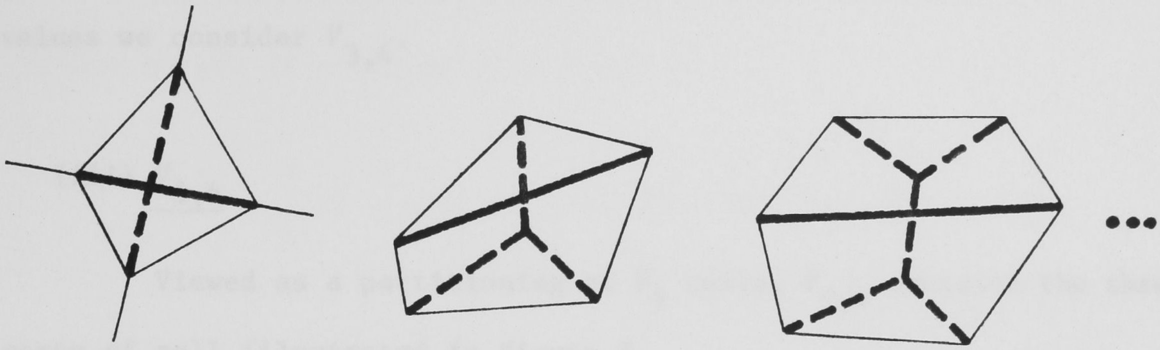

Figure 12

In Figure 12 we have included, for clarification purposes, the single V_1 side which is contained in every V_2 cell. This makes two of the V_2 cell's vertices (1,2) vertices, and the rest must be (2,3) vertices. Note that each V_2 i-gon contains (i - 5) $\mathcal{L}_3(+,+)$ sides (i ⩾ 5) and (i - 4) (3,4) vertices (i ⩾ 4). Hence

$$\sum_4^\infty (i - 4)\sigma_2(i) = \sigma(3,4) = 6\rho$$

and since $\sigma_2 = \sum_4^\infty \sigma_2(i) = 3\rho$,

$$E(\text{no of sides of } V_2 \text{ cell}) = \sum_4^\infty i\sigma_2(i) \Big/ \sum_4^\infty \sigma_2(i) = \frac{18\rho}{3\rho} = 6 \quad ,$$

as expected.

More important, however, is the one-to-one correspondence between V_2 quadrilaterals and $\mathcal{L}_3(-,-)$ sides which follows directly from the cell types shown in Figure 12, for the only V_2 cell which contains an $\mathcal{L}_3(-,-)$ side is the quadrilateral. Hence we have the interesting formula

$$\sigma_2(4) = \sigma_3(-,-) \quad . \tag{2.1}$$

To investigate whether this correspondence carries on for higher n values we consider $V_{3,4}$.

(iii) $\underline{V_{3,4}}$

Viewed as a partitioning of V_4 cells, $V_{3,4}$ contains the three sorts of cell illustrated in Figure 8.

Viewed as a partitioning of V_3 cells, Figure 7 shows that the cell types are as listed in Figure 13. In Figure 13 the V_2 segments are also included.

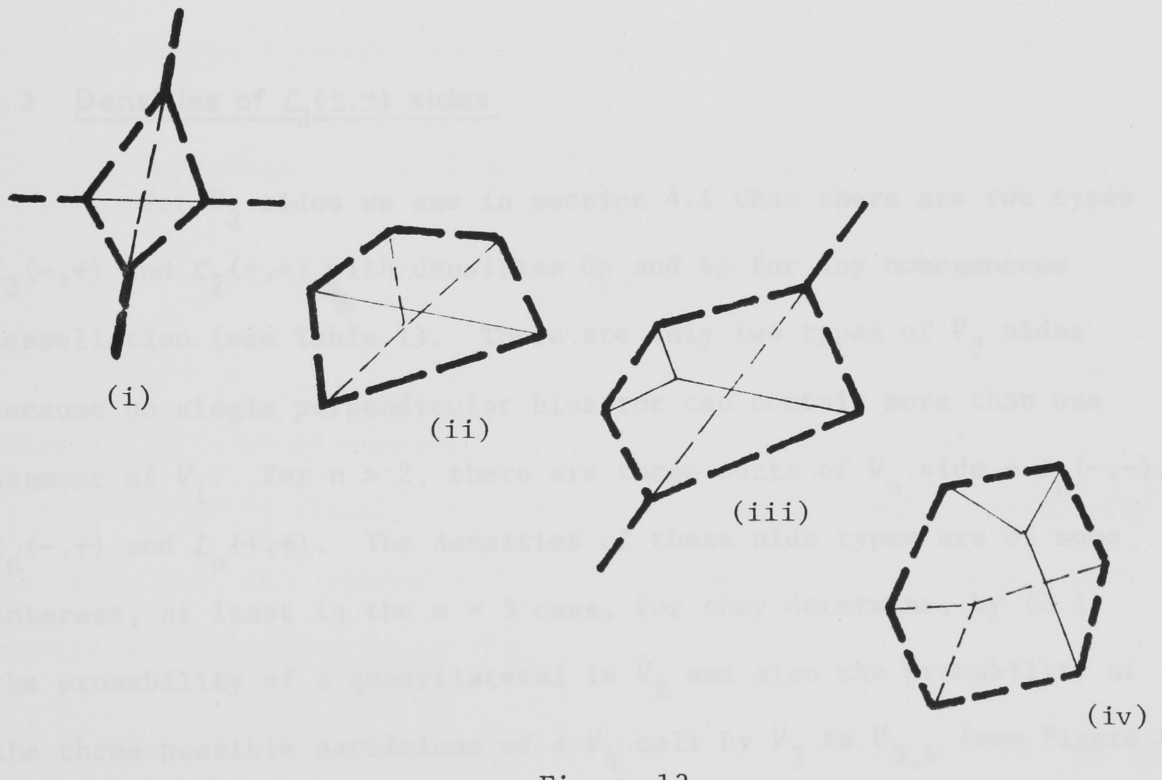

Figure 13

Note that Figure 13 simply gives illustrations of possible cell partitions for V_3 cells with a small number of sides. For example the V_2 side in diagram (ii) could cut the V_4 sides just once, instead of twice.

However because of the two possibilities for V_2 sides inside

V_3 cells we lose any correspondence between $\mathcal{L}_4(-,-)$ sides and quadrilaterals in V_3 - see (iii) in Figure 13.

Also totalling the (1,2) vertices and (4,5) vertices in each V_2 i-gon we get (i - 4), so

$$\sum_4^\infty (i - 4)\sigma_3(i) = \sigma(1,2) + \sigma(4,5) = 10\rho$$

and we can again verify that

$$E(\text{no of sides of } V_3 \text{ cell}) = \sum_4^\infty i\sigma_3{}^i \sum_4^\infty \sigma_3{}^i$$

$$= 30/5 = 6 \quad .$$

4.3 Densities of $\mathcal{L}_3(\pm,\pm)$ sides

For V_2 sides we saw in section 4.1 that there are two types $\mathcal{L}_2(-,+)$ and $\mathcal{L}_2(+,+)$ with densities 6ρ and 4ρ for any homogeneous tessellation (see Table 1). There are only two types of V_2 sides because no single perpendicular bisector can contain more than one segment of V_1. For $n > 2$, there are three sorts of V_n side - $\mathcal{L}_n(-,-)$, $\mathcal{L}_n(-,+)$ and $\mathcal{L}_n(+,+)$. The densities of these side types are of some interest, at least in the $n = 3$ case, for they determine, by (2.1) the probability of a quadrilateral in V_2 and also the probability of the three possible partitions of a V_4 cell by V_3 in $V_{3,4}$ (see Figure 8).

In Theorem 2 we obtained two equations (1.9), (1.10) involving the required side densities i.e.

$$2\sigma_{n-1}(-,-) + \sigma_{n-1}(-,+) = 6(n - 2)\rho \qquad (3.1)$$

$$\sigma_{n-1}(-,+) + 2\sigma_{n-1}(+,+) = 6(n - 1)\rho \qquad (3.2)$$

Adding (3.1) and (3.2) gives $2\{3[2(n-1)-1]\rho\}$, twice the density of V_{n-1} sides which follows also from the known density of V_{n-1} cells (Theorem 2). However the author has been unable to derive another independent equation for these densities for the general homogeneous case. Instead we assume a Poisson process as the generating process and calculate $\sigma_3(-,-)$ using the stochastic constructions in section 3.5.

We choose a random V_3 side, L_3, in the following manner.

(i) choose a (2,3) vertex with probability 2/5
or a (3,4) vertex with probability 3/5

and then

(ii) choose a random side of V_3 meeting this vertex.

We define $\quad p_3(\pm,\pm) \equiv P(L_3 \in \mathcal{L}_3(\pm,\pm))$

$$= \lim_{|X|\to\infty} \frac{N_{\pm\pm}(X)}{N_3(X)}$$

where $N_{\pm\pm}(X)$ = no of members of $\mathcal{L}_3(\pm,\pm)$ contained in X and $N_3(X)$ = no. of V_3 sides in X, i.e. $p_3(\pm,\pm)$ is the ergodic probability that a V_3 side is a member of $\mathcal{L}_3(\pm,\pm)$. Note that $\sigma_3(\pm,\pm) = p_3(\pm,\pm)\times$ density of V_3 sides $= 15p_3(\pm,\pm)\rho$.

Now, conditioning on the vertex type ν, chosen in (i), we have

$$p_3(-,-) = P(L_3 \in \mathcal{L}_3(-,-)\,|\,\nu = (2,3)\text{ vertex})P(\nu = (2,3)\text{ vertex})$$
$$+ P(L_3 \in \mathcal{L}_3(-,-)\,|\,\nu = (3,4)\text{ vertex})P(\nu = (3,4)\text{ vertex})$$
$$= \frac{2}{5}\cdot P(L_3 \in \mathcal{L}_3(-,-)\,|\,\nu = (2,3)\text{ vertex})$$
$$\equiv \frac{2}{5}\, P(232|23) \quad \text{say} \quad . \tag{3.3}$$

Hence it suffices to calculate $P(232|23)$. We use the ergodic structure of a (2,3) vertex specified in Lemma 3.10. Referring to Figure 14, we know that

R = radius of vertex $\sim \Gamma_2(6,\pi\rho)$ with

p.d.f. $g(R) = \pi^3\rho^3R^5\exp\{-\rho\pi R^2\} \quad 0 < R < \infty$

α has same distribution as a random angle from a Delaunay triangle (since $\alpha = \beta$ in Figure 14) with p.d.f.

$f(\alpha) = \frac{4}{3\pi}\sin\alpha[(\pi - \alpha)\cos\alpha + \sin\alpha], \; 0 < \alpha < \pi,$

obtained from density (3.5.5)

and ω, the filling particle, is uniformly distributed on the vertex.

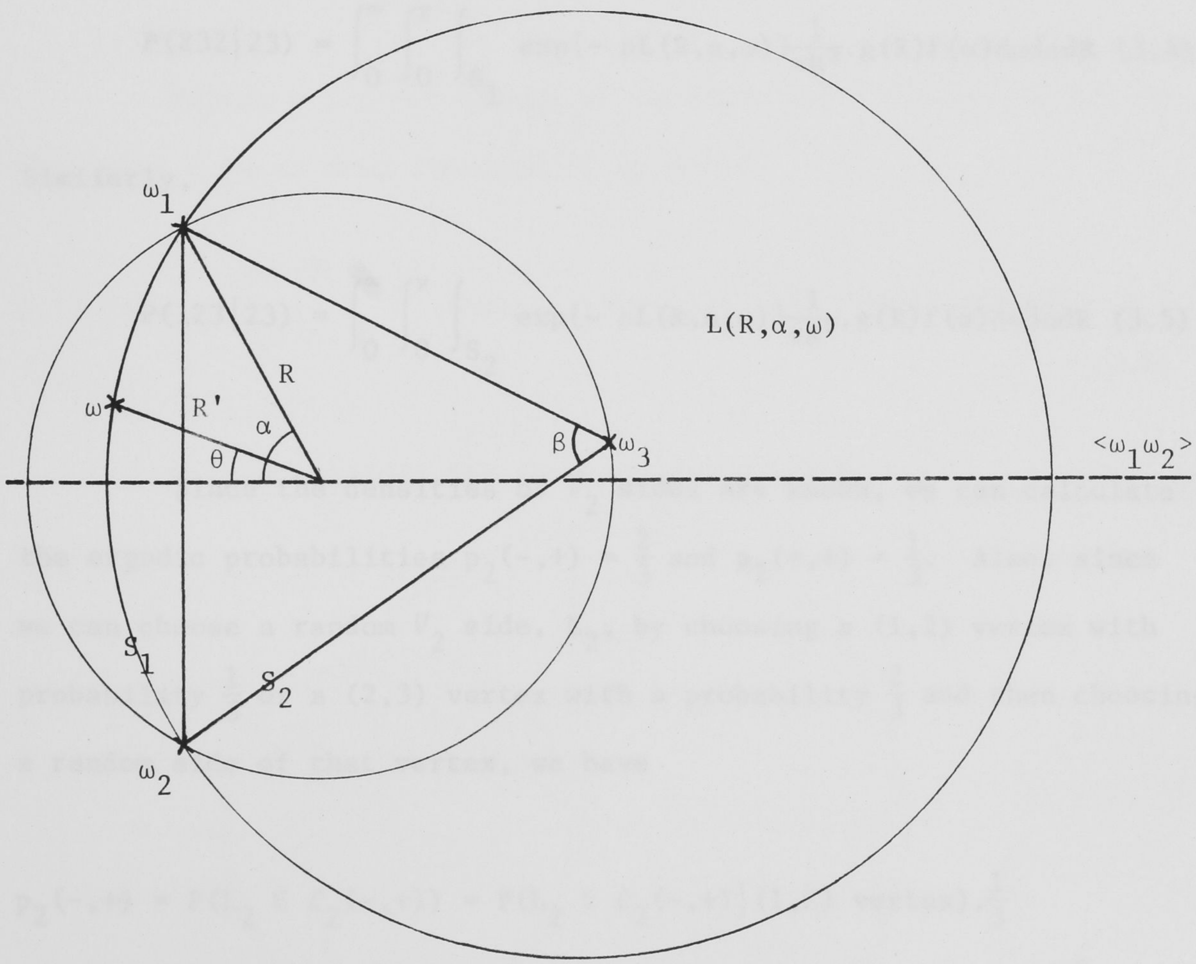

$S_1[S_2]$ is region in vertex circumdisc to left [right] of line joining ω_1 and ω_2.

Figure 14

Note that R and α are independent, and that the third circumferential particle lies outside the 2α arc between the randomly chosen pair ω_1, ω_2 whose perpendicular bisector $<\omega_1\omega_2>$ contains the $\mathcal{V}_3$ side of interest.

Consider moving along $<\omega_1\omega_2>$, along the $\mathcal{V}_3$ segment. We meet a $\mathcal{V}_2$ segment iff ω lies in region S_1 and $L(R,\alpha,\omega)$ is empty, where $L(R,\alpha,\omega)$ = area of $Q(\omega_1,\omega_2,\omega)$ outside of the vertex.

Hence

$$P(232|23,R,\alpha,\omega) = \begin{cases} 0 & \omega \in S_2 \\ \exp\{-\rho L(R,\alpha,\omega)\} & \omega \in S_1 \end{cases}$$

and

$$P(232|23) = \int_0^\infty \int_0^\pi \int_{S_1} \exp\{-\rho L(R,\alpha,\omega)\} \frac{1}{\pi R^2} . g(R) f(\alpha) d\omega d\alpha dR \quad (3.4)$$

Similarly,

$$P(123|23) = \int_0^\infty \int_0^\pi \int_{S_2} \exp\{-\rho L(R,\alpha,\omega)\} \frac{1}{\pi R^2} . g(R) f(\alpha) d\omega d\alpha dR \quad (3.5)$$

Since the densities of $\mathcal{V}_2$ sides are known, we can calculate the ergodic probabilities $p_2(-,+) = \frac{2}{3}$ and $p_2(+,+) = \frac{1}{3}$. Also, since we can choose a random $\mathcal{V}_2$ side, L_2, by choosing a (1,2) vertex with probability $\frac{1}{3}$ or a (2,3) vertex with a probability $\frac{2}{3}$ and then choosing a random side of that vertex, we have

$$p_2(-,+) = P(L_2 \in \mathcal{L}_2(-,+)) = P(L_2 \in \mathcal{L}_2(-,+)|(1,2) \text{ vertex}).\frac{1}{3}$$
$$+ P(L_2 \in \mathcal{L}_2(-,+)|2,3 \text{ vertex}).\frac{2}{3}$$

$$p_2(+,+) = \frac{2}{3} P(L_2 \in \mathcal{L}_2(+,+)|2,3 \text{ vertex}) .$$

Solving for the conditional probability gives

$$P(L_2 \in \mathcal{L}_2(-,+) \mid (2,3) \text{ vertex}) = P(123|23) = \tfrac{1}{2} . \qquad (3.6)$$

Note that this does not give us the value of $P(232|23)$, since the integrals in (3.4) and (3.5) are unequal due to the lack of symmetry of $f(\alpha)$ about $\pi/2$.

Utilizing (3.4) - (3.6), and parametrizing ω by polar co-ordinates (R',θ) $0 < R' < R$, $-\pi < \theta < \pi$, we can obtain

$$P(232|23) = \int_0^\infty \int_0^\pi \int_{-\pi}^{\pi} \int_0^R \exp\{-\rho L(R,\alpha,R',\theta)\} \frac{1}{\pi R^2} g(R) f(\alpha) R' dR' d\theta d\alpha dR - \tfrac{1}{2}.$$

Making a further change of variable $u = R'/R$, and using the fact that L is an even function of θ, gives

$$P(232|23) = 2 \int_0^\infty \int_0^\pi \int_0^\pi \int_0^1 \exp\{-\rho L(R,\alpha,u,\theta)\} \frac{1}{\pi} g(R) f(\alpha) u . du d\theta d\alpha dR - \tfrac{1}{2} . \qquad (3.7)$$

We now consider the functional form of L.

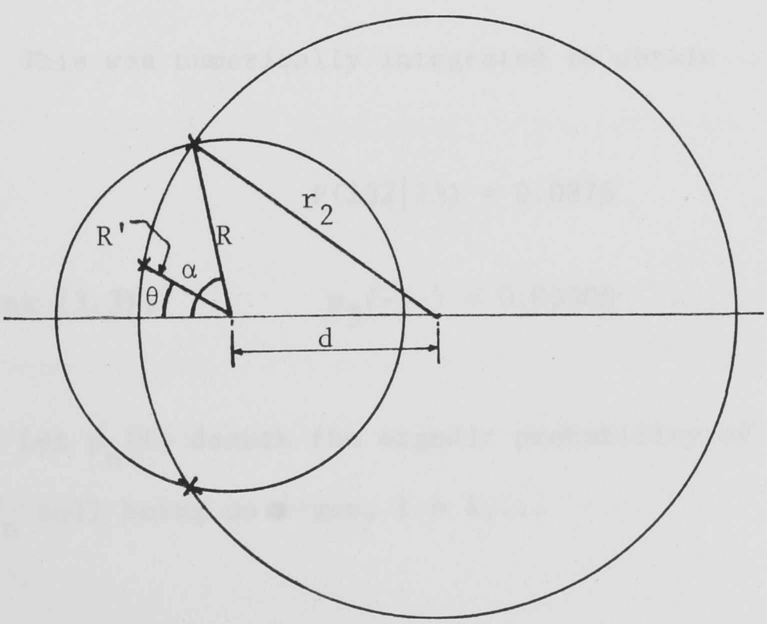

Figure 15

From Figure 15,

$$d = \frac{1 - u^2}{2(\cos\alpha - u\cos\theta)} . R = d(u,\alpha,\theta)R$$

$$r_2 = R.[\sin^2\alpha + (\cos\alpha - d(u,\alpha,\theta))^2]^{\frac{1}{2}} = r_2(u,\alpha,\theta)R \quad .$$

No matter where (R',θ) is in the vertex, $(S_1$ or $S_2)$,

$$L(R,\alpha,u,\theta) = \pi r_2{}^2 - A(R,r_2,|d|)$$

where $A(x,y,d)$ = area of intersection of two circles radii

x and y separated by distance d.

$$L(R,\alpha,u,\theta) = R^2\{\pi r_2{}^2(u,\alpha,\theta) - A(1,r_2(u,\alpha,\theta),|d(u,\alpha,\theta)|)\}$$

$$\equiv h(u,\alpha,\theta)R^2 \quad . \tag{3.8}$$

Substituting (3.8) into (3.7) and integrating out R gives

$$P(232|23) = 2\int_0^{\pi}\int_0^{\pi}\int_0^1 \frac{\pi^2 uf(\alpha)}{(\pi + h(u,\alpha,\theta))^3}\, du\,d\theta\,d\alpha - \tfrac{1}{2} \; .$$

This was numerically integrated to obtain

$$P(232|23) = 0.0876$$

and, using (3.3), $\quad p_3(-,-) = 0.03505 \quad .$ (3.9)

Let $p_n(i)$ denote the ergodic probability of a uniform random V_n cell being an i-gon, i = 4,...

Theorem 3

For a V_2 tessellation with generating process $\mathbb{P}$,

$$p_2(4) = 0.175 \quad .$$

Proof

From (2.1), (3.9) and Table 1

$$p_2(4) = \frac{\sigma_2(4)}{\sigma_2} = \frac{\sigma_3(-,-)}{\sigma(V_3 \text{ sides})} \frac{\sigma(V_3 \text{ sides})}{\sigma_2}$$

$$= p_3(-,-).\frac{15}{3}$$

$$= 2P(232|23)$$

$$= 0.175 \quad .$$

Thus 17.5% of V_2 cells are quadrilaterals. This compares with 1.1% triangles and 10.7% quadrilaterals for V_1. (Simulation estimates by Hinde and Miles [1980].)

From (3.1), (3.2) and (3.9) we can deduce the ergodic probabilities $p_3(\pm,\pm)$ that a uniform random V_3 side is a member of $\mathcal{L}_3(\pm,\pm)$, which are shown, together with the different side densities in Table 2.

Also using (1.1), and Table 2, we can deduce the densities $\sigma_4{}^i$, and thus the ergodic probabilities $p_4{}^i$ that a uniform random V_4 cell contains i (2,3) vertices - i.e. the probabilities of the three possible partitionings of a V_4 cell shown in Figure 8. These are shown in Table 3.

Table 2

Side type	$\mathcal{L}_3(-,-)$	$\mathcal{L}_3(-,+)$	$\mathcal{L}_3(+,+)$
density	$0.526\ \rho$	$10.95\ \rho$	$3.524\ \rho$
probability	0.035	0.73	0.235

Table 3

i	0	1	2
$\sigma_4^{\,i}$	$3.524\ \rho$	$0.95\ \rho$	$0.526\ \rho$
$p_4^{\,i}$	0.705	0.105	0.19

From Table 3 we see that 70.5% of V_4 cells will have just two n^- vertices, 10.5% three and 19.5% five n^- vertices.

In section 4.6 use is also made of (3.9) to calculate the probabilities of the three types of perpendicular bisector under the condition that $<\omega_1\omega_2 \to 2>$ i.e. that at least one V_2 segment appears on $<\omega_1\omega_2>$.

Obviously an expression similar to that for $P(232|23)$ can be written down for general n, although it is considerably more complex. However from (3.1) and (3.2),

$$\sigma_n(+,+) - \sigma_n(-,-) = 3\rho$$

and hence

$$p_n(+,+) - p_n(-,-) = \frac{1}{(2n-1)} .$$

Thus $p_n(+,+)$ and $p_n(-,-)$ are asymptotically equal.

For general homogeneous processes the best we can do is give the upper bound $p_2(4) \leqslant \frac{2}{3}$ which follows from the first equation in Theorem 2, (1.1) and noting that $\sigma_4^{\,1} > 0$.

4.4 Some Moment Expressions for Voronoi and Generalized Voronoi Cells

A number of different expressions can be written down for the second moment of the area of V_n cells, for both the n = 1 and n > 1 cases when the generating process is $\mathbb{P}$. The relationships between these expressions often reflect more fundamental geometrical identities, such as those in section 1.3.

Voronoi Tessellation

The situation is simplified for n = 1 since, as we have seen in section 2.3, we generate a typical V_1 polygon by placing a particle at the origin and surrounding it by a Poisson process. If A_1 denotes the area of a typical cell P, then

$$A_1 = \int I_1(\underline{x})d\underline{x} \quad , \tag{4.1}$$

where
$$I(\underline{x}) = \begin{cases} 1 & \underline{x} \in P \\ 0 & \text{otherwise} \end{cases} .$$

From (4.1) we quickly obtain $E(A_1) = \rho^{-1}$. Extending this technique to the second moment,

$$\begin{aligned} E(A_1{}^2) &= E \iint I(\underline{x})I(\underline{y})d\underline{x}d\underline{y} \\ &= \iint P(\underline{x} \text{ and } \underline{y} \in P)d\underline{x}d\underline{y} \\ &= \iint \exp\{-\rho A(\underline{x},\underline{y})\}d\underline{x}d\underline{y} \quad , \end{aligned}$$

where $A(\underline{x},\underline{y})$ represents the area which must be empty for both $\underline{x}$ and $\underline{y}$ to be in the V_1 cells of the origin particle (see Figure 16).

Changing to polar co-ordinates and using (1.3.3),

$$E(A_1{}^2) = 4\pi \int_0^{\pi} \int_0^{\infty} \int_0^{\infty} \exp\{-\rho A(r_1 r_2 \psi) r_1 r_2 dr_1 dr_2 d\psi\} \ , \quad (4.2)$$

where ψ is the angular separation of the points. Putting $r_1 = ur_2$ yields $A(r_1 r_2 \psi) = A(u,\psi) r_2{}^2$, and integrating out r_2 gives

$$E(A_1{}^2) = \frac{2\pi}{\rho^2} \int_0^{\pi} \int_0^{\infty} \frac{u}{A(u,\psi)^2} \, du d\psi \quad (4.3)$$

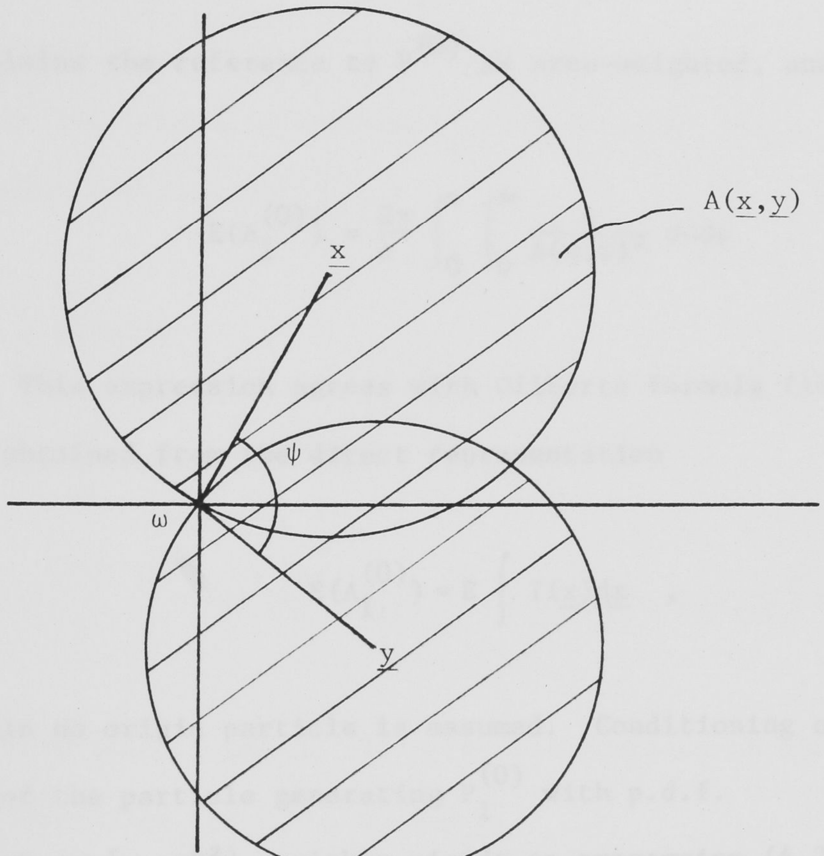

Figure 16

We now consider an ordinary realization of $\mathbb{P}$ over the plane with no assumption of a particle at the origin and let $A_1^{(0)}$ denote the area of the V_1 cell $P^{(0)}$ which happens to contain the origin. This cell is no longer a typical cell - in fact it is area-weighted.

Let $f(A)$ denote the p.d.f. of A_1 and $g(A)$ the p.d.f. of $A_1^{(0)}$.

Heuristically,

$$g(a)da = P(\text{typical } P \text{ has area } (a,a+da) \text{ and is hit by random pt})$$

$$= P(\text{hit by random pt} \mid \text{area } a)P(P \text{ has area } a)$$

$$\propto af(a)da\,.$$

Hence
$$g(a) = \frac{af(a)}{E(A_1)}\,,\quad E(A_1^{(0)}) = \frac{E(A_1{}^2)}{E(A_1)} \tag{4.4}$$

(4.4) explains the reference to $P^{(0)}$ as area-weighted, and with (4.3) yields

$$E(A_1^{(0)}) = \frac{2\pi}{\rho}\int_0^{\pi}\int_0^{\infty}\frac{u}{A(u,\psi)^2}\,du\,d\psi\quad . \tag{4.5}$$

This expression agrees with Gilberts formula (14) [1962], which he obtained from the direct representation

$$E(A_1^{(0)}) = E\int I(\underline{x})d\underline{x}\quad ,$$

where again no origin particle is assumed. Conditioning on the radial distance of the particle generating $P_1^{(0)}$ with p.d.f. $h(R) = 2\pi\rho R\exp\{-\rho\pi R^2\}$, quickly yields an expression (4.2) with an additional ρ factor due to (4.4), since $E(A_1) = \rho^{-1}$.

Numerical integration (Gilbert [1962]) of (4.3) yields

$$E(A_1{}^2) = 1.28\,\rho^{-2}\quad ,\qquad \mathrm{Var}(A_1) = 0.28\,\rho^{-2}$$

which agree with independent methods used in section 4.5.

<u>Extension of Methods to V_n n > 1</u>

The immediate difficulty is the generation of a typical V_n cell - there is no convenient method analogous to the V_1 construction. However the area-weighted V_n gons containing the origin can be investigated. Let $P_2^{(0)}$ be the V_2 cell which contains the origin, with area $A_2^{(0)}$. (4.4) and Theorem 1 give

$$E(A_2^{(0)}) = 3\rho E(A_2{}^2) \tag{4.6}$$

where A_2 is the area of a typical V_2 cell ($E(A_2) = {}^1/_{3\rho}$). If $I(\underline{x})$ is the indicator function of $P_2^{(0)}$,

$$\begin{aligned} E(A_2^{(0)}) &= \int EI(\underline{x})d\underline{x} \\ &= 2\pi \int_0^\infty rP(r \in P_2^{(0)})dr \\ &= 2\pi \int_0^\infty \int .. \int rP(r \in P_2^{(0)} | R_1, \theta_1, R_2, \theta_2) f(R_1) g(R_2) \left(\frac{1}{2\pi}\right)^2 dR_1 dR_2 d\theta_1 d\theta_2 dr, \end{aligned}$$

where we have conditioned on the polar co-ordinates of the two proximity particles for $P_2^{(0)}$, ω_1 and ω_2.

Since the point r is in $P_2^{(0)}$ iff ω_1 and ω_2 are its two closest particles, $P(r \in P_2^{(0)} | R_1 \theta_1 R_2 \theta_2) = \exp\{-\rho A(r, R_1, \theta_1, R_2, \theta_2)\}$, where A is the area outside $Q(\underline{0}, R_1)$ but inside a circle, centered at r, with radius to the furthest of ω_1 and ω_2 (see Figure 17). Similar expressions can be obtained for higher n values, however a more natural approach to this problem, which also yields information about the transect distributions, is used to do the calculations (see section 4.5).

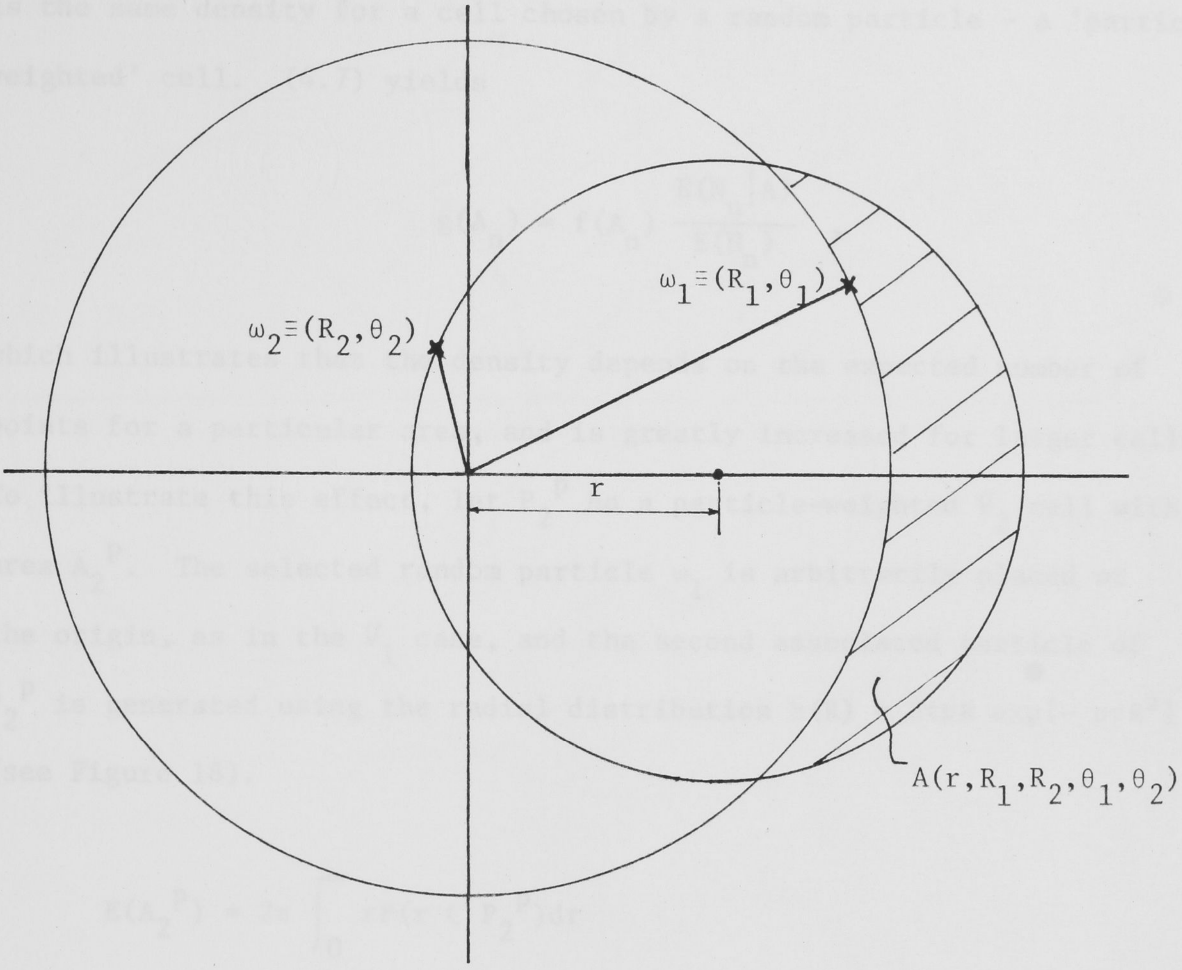

Figure 17

We can utilize the Voronoi theory in one sense in the generalized Voronoi case, to analyse the V_n cell distribution when we choose a V_n cell by choosing a random particle. Since every V_1 cell contains exactly one particle, we know that the cell containing a random particle is a typical cell. For $n > 1$, a V_n cell can contain $0,1,2,\ldots n$ particles. The distribution of N_n, the number of particles in a typical V_n cell, is investigated in section 3.7.

If we choose a V_n cell by choosing a random particle, the probability of any cell being chosen is proportional to the number of particles it contains. Hence

$$g(N_n, A_n) \propto N_n f(N_n, A_n) \ , \qquad (4.7)$$

where f is the joint density of N_n and A_n for a typical cell, and g is the same density for a cell chosen by a random particle - a 'particle weighted' cell. (4.7) yields

$$g(A_n) = f(A_n) \frac{E(N_n|A)}{E(N_n)} ,$$

which illustrates that the density depends on the expected number of points for a particular area, and is greatly increased for larger cells. To illustrate this effect, let P_2^P be a particle-weighted V_2 cell with area A_2^P. The selected random particle ω_1 is arbitrarily placed at the origin, as in the V_1 case, and the second associated particle of P_2^P is generated using the radial distribution $h(R) = 2\pi\rho R \exp\{-\rho\pi R^2\}$ (see Figure 18).

$$E(A_2^P) = 2\pi \int_0^\infty rP(r \in P_2^P)dr$$

$$= 2\pi \int_0^\infty r \int_0^\infty \int_0^{2\pi} P(r \in P_2^P|R,\theta)h(R) \frac{1}{2\pi} d\theta dRdr$$

$$= 2\pi \int_0^\infty \int_0^{2\pi} \int_0^\infty r\exp\{-\rho A(r,R,\theta)\}\rho R\exp\{-\rho\pi R^2\}dRd\theta dr ,$$

where $A(r,R,\theta)$ is the area in a circle, centre r, radius to the furthest of ω_1, ω_2, excluding the area in $Q(\underline{0},R)$ (see Figure 18). This excluded area is accounted for by the exponential term in h(R). Putting R = ur, and integrating out r, gives

$$E(A_2^P) = \frac{2\pi}{\rho} \int_0^\infty \int_0^\pi \frac{u}{A(u,\theta)^2} d\theta du , \qquad (4.7)$$

which is exactly analogous to (4.5), the expression for the mean area of an area-weighted V_1 gon, with a different interpretation for $A(u,\theta)$. In this case $A(u,\theta)$ = total area of $Q(\underline{0},u)$ and a circle centre (1,0)

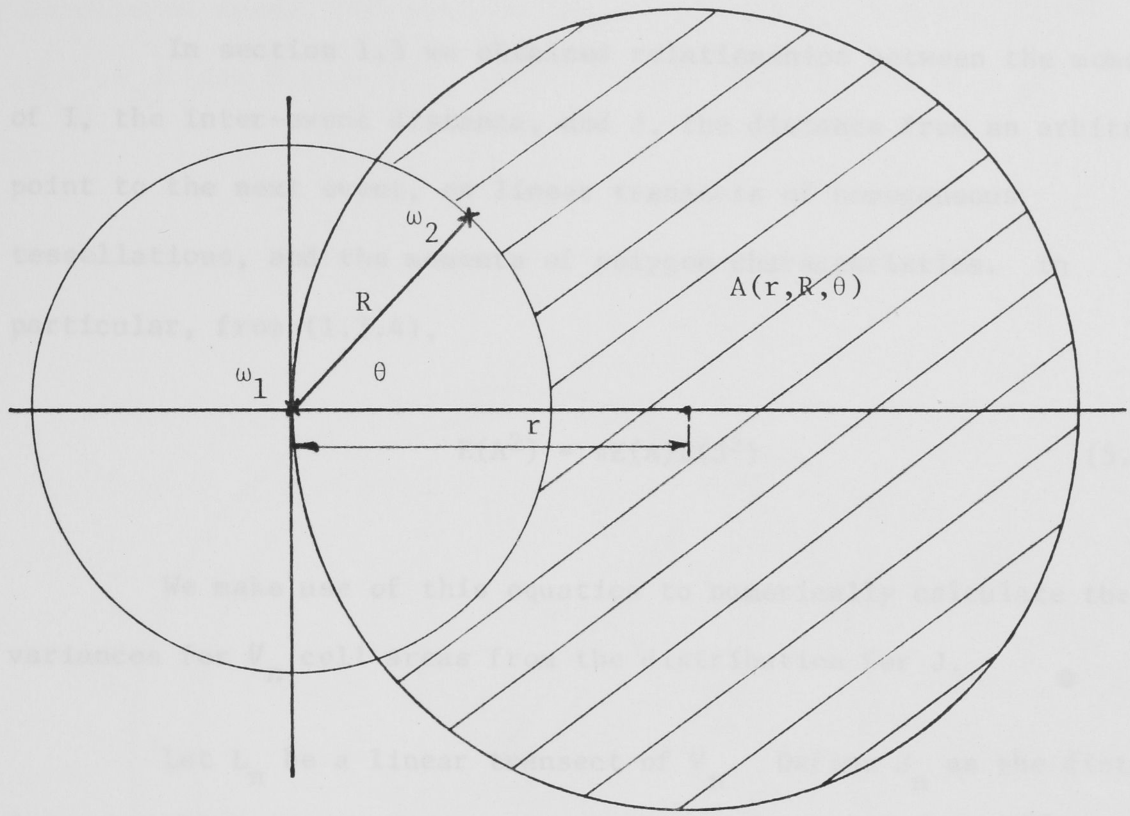

Figure 18

with radius to furthest of $\underline{0}$ and (u,θ).

Numerical integration of (4.7) gives

$$E(A_2{}^p) = 0.542\ \rho^{-1} \quad ,$$

which is larger than $E(A_2) = \frac{1}{3}\rho^{-1}$, the mean area for a uniform random V_2 cell, but smaller than $E(A_2^{(0)}) = 0.78\ \rho^{-1}$, the mean area for an area-weighted V_2 cell, which follows from (4.6) and the variance of A_2 calculated in section 4.5.

4.5 Transect Distributions for V_n and the variance of V_n cell areas

In section 1.3 we obtained relationships between the moments of I, the inter-event distance, and J, the distance from an arbitrary point to the next event, on linear transects of homogeneous tessellations, and the moments of polygon characteristics. In particular, from (1.3.4),

$$E(A^2) = \pi E(A)E(J^2) \quad . \tag{5.1}$$

We make use of this equation to numerically calculate the variances for V_n cell areas from the distribution for J.

Let L_n be a linear transect of V_n. Define J_n as the distance from an arbitrary point on L_n to the next event, and $J_n' = \sqrt{n}J_n$. The limiting distribution of J_n' is investigated in section 6.2.

Moments of J_n'

Take L_n passing through the origin, and the origin as our arbitrary starting position. We generate the n nearest particles to $\underline{0}$ by generating R_{n+1}, the distance to the $(n + 1)^{st}$ closest particle and then uniformly distributing n particles on the disk $Q(\underline{0},R_{n+1})$. These n particles are the proximity particles of the V_n cell containing the origin, $\omega_1,\omega_2,\ldots,\omega_n$ say. We define

$$S_n = \max_{i=1,2..n} \left|\omega_i - \left(\frac{x}{\sqrt{n}},0\right)\right| \quad .$$

S_n is the distance from $\left(\frac{x}{\sqrt{n}},0\right)$ to the furthest of $\underline{0}$'s proximity particles, so for the point $\left(\frac{x}{\sqrt{n}},0\right)$ to have the same n proximity particles as $\underline{0}$, $Q\left(\left(\frac{x}{\sqrt{n}},0\right),S_n\right)$ must contain no particles other than $\omega_1,\omega_2,..,\omega_n$. Note that $0 < S_n < R_{n+1} + \frac{x}{\sqrt{n}}$. We define

$A_n = Q\left(\frac{x}{\sqrt{n}}, S_n\right) - Q(\underline{0}, R_{n+1})$, $B_n = Q(\underline{0}, R_{n+1}) - Q\left(\frac{x}{\sqrt{n}}, S_n\right)$ (these areas are considered open), and $q(\alpha)$ is the arc of $Q(\underline{0}, R_{n+1})$ lying inside $Q\left(\frac{x}{\sqrt{n}}, S_n\right)$ (see Figure 19). We write $|S|$ for the area of S.

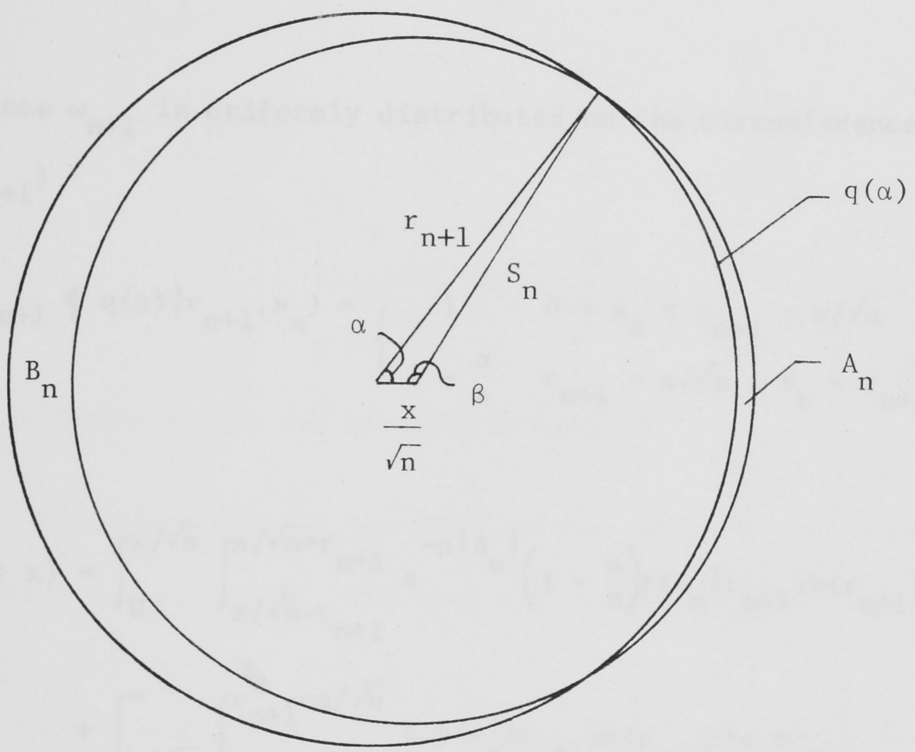

Figure 19

$$\text{Consider } P(J_n' > x) = P\left(\frac{x}{\sqrt{n}} \text{ has same proximity particles as the origin}\right)$$

$$= P(A_n \text{ is empty of particles and } \omega_{n+1} \text{ does not lie on } q(\alpha))$$

$$= \iint P(A_n \text{ empty and } \omega_{n+1} \notin q(\alpha) \,|\, r_{n+1}, s_n) f(s_n | r_{n+1}) h(r_{n+1}) ds_n dr_{n+1}, \tag{5.2}$$

where f is the conditional density of S_n given R_{n+1} and h is the marginal density of R_{n+1}.

We note that the support of f depends on whether $x/\sqrt{n}$ lies inside or outside of $Q(\underline{0},r_{n+1})$. The support is $(0,r_{n+1} + x/\sqrt{n})$ if $x/\sqrt{n} < r_{n+1}$, and $(x/\sqrt{n} - r_{n+1}, x/\sqrt{n} + r_{n+1})$ if $x/\sqrt{n} > r_{n+1}$. Also,

$$P(A_n \text{ empty} | r_{n+1}, s_n) = \begin{cases} 1 & 0 < s_n < r_{n+1} - x/\sqrt{n} \\ \exp\{-\rho|A_n|\} & r_{n+1} - x/\sqrt{n} < s_n < r_{n+1} + x/\sqrt{n} \end{cases} \tag{5.3}$$

and, since ω_{n+1} is uniformly distributed on the circumference of $Q(\underline{0},R_{n+1})$

$$P(\omega_{n+1} \notin q(\alpha) | r_{n+1}, s_n) = \begin{cases} 1 & 0 < s_n < r_{n+1} - x/\sqrt{n} \\ 1 - \frac{\alpha}{\pi} & r_{n+1} - x/\sqrt{n} < s_n < r_{n+1} + x/\sqrt{n} \end{cases}$$

Hence

$$\begin{aligned} P(J_n' > x) = &\int_0^{x/\sqrt{n}} \int_{x/\sqrt{n}-r_{n+1}}^{x/\sqrt{n}+r_{n+1}} e^{-\rho|A_n|}\left(1 - \frac{\alpha}{\pi}\right) f(s_n|r_{n+1}) h(r_{n+1}) ds_n dr_{n+1} \\ &+ \int_{x/\sqrt{n}}^{\infty} \int_0^{r_{n+1}-x/\sqrt{n}} 1.f(s_n|r_{n+1}) h(r_{n+1}) ds_n dr_{n+1} \\ &+ \int_{x/\sqrt{n}}^{\infty} \int_{r_{n+1}-x/\sqrt{n}}^{r_{n+1}+x/\sqrt{n}} e^{-\rho|A_n|}\left(1 - \frac{\alpha}{\pi}\right) f(s_n|r_{n+1}) h(r_{n+1}) ds_n dr_{n+1} \end{aligned} \tag{5.4}$$

$$= I_1 + I_2 + I_3 \text{ say} \quad .$$

Simple geometric argument shows that $R_{n+1} \sim \Gamma_2(2n + 2, \pi\rho)$, and hence $h(r_{n+1})$ is given by (3.5.4). To obtain the form of f, consider

$$F(s_n|r_{n+1}) = \text{d.f. of } S_n \text{ given } R_{n+1} = r_{n+1}$$

$$= P(S_n \leqslant s_n|r_{n+1})$$

$$= P(B_n \text{ empty})$$

$$= \left(1 - \frac{|B_n|}{\pi r_{n+1}^2}\right)^n$$

$$f(s_n|r_{n+1}) = \frac{-n}{\pi r_{n+1}^2}\left(1 - \frac{|B_n|}{\pi r_{n+1}^2}\right)^{n-1} \frac{d|B_n|}{ds_n}$$

$$= \frac{2n\beta}{\pi r_{n+1}^2}\left(1 - \frac{|B_n|}{\pi r_{n+1}^2}\right)^{n-1} s_n \quad , \qquad (5.5)$$

by use of Lemma 4 (see end of this section).

The exact form of the distribution of J for all n is complicated, so we simply calculate the second moment.

$$E(J_n'^2) = 2\int_0^\infty xP(J_n' > x)dx = \sum_{j=1}^{3} 2\int_0^\infty xI_j dx = \sum_{j=1}^{3} K_j$$

Consider $K_2 = 2\int_0^\infty xI_2 dx = 2\int_0^\infty \int_0^{\sqrt{n}r_{n+1}} x.P(S_n < r_{n+1} - x/\sqrt{n}|r_{n+1})h(r_{n+1}) \times dxdr_{n+1}$.

Note that $P(S_n < r_{n+1} - x/\sqrt{n}|r_{n+1}) = P(C_n \text{ empty})$ (see Figure 20)

$$= \left(1 - \frac{|C_n|}{\pi r_{n+1}^2}\right)^n \quad , \qquad (5.6)$$

where $|C_n| = \pi r_{n+1}^2 - \pi(r_{n+1} - x/\sqrt{n})^2 = \pi C(p_1)r_{n+1}^2$, if $x = p_1 r_{n+1}$ and $C(p) = 2p_1/\sqrt{n} - p_1^2/n$.

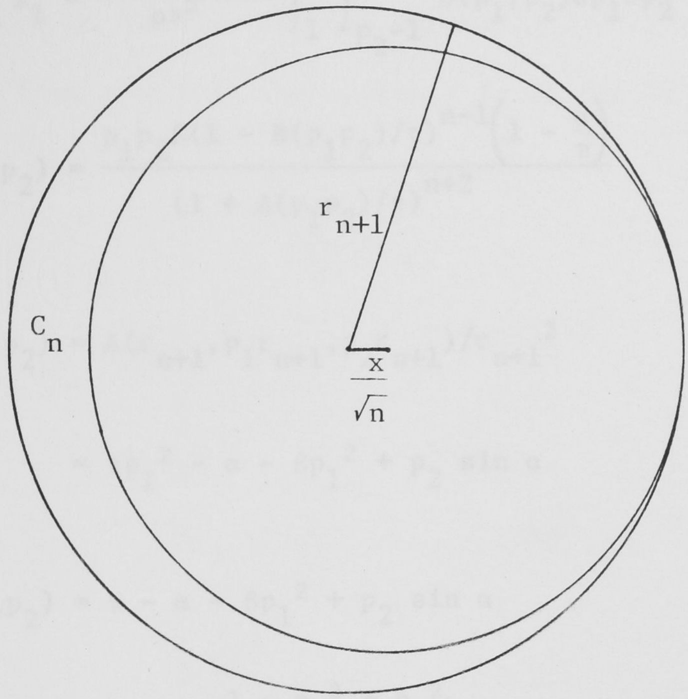

Figure 20

Hence, substituting for h,

$$K_2 = \frac{4(\pi\rho)^{n+1}}{n!} \int_0^\infty \int_0^{\sqrt{n}} p_1 r_{n+1}(1 - C(p_1))^n r_{n+1}{}^{2n+1} e^{-\rho\pi r_{n+1}{}^2} r_{n+1} dp_1 dr_{n+1}$$

$$= \frac{4(\pi\rho)^{n+1}}{n!} \int_0^{\sqrt{n}} p_1(1 - C(p_1))^n \frac{\Gamma(n + 2)}{2(\rho\pi)^{n+2}} dp_1$$

$$= \frac{2n(n + 1)}{\rho\pi} \int_0^1 y(1 - y)^{2n} dy$$

$$= \frac{2n(n + 1)}{\rho\pi} \frac{\Gamma(2)\Gamma(2n + 1)}{\Gamma(2n + 3)} = \frac{n}{\rho\pi(2n + 1)} \quad . \tag{5.7}$$

Consider

$$K_1 = 2\int_0^\infty \int_{\sqrt{n}r_{n+1}}^\infty \int_{x/\sqrt{n}-r_{n+1}}^{x/\sqrt{n}+r_{n+1}} x.\exp\{-\rho|A_n|\}\left(1 - \frac{\alpha}{\pi}\right) f(s_n|r_{n+1}) h(r_{n+1}) ds_n dx dr_{n+1} .$$

Again substituting for f and h, and putting $s_n = p_1 r_{n+1}$, $x = p_2 r_{n+1}\sqrt{n}$, and integrating out r_{n+1} yields

$$K_1 = \frac{4n^2(n+1)}{\rho\pi^2} \int_1^{\infty} \int_{p_2-1}^{p_2+1} D(p_1,p_2)dp_1dp_2 \quad , \qquad (5.8)$$

where $$D(p_1,p_2) = \frac{p_1p_2\beta(1 - B(p_1p_2)/\pi)^{n-1}\left(1 - \frac{\alpha}{\pi}\right)}{(1 + A(p_1p_2)/\pi)^{n+2}}$$

$$A(p_1,p_2) = A(r_{n+1}, p_1r_{n+1}, p_2r_{n+1})/r_{n+1}^2$$

$$= \pi p_1^2 - \alpha - \beta p_1^2 + p_2 \sin\alpha$$

$$B(p_1,p_2) = \pi - \alpha - \beta p_1^2 + p_2 \sin\alpha$$

$$\alpha = \cos^{-1}\left(\frac{1 - p_1^2 + p_2^2}{2p_2}\right), \qquad \beta = \cos^{-1}\left(\frac{p_1^2 - 1 + p_2^2}{2p_1p_2}\right)$$

These formulae follow directly from Lemma 4.

Similarly, $$K_3 = \frac{4n^2(n+1)}{\pi^2\rho} \int_0^1 \int_{1-p_2}^{1+p_2} D(p_1p_2)dp_1dp_2 \quad . \qquad (5.9)$$

Collecting (5.7), (5.8), (5.9) gives

$$E(J_n'^2) = \left[\frac{4n^2(n+1)}{\pi^2}\left[\int_0^1 \int_{1-p_2}^{1+p_2} D(p_1,p_2)dp_1dp_2 + \int_1^{\infty}\int_{p_2-1}^{p_2+1} D(p_1p_2)dp_1dp_2\right] + \frac{n}{\pi(2n+1)}\right]\rho^{-1} \quad .$$

This was numerically evaluated for various values of n.

In Table 4 we present the variances for the scaled sequence of tessellations $\sqrt{(2n-1)\rho}V_n$ with mean areas normed to unity for all n i.e. $A_n' = (2n-1)\rho A_n$. These normed variances tend to the limiting variance calculated in section 6.2.

Note that $$\mathrm{Var}(A_n') = \frac{(2n-1)\pi\rho}{n} E(J_n'^2) - 1 \quad .$$

The value for $n = 1$ agrees with Gilbert's [1962] calculation. We note that most of the convergence occurs in the first few n values so that by the time $n = 128$, the variance is within 2% of its limiting value.

Table 4

n	$Var(A_n')$
1	0.28
2	1.34
3	1.80
4	2.14
5	2.22
6	2.33
7	2.41
8	2.48
9	2.53
10	2.57
16	2.71
32	2.83
64	2.89
128	2.91
∞	2.95

Lemma 4

Consider intersecting circles as in Figure 21.

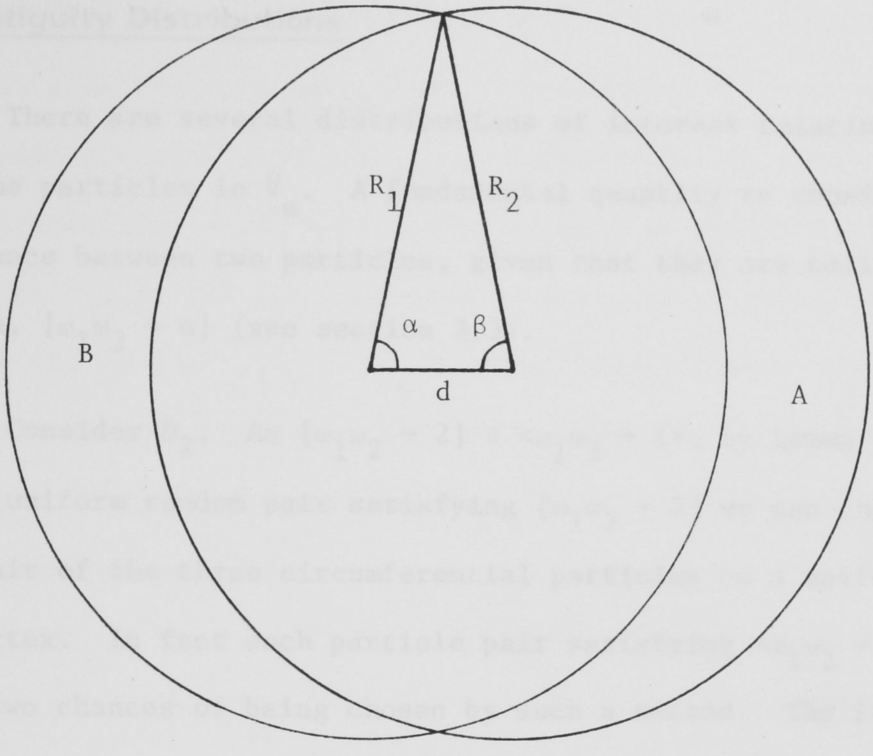

Figure 21

By considering relevant areas of sectors and triangles,

$$B(R_1,R_2,d) = \pi R_1^{\,2} - \frac{2\alpha}{2\pi}.\pi R_1^{\,2} - \frac{2\beta}{2\pi}.\pi R_2^{\,2} + 2.\tfrac{1}{2}.R_1 d \sin\alpha$$

$$= \pi R_1^{\,2} - \alpha R_1^{\,2} - \beta R_2^{\,2} + R_1 d \sin\alpha ,$$

and $$A(R_1,R_2,d) = \pi R_2^{\,2} - \alpha R_1^{\,2} - \beta R_2^{\,2} + R_1 d \sin\alpha .$$

Here $\cos\alpha = (R_1^{\,2} - R_2^{\,2} + d^2)/2R_1 d$, $\cos\beta = (R_2^{\,2} - R_1^{\,2} + d^2)/2R_2 d$,

$0 < \alpha,\ \beta < \pi$.

As is obvious from Figure 21,

$$\frac{dB}{dR_2} = -\,2\beta R_2 \ .$$

4.6 Contiguity Distributions

There are several distributions of interest relating to contiguous particles in V_n. A fundamental quantity to consider is D_n, the distance between two particles, given that they are cell-contiguous in V_n i.e. $[\omega_1\omega_2 \to n]$ (see section 3.3).

Consider D_2. As $[\omega_1\omega_2 \to 2] \equiv \langle\omega_1\omega_2 \to 1\rangle$, by Lemma 3.4, to choose a uniform random pair satisfying $[\omega_1\omega_2 \to 2]$ we can choose a random pair of the three circumferential particles on a uniform random (1,2) vertex. In fact each particle pair satisfying $\langle\omega_1\omega_2 \to 1\rangle$ has exactly two chances of being chosen by such a method. The line joining ω_1 and ω_2, chosen in the above manner is just a uniform random side of a Delaunay triangle, whose distribution and moments follow from the Stochastic Construction for a uniform random V_1 vertex (Lemma 3.10) for the case where the generating particles process is $\mathbb{P}$.

From Miles [1970], p 113,

$$E[D_2{}^k] = \frac{2^{k+3}\Gamma((k + 5)/2)}{3(k + 2)\pi^{(k+1)/2}\rho^{k/2}} \quad . \tag{6.1}$$

The density $f_2(x)$ of D_2 has the interesting form

$$f_2(x) = \frac{2\pi x}{3}\left[1 - \Xi\left(x\sqrt{\frac{\pi}{2}}\right) + x\sqrt{\frac{\pi}{2}}\xi\left(x\sqrt{\frac{\pi}{2}}\right)\right] \quad , \tag{6.2}$$

where $\Xi(x)$ and $\xi(x)$ are the d.f. and p.d.f. of the standard normal distribution (Sibson [1980b]). (6.2) assumes $\rho = 1$. Since ρ is simply a scale parameter the p.d.f. for general ρ is $f_2(x;\rho) = \rho^{\frac{1}{2}}f_2(x\rho^{\frac{1}{2}})$.

Now consider D_3. Again applying Lemma 4, we are concerned with particle pairs satisfying $\langle\omega_1\omega_2 \to 2\rangle$. However if we choose a particle pair randomly from a uniform random (2,3) vertex, not all pairs satisfying $<\omega_1\omega_2 \to 2>$ will have equal chances of being chosen. This is because there is more than one pattern of V_n segments on $<\omega_1\omega_2>$ under the condition $<\omega_1\omega_2 \to 2>$ compared to the single pattern under the condition $<\omega_1\omega_2 \to 1>$. (For details on segmentation of $<\omega_1\omega_2>$ see section 5.2.) The three classes of patterns on $<\omega_1\omega_2>$ are listed in Figure 22. Write $<\omega_1\omega_2 \to 2>_i$ for the condition that $<\omega_1\omega_2>$ has pattern i as listed in Figure 22. Then, under the above sampling scheme, particle pairs satisfying $<\omega_1\omega_2 \to 2>_1$ or $<\omega_1\omega_2 \to 2>_2$ have equal chances of being chosen but $<\omega_1\omega_2 \to 2>_3$ pairs have a double weighting due to the four (2,3) vertices contained in that arrangement.

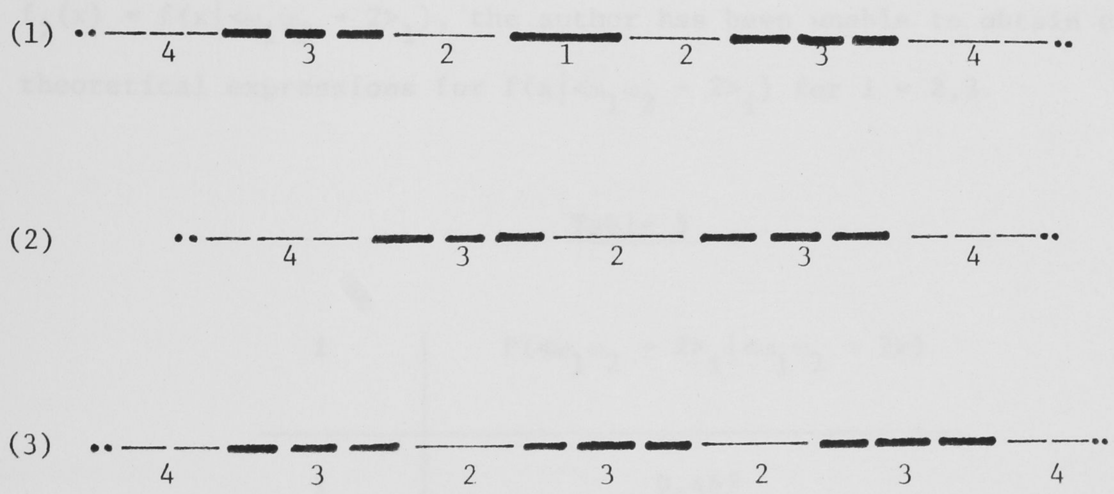

Figure 22

It seems natural to condition on the pattern type, and if $f_3(x)$ is the p.d.f. of D_3 we have

$$f_3(x|<\omega_1\omega_2 \to 2>) = \sum_{i=1}^{3} f(x|<\omega_1\omega_2 \to 2>_i)P(<\omega_1\omega_2 \to 2>_i|<\omega_1\omega_2 \to 2>) .$$

Using the side densities calculated in sections 4.1 and 4.3, the conditional probabilities of the three pattern types can be calculated. Let ψ_i be the density of perpendicular bisectors with arrangement i. Then from Figure 22,

$$\psi_1 = \text{density of } V_1 \text{ sides} = 3\rho \quad \text{(Table 1)}$$

$$\psi_2 + 2\psi_3 = \sigma_2(+,+) = 4\rho \quad \text{(Table 1)}$$

and $$\psi_3 = \sigma_3(-,-) = 0.526\,\rho \quad \text{(Table 3)}$$

Table 5 gives the resulting conditional probabilities for the three arrangements. Although we have D_3 expressed as a mixture of three related contiguity distributions, one of which is known since $f_2(x) = f(x|<\omega_1\omega_2 \to 2>_1)$, the author has been unable to obtain even theoretical expressions for $f(x|<\omega_1\omega_2 \to 2>_i)$ for i = 2,3.

Table 5

i	$P(<\omega_1\omega_2 \to 2>_i \| <\omega_1\omega_2 \to 2>)$
1	0.463
2	0.455
3	0.082

Another measure of the separation of contiguous particles ω_1, ω_2 in V_n is the number of particles which are closer to ω_1 than ω_2 is (or vice versa). Let ω_1 and ω_2 be a uniform random pair of cell contiguous particles in V_2 generated by $\mathbb{P}$, and let ω_2 be the I^{th} closest particle to ω_1 (where I is random). Let q_i denote $P(I = i)$, i = 1,2,... . Using (6.2) we have (ρ = 1),

$$q_i = \int_0^\infty P(I = i|r) f_2(r) dr ,$$

(where $P(I = i|r) = P(\text{circle radius } r \text{ is } (i-1) \text{ filled})$

$$= e^{-\pi r^2} (\pi r^2)^{i-1}/(i-1)!$$

Hence $$q_i = \frac{(2i)!}{3i!(i-1)!} \left\{ \frac{1}{5^{i+\frac{1}{2}}} + \int_1^\infty \frac{dx}{(4+x^2)^{i+\frac{1}{2}}} \right\} .$$

The q_i values for $i = 1,2,..15$ are listed in Table 6. We note that

$$E(I) = \sum_{i=1}^{\infty} iq_i$$

$$= \int_0^\infty (1 + \pi r^2) f_2(r) dr$$

$$= 1 + \pi E(D_2{}^2)$$

$$= 6 ,$$

by use of (6.1). Since the closest particle to ω_1 is always contiguous and the mean number of sides is 6 we would expect (approximately) that $P(I = 1) = {}^1/6$, which is supported by Table 6. The mean value $E(I) = 6$, which may seem too large given that $E(N) = 6$, can be explained by realizing that particles near to ω_1 can miss out on contiguity if closer particles intervene. This spreads out the distribution for I. In fact, $E(I^2) = 1 + 3\pi E(D_2{}^2) + \pi^2 E(D_2{}^4)$, which gives $Var(I) = 220/3$.

Table 6

i	q_i	i	q_i	i	q_i
1	0.1516	6	0.071	11	0.0284
2	0.1339	7	0.0596	12	0.0235
3	0.1160	8	0.0498	13	0.0194
4	0.0993	9	0.0414	14	0.0159
5	0.0843	10	0.0344	15	0.0131

4.7 Basic Results for V_n relative to $\mathbb{P}$

The results in this section summarize joint work between R.E. Miles and the author. See Miles and Maillardet [1982].

To enable us to write down probability statements for an N-gon of V_n we have to establish a link between the V_n cell and the particles which generate it. This can be done using the geometry of V_n N-gons in section 3.6, and particularly Lemma 3.14. From this geometry it is clear that associated with any N-gon T in V_n are N particles whose perpendicular bisectors determine the sides of T (see Figure 3.16). We refer to these N particles as the generating particles of the cell; they are just the inner and outer particles of T. Compare this situation with a V_1 N-gon, whose sides are generated by N + 1 particles, with the nucleus particle free to occupy any point inside the cell.

We wish to establish a correspondence between N-gons and their N generating particles. Consider N particles in the plane. The collection of possible cells which they generate in V_n is just the collection of cells in their V_2, for any cell they generate in V_2 they will generate in V_n simply by introducing the requisite number of interior particles into the area Λ (see Lemma 3.14). The V_2 of four particles contains a quadrilateral if they have a quadrilateral convex hull, otherwise it contains no finite polygonal region. The V_2 of five particles contains a pentagon, a quadrilateral, and a certain number of infinite polygonal regions (the number depending on whether the particles have a triangular, quadrilateral or pentagonal convex hull). See Figure 23 for the quadrilateral convex hull case. It seems intuitively plausible that five particles will generate at most one pentagon in their V_2, and indeed that N particles will generate at most one N-gon in their V_2. We assume that this is so, but have yet to determine a proof.

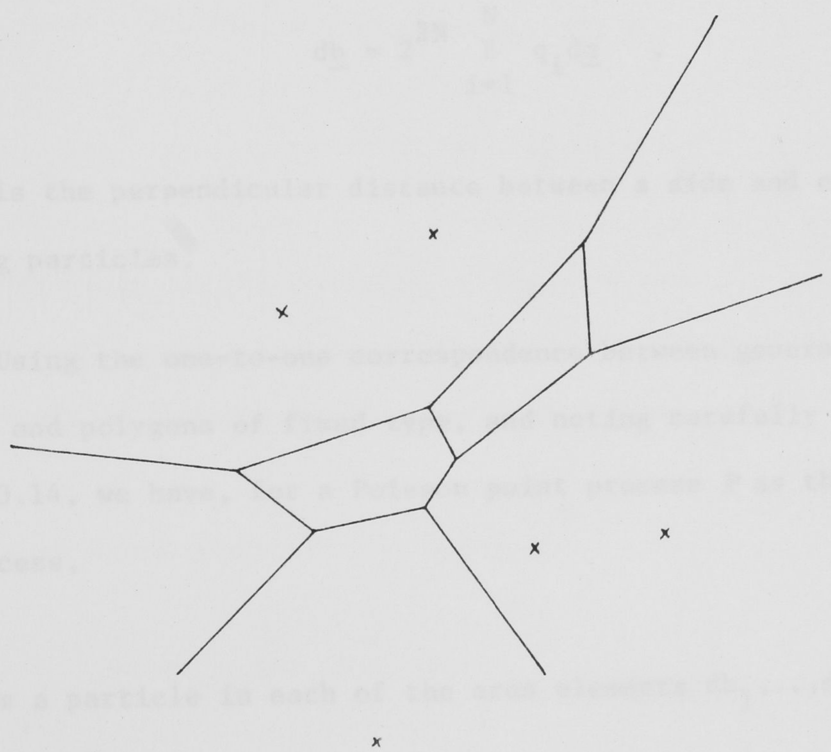

The V_2 of five particles with a quadrilateral convex hull.

Figure 23

Now consider an N-gon in V_n, parameterized by its N vertices $\underline{\nu} = (\nu_1, \nu_2, .. \nu_N)$ say. Is there a unique set of generating particles associated with it? The answer, in general, is no, for since vertices in V_n can be of two sorts, inner and outer, an N-gon will have a range of permissible types to which it could belong (see section 3.6). And it is easy to construct examples of two identical cells of different types with different generating particles. However, for a polygon of fixed type ϕ, Miles [1982] has shown that there is a unique set of N generating particles, and has determined the Jacobian of the transformation between those particles $\underline{b} = (b_1, b_2, .. b_N)$ and $\underline{\alpha} = (p_1, \theta_1, .., p_N, \theta_N)$, the parametrization of T in terms of its sides (see section 2.4). Thus we have

$$d\underline{b} = 2^{2N} \prod_{i=1}^{N} q_i d\underline{\alpha} \quad , \tag{7.1}$$

where q_i is the perpendicular distance between a side and either of its generating particles.

Using the one-to-one correspondence between generating particles and polygons of fixed type, and noting carefully the geometry of Lemma 3.14, we have, for a Poisson point process $\mathbb{P}$ as the underlying point process,

P(there is a particle in each of the area elements $db_1, .., db_N$ generating an N-gon in V_n)

$$= \left(\prod_{i=1}^{N} \rho db_i\right) \Pr\left(\text{there are } (n-m) \text{ particles in int } \Lambda, \text{ and no particles in int}(V - \Lambda)\right)$$

$$= \left(\prod_{i=1}^{N} \rho db_i\right) \left\{(\rho|\Lambda|)^{n-m} e^{-\rho|\Lambda|}/(n-m)!\right\} e^{-\rho|V-\Lambda|}$$

$$= \rho^{N+n-m} |\Lambda|^{n-m} e^{-\rho|V|} (n-m)!^{-1} d\underline{b} \quad .$$

Hence, using (7.1) we have

P(there is an N-gon member of $\mathcal{V}_n$ within the side limitations $d\underline{\alpha}$)

$$= 2^{2N} \sum_{\phi\in\Phi} \rho^{N+n-m}|\Lambda|^{n-m} \exp\{-\rho|V|\}(n-m)!^{-1}\left(\prod_{i=1}^{N} q_i\right)d\underline{\alpha} \quad , \quad (7.2)$$

where we have summed over the collection Φ of permissible types ϕ for the cell. Using (2.4.4), we can transform to the vertex parametrization of T and hence to 'structural N-gon co-ordinates' $\eta = (z,\ell,\underline{\sigma})$, where

$$\nu_1 = z$$

$$\nu_2 = z + \ell(\cos\psi_2, \sin\psi_2)$$

$$\nu_i = z + \ell\lambda_i(\cos\psi_i, \sin\psi_i) \qquad i = 3,4,..,N$$

Here z gives the position, ℓ the size and $\underline{\sigma} = (\lambda_3,..,\lambda_N,\psi_2,..,\psi_N)$ the shape of T. So for certain functions g and h, $\Lambda = g(\underline{\sigma})\ell^2$ and $V = h(\underline{\sigma})\ell^2$, and (7.2) becomes

P(there is an N-gon member of $\mathcal{V}_n$ in $d\eta$)

$$= 2^{2N} \sum_{\phi\in\Phi} \rho^{N+n-m} g(\underline{\sigma})^{n-m} \ell^{2N+2n-2m-3} \exp\{-\rho h(\underline{\sigma})\ell^2\}(n-m)!^{-1}$$

$$\times \prod_{i=1}^{N} (|\sin\psi_i|q_i/L_i) \prod_{i=3}^{N} \lambda_i \quad . \quad (7.3)$$

Since the area and perimeter of the cell can be written as $A = a(\underline{\sigma})\ell^2$ and $S = s(\underline{\sigma})\ell$, (7.3) shows that for a given shape, the conditional distributions of A and S are mixtures of the generalized gamma distributions defined by Miles [1970] p 88.

CHAPTER 5

COMPUTATION OF VORONOI AND GENERALIZED VORONOI TESSELLATIONS

The generalized Voronoi tessellations, even for regular lattices of particles rather than random particles in general position, are difficult to visualize and think about without a picture. The task of constructing these tessellations by hand, even for small values of n, is extremely laborious, as Miles comments in his initial work. It was essential that a program for producing these tessellations over large areas was developed.

A summary of developed techniques for efficient computation of Voronoi tessellations is given in section 5.1, together with an assessment of transferring the same techniques to the V_n case. Section 5.2 gives the geometric background to the program we use, which is explained in detail in section 5.3. Section 5.4 specifies a more efficient alternative program for generation of V_n for n very large. Section 5.5 investigates calculations based on a degenerate square grid of particles.

5.1 Computation of Voronoi Tessellations

The computation of the Voronoi tessellation has become a subject of considerable interest over the last few years. This is no doubt due to its increasing importance and use in a wide variety of modelling situations.

The history of the computation of V_1, at least for the planar case, is summarized in Green and Sibson [1978], where an efficient technique for the computation of planar Voronoi tessellations over a region bounded by linear constraints is developed. This program is very fast, and works by iteratively modifying an established tessellation by the successive addition of new particles.

This works well for V_1, since the only cells which are modified are those which are edge-contiguous with the added particle. Figure 1 illustrates how the cell of an added particle captures its territory from the cells of edge-contiguous particles.

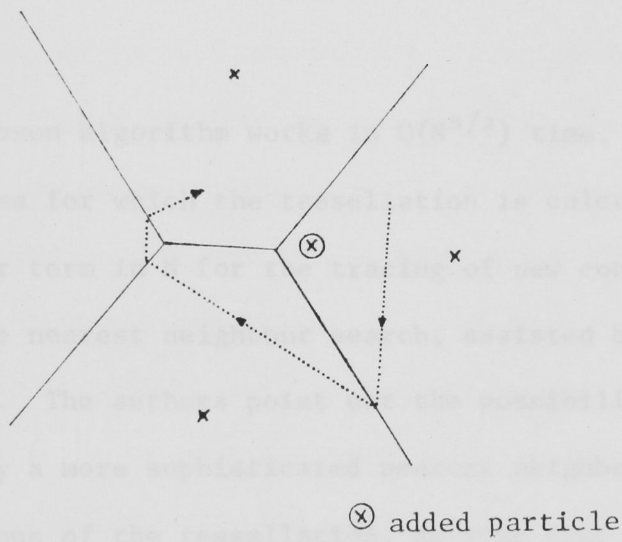

Figure 1

The Green/Sibson algorithm begins with a nearest neighbour search, since a new particle will always be edge-contiguous with its nearest neighbour, and the new contiguities are traced out as indicated in Figure 1. Use is made of the established tessellation to decrease the time of this nearest neighbour search.

Applying a similar approach to the computation of V_n is unworkable. As an example consider adding a particle ω to an established V_{50} tessellation. Let $A_{\omega,50}$ be the 50-Area of ω relative to the existing particles.

Over the whole of $A_{\omega,50}$ the tessellation is changed, and the cells within this area have different proximity particles due to the inclusion of ω. Around the edge of $A_{\omega,50}$ there are other cells with the same proximity particles but which now have a side (part of the perpendicular bisector between one of their proximity particles and ω) which has modified their geometry. For n = 50, Lemma 3.3 indicates a mean number of 4950 cells will be effected by having their proximity particles changed. These considerations obviously rule out any straightforward application of the Green/Sibson approach to the V_n case.

The Green/Sibson algorithm works in $O(N^{3/2})$ time, where N is the number of particles for which the tessellation is calculated. This is made up of a linear term in N for the tracing of new contiguities and an $N^{\frac{1}{2}}$ term for the nearest neighbour search, assisted by the existing tessellation. The authors point out the possibility of an O(N log N) run time by a more sophisticated nearest neighbour search over several generations of the tessellation, at some cost in storage.

Further work aimed at improving the efficiency of V_1 computation is currently being carried out by Murota (University of Tokyo), who has implemented an O(N log N) algorithm based on an efficient version by Horspool [1979] of an algorithm originally described in Shamos and Hoey [1975] (personal communication). Murota is also currently working on an improvement to the Green/Sibson algorithm which could run in O(n) time on average.

There has also been recent work on extending the Green/Sibson algorithm to the computation of Voronoi and Delaunay tessellations in k-dimensions (Bowyer [1981]). Bowyer computes the dual Delaunay tessellation by a natural extension of the two-dimensional algorithm, performing a tessellation assisted search to find the added particles nearest neighbour, and a vertex search through the established Delaunay vertices to calculate the contiguities generated or removed by the new particle. Watson [1981] has tackled the problem in a similar fashion.

It is important to remember that there are two sorts of problems in the generation of tessellations, which are computationally clearly distinct. One is the generation of the tessellation over a certain area, the other the generation of an individual typical polygon for simulation purposes, to investigate polygon characteristics beyond theoretical treatment. These problems are related, and the former could always be solved by an iterative application of the latter to build up the tessellation, polygon by polygon, over a region (see sections 5.3, 5.4). For the Voronoi case the generation of individual polygons is straightforward, using the typical cell $[\omega_0]$ generated by $\mathbb{P} \cup \{\omega_0\}$, as described in section 2.3. A large scale Monte Carlo study of Voronoi cells was carried out by Hinde and Miles [1980], using this technique.

5.2 The partitioning of $<\omega_1\omega_2>$ into $\mathcal{V}_n$ segments

Consider two particles of the generating process of the tessellation, which is assumed to be of type Π_2, and their perpendicular bisector $<\omega_1\omega_2>$. This is partitioned by the other particles of Π_2 into segments of $\mathcal{L}_n$. In fact any point $\underline{x}$ on $<\omega_1\omega_2>$ is contained in an $\mathcal{L}_n$ segment if the circle, centered at $\underline{x}$ and passing through ω_1 and ω_2 i.e. $Q(\underline{x},|\underline{x} - \omega_1|)$ is $(n - 1)$-filled, $n = 1,2,3,\ldots$. (see Figure 2) and we write $n(\underline{x}) = n$. Such a circle is referred to as a centered circle.

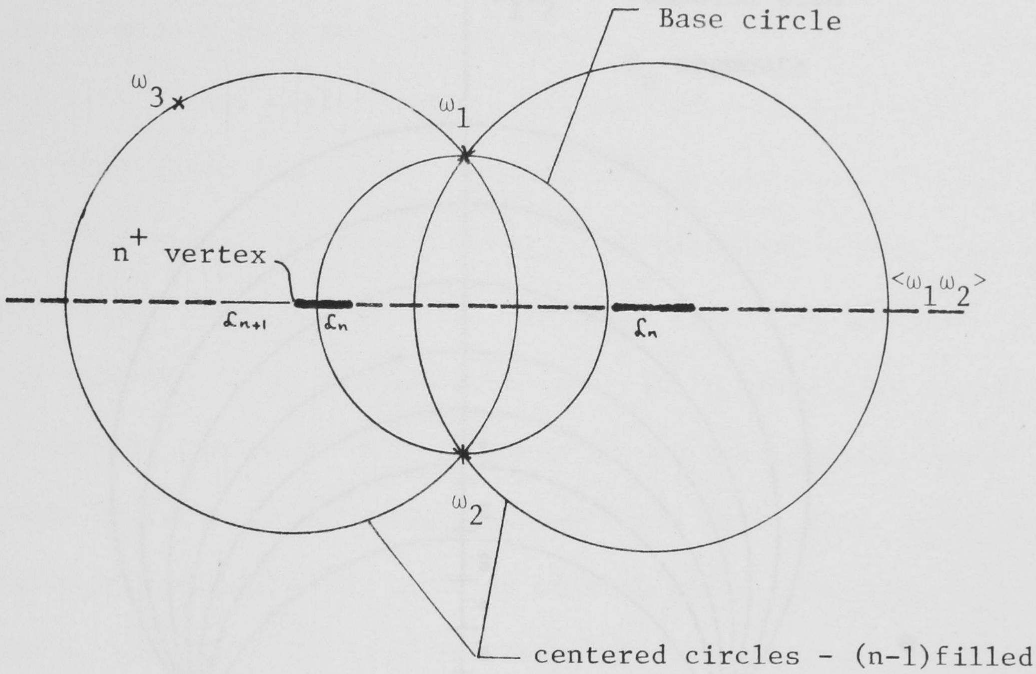

Figure 2

The endpoints of the $\mathcal{V}_n$ segments are the circumcentres $<\omega_1\omega_2\omega_i>$ where ω_i ranges over the other particles of Π_2.

The main processes of interest in an analysis of the partitioning of $<\omega_1\omega_2>$ are

(i) the point process of circumcentres $\{<\omega_1\omega_2\omega_i>, \omega_i \in \Pi_2\}$, $C(d)$, and

(ii) the random step function $\{n_d(\underline{x}), \underline{x} \in <\omega_1\omega_2>\}$, where $n_d(\underline{x}) = n$ if $\underline{x} \in \mathcal{L}_n$ segment.

Since no meaning can be ascribed to an arbitrary or typical pair of particles or equivalently a typical perpendicular bisector, we always condition on the distance between ω_1 and ω_2 - hence $n_d(\underline{x})$ and $C(d)$.

A typical realization of $n_d(\underline{x})$ is given in Figure 3.

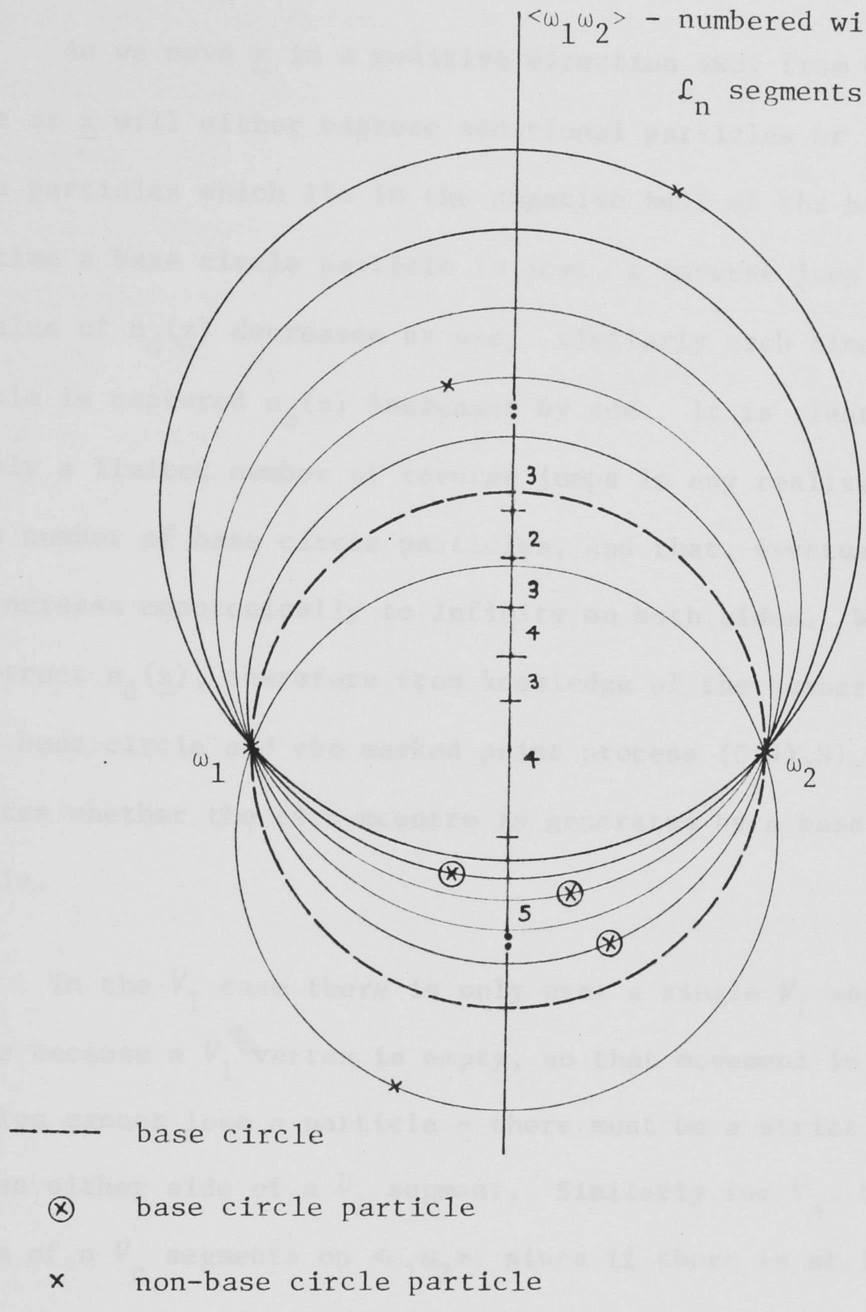

Figure 3

Although similar arguments apply relative to an origin fixed anywhere on $<\omega_1\omega_2>$, we arbitrarily fix the origin at the midpoint between ω_1 and ω_2 and refer to the circle, centre origin which passes through ω_1 and ω_2 as the base circle (Figure 2).

If there are n particles in the base circle, the origin is in an $\mathcal{L}_{n+1}$ segment. We call these particles *base circle* particles. Note that the $\mathcal{L}_{n+1}$ segment centered on the base circle is not necessarily the minimum $\mathcal{L}_n$ which appears on $<\omega_1\omega_2>$.

As we move $\underline{x}$ in a positive direction away from $\underline{0}$, the centered circle at $\underline{x}$ will either capture additional particles or lose base circle particles which lie in the negative half of the base circle. Each time a base circle particle is lost, a reverse jump occurs and the value of $n_d(\underline{x})$ decreases by one; similarly each time another particle is captured $n_d(\underline{x})$ increases by one. It is clear that there are only a limited number of reverse jumps in any realization, equal to the number of base circle particles, and that, eventually, $n_d(\underline{x})$ will increase monotonically to infinity on both sides. We can reconstruct $n_d(\underline{x})$, therefore from knowledge of the number of particles in the base circle and the marked point process (C(d),S) where S indicates whether the circumcentre is generated by a base circle particle.

In the V_1 case there is only ever a single V_1 segment on $<\omega_1\omega_2>$. This is because a V_1 vertex is empty, so that movement in either direction cannot lose a particle - there must be a strict monotonic increase either side of a V_1 segment. Similarly for V_n, there is a maximum of n V_n segments on $<\omega_1\omega_2>$, since if there is at least one such segment there is an (n - 1)-filled centered circle on $<\omega_1\omega_2>$ which limits the number of reverse jumps either side of it to (n - 1) and hence the number of V_n segments to a maximum of n, in the case where the (n - 1) reverse jumps alternate with positive jumps.

5.3 Computation of the V_n tessellation

Efficiency is not an overriding consideration in the computation of V_n; the aim was for a program that would generate the tessellation over large areas for a range of values of n.

The technique used is to concentrate attention not on whole polygons, but on the perpendicular bisectors of all particles that are sufficiently close that there is a fair probability of them containing a V_n segment. For each $<\omega_1\omega_2>$ chosen we find $<\omega_1\omega_2\omega_k>$ for the other particles ω_k, noting each time whether ω_k is a base circle particle or not, and simultaneously finding the total number of particles in the base circle - NBC say. This information amounts to knowing (C(d),S) for the $<\omega_1\omega_2>$ under consideration.

The program uses vector parametric form for $<\omega_1\omega_2>$ and stores circumcentres by storing the appropriate parameter value - positive values in one array and negative values in another, so that the sign can be used to indicate the presence of a 'base-circle particle' generated circumcentre (-) or otherwise (+) (see Figure 4).

Once all circumcentres are calculated, both arrays are ordered (by absolute value). The central segment on $<\omega_1\omega_2>$, which cuts through the origin, is a V_{NBC+1} segment with endpoints at the smallest positive and largest negative circumcentres. Further V_n segments extend between successive circumcentres, with n values dictated by the S value corresponding to their circumcentre nearest to $\underline{0}$, in the fashion explained in section 5.2. The program simply proceeds along $<\omega_1\omega_2>$ in the positive and then negative directions and stores segments of any V_n which is being generated into an appropriate data file (see Figure 4). The search along $<\omega_1\omega_2>$ terminates when the segments are no longer in the recorded region, or when it becomes clear that no more V_n segments can occur since all base-circle reverse jumps have been exhausted.

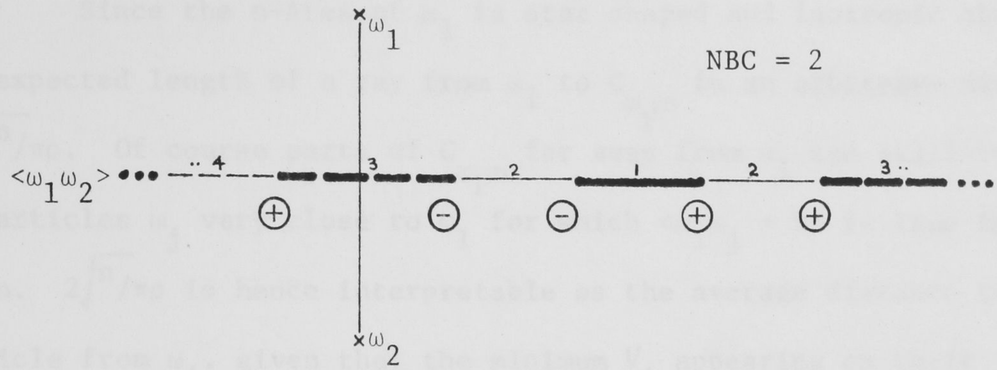

Figure 4

This procedure is repeated for all choices of pairs of particles. If we fix ω_1 and allow ω_2 to vary over the possible pairs, the program generates all V_n segments in which ω_1 plays a part. Such a V_n segment, on $\langle\omega_1\omega_i\rangle$ say, is the boundary between two V_n cells of the form $[\omega_1\Omega_2 .. \Omega_n]$ and $[\omega_i\Omega_2 .. \Omega_n]$, and hence clearly forms part of the boundary of ω_1's n-Area - i.e. part of ω_1's n-Circuit $C_{\omega_1,n}$ (see section 3.2). Hence the program essentially computes the n-Circuits for all particles. This is strictly true only for the first particle, for later particles are paired only with particles they have not yet been paired with, which means that only parts of their n-Circuit not previously computed will be generated.

Choice of particle pairs

Given a particle ω_1 the question is what other particles should be paired with it to ensure that all perpendicular bisectors containing V_n segments are considered. We can get some indication from Lemma 3.2, which showed that

$$E(A_{\omega,n}) = n/\rho \quad .$$

Since the n-Area of ω_1 is star shaped and isotropic about ω_1, the expected length of a ray from ω_1 to $C_{\omega_1,n}$ in an arbitrary direction is $\sqrt{n/\pi\rho}$. Of course parts of $C_{\omega_1,n}$ far away from ω_1 can still be due to particles ω_j very close to ω_1 for which $<\omega_1\omega_j \rightarrow k>$ is true for some $k < n$. $2\sqrt{n/\pi\rho}$ is hence interpretable as the average distance to a particle from ω_1, given that the minimum V_i appearing on their perpendicular bisector is a V_n.

For smaller values of n, depending on the size of the area of tessellation generated, some time saving is possible by griding the plane and considering only those particles in certain grids near to ω_1. Since such an approach is probabilistic, rather than geometric, there is always a possibility that a V_n segment is missed. This difficulty need not be faced, however, for when we are interested in calculating a series of V_n's the highest n value determines the pair selection and this often means choosing all possible pairs.

For example, to generate the plots in Figure 5, which shows a sequence of V_n's for n = 4, 16, 64 and 256, and the V_{300} in Figure 6, 500 random particles were placed in the unit square, and areas of the different V_n's were stored over the regions shown in Figure 7. All possible particle pairs were considered. In this case we can be virtually certain that the tessellations produced over their respective areas will be complete, since, with high probability, each point in these areas has its n nearest particles determined by the particles inside the unit square, so there is a corresponding high probability that all edge-contiguous particle pairs will be considered.

We note that in calculating V_{300} this program must also calculate V_i for all i < 300, since all such V_i segments must be

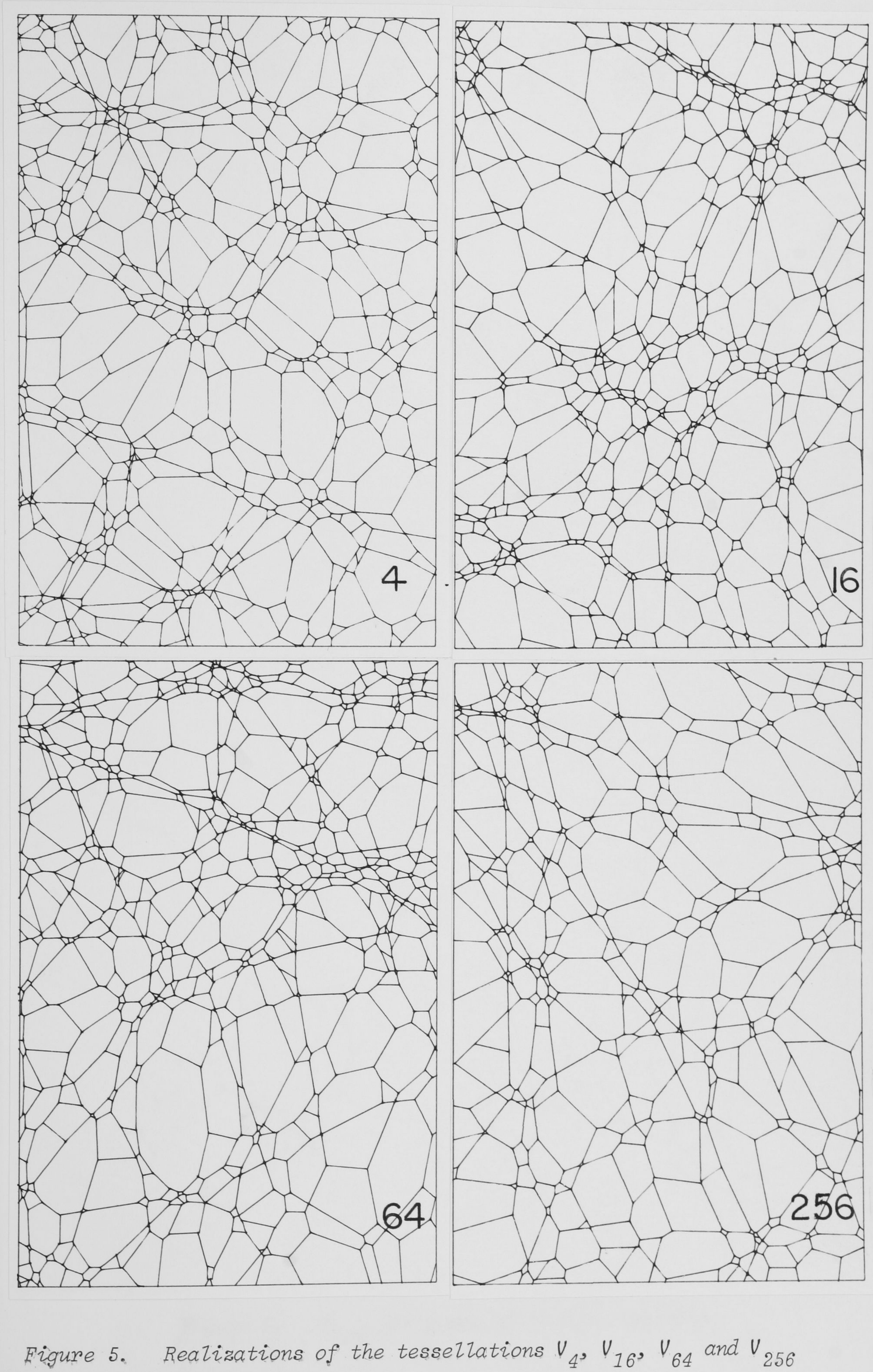

Figure 5. Realizations of the tessellations V_4, V_{16}, V_{64} and V_{256} scaled so as to have equal mean areas.

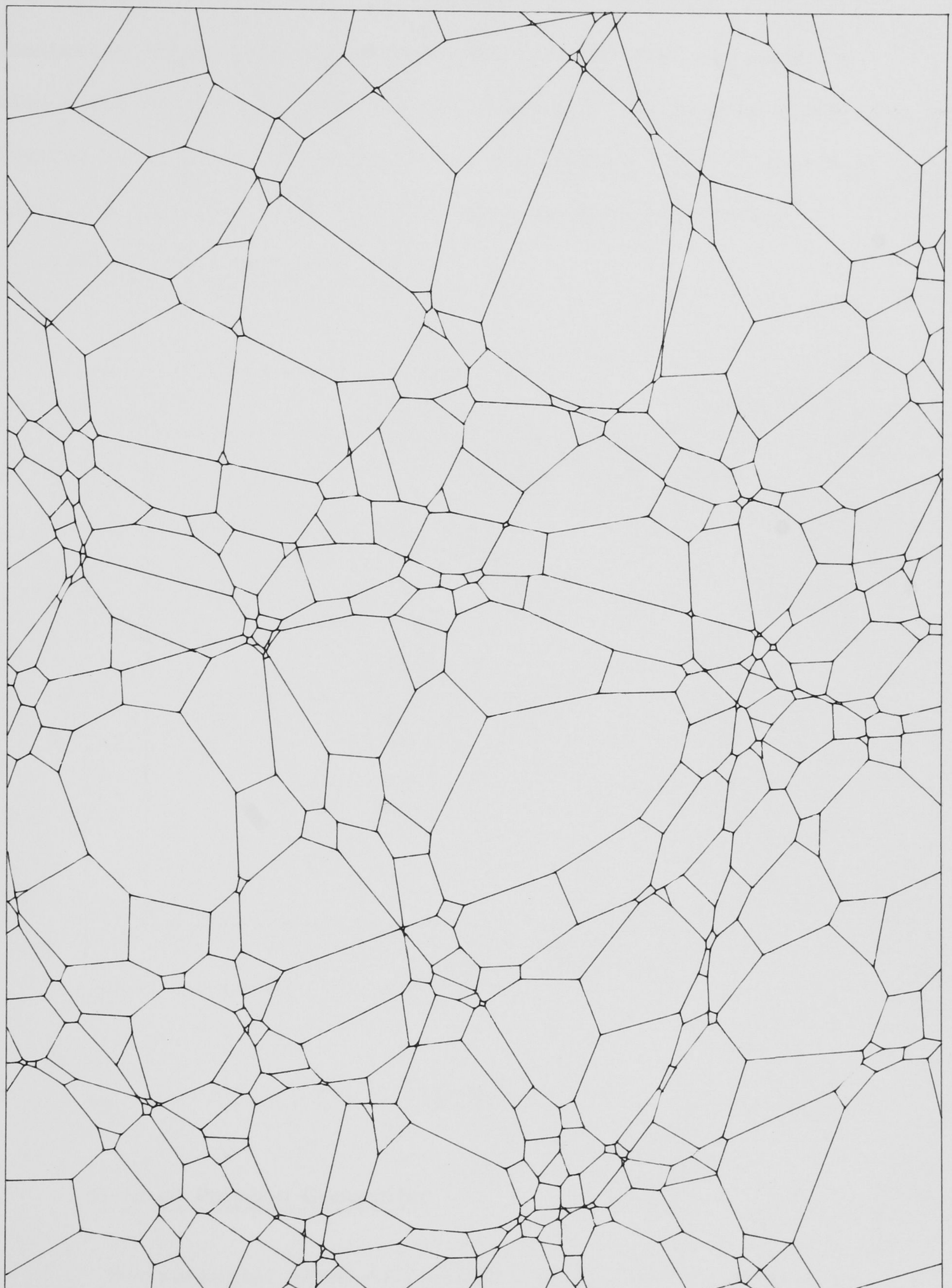

Figure 6. V_{300} *for a set of random particles*

considered in passing along each perpendicular bisector. The only limitation, then, is the amount of data storage available, and the time spent actually storing the required data. The program generating Figures 5 and 6 ran for approximately one hour on a Dec-20 System of the R.S.S.S., A.N.U.. If required, data on all tessellations $V_1, \ldots, V_{300}$ could have been stored.

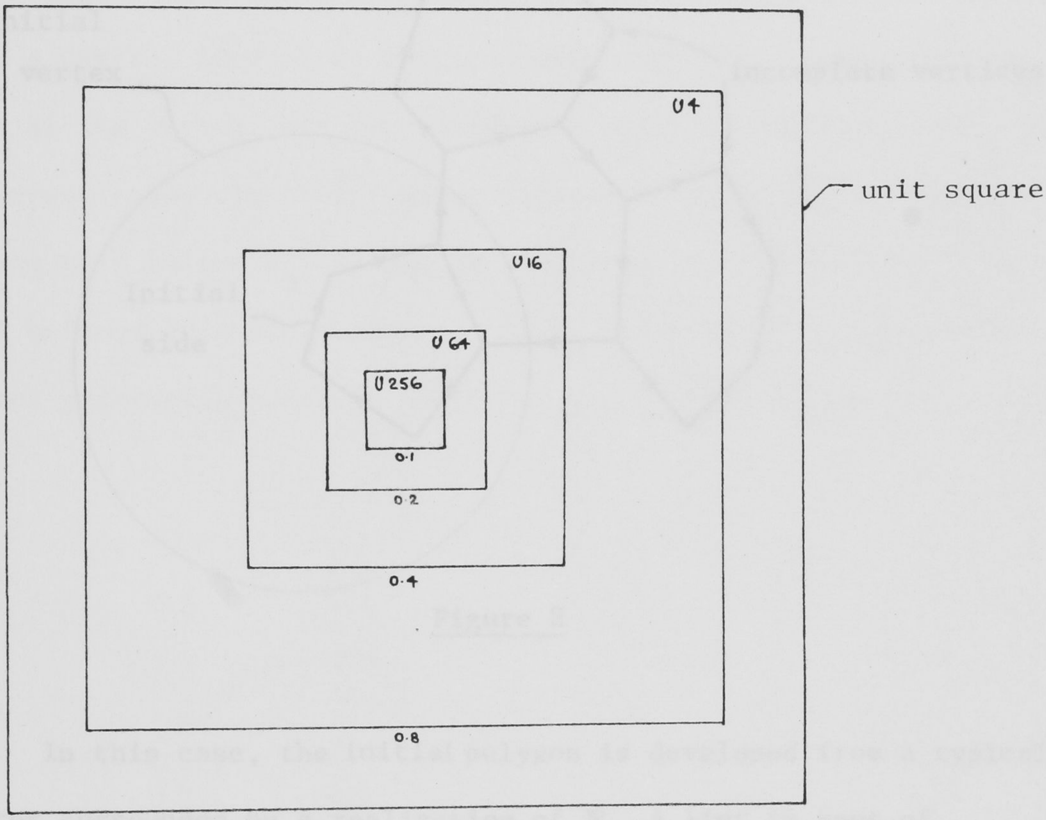

Figure 7

5.4 Individual Polygon Generation

For potential simulation studies of V_n, another program was developed for the generation of individual V_n polygons. This was based on the Stochastic Construction of a typical V_n cell.

The program presents some interesting logical problems in terms of keeping track of particles, base circle or otherwise, in searching appropriate areas for the next vertex, and in proceeding around the polygon in the correct manner, but is basically a straightforward application of the logic of Lemma 3.11. This program can also be used for building up plots of large regions of V_n by applying the algorithm repeatedly to add polygons adjacent to those already generated (see Figure 8).

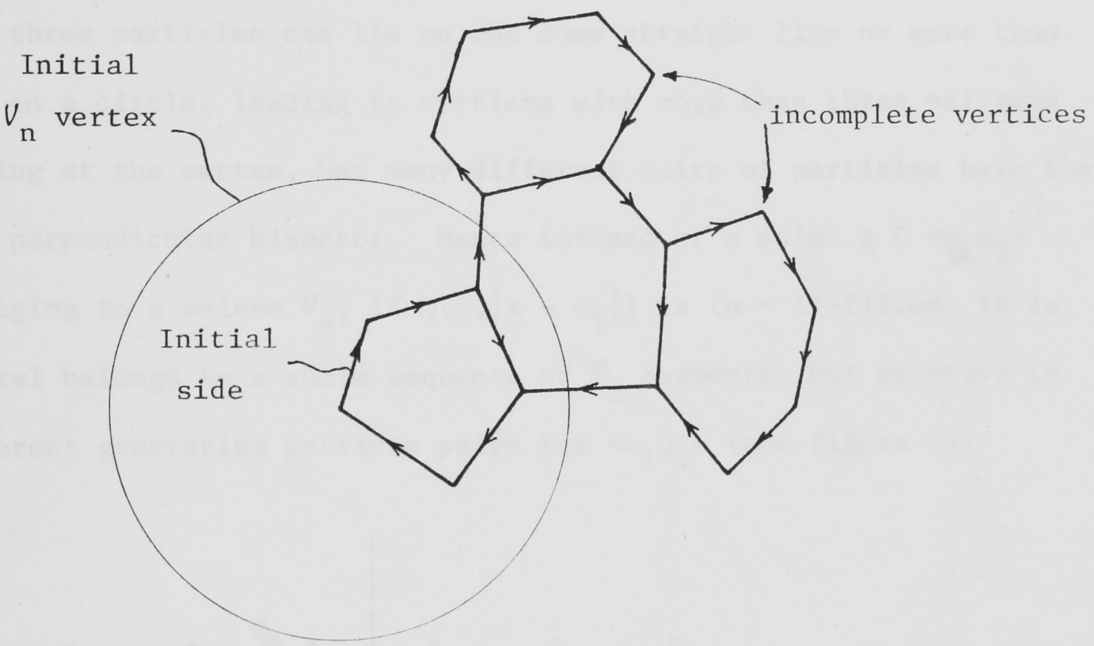

Figure 8

In this case, the initial polygon is developed from a typical V_n vertex surrounded by a realization of $\mathbb{P}$. A list is kept of incomplete vertices i.e. vertices with only two segments joining. The program iterates through the incomplete vertex list, adding the polygon which completes that vertex and an adjacent vertex, and at the same time adding the new incomplete vertices associated with that polygon to the incomplete vertex list. This iteration continues until a specified area is tessellated. A working version of this program was used to generate V_1. It could be applied to the generation of V_n's for very large n with reasonable run times i.e. n $\overline{\sim}$ 2000.

5.5 $\underline{V_n}$'s based on a degenerate square grid

A program was developed for the computation of V_n's based on a degenerate square grid of particles. This was similar in structure to that used for random particles in general position, but there are some interesting fundamental differences between the two cases.

(i) a square grid is degenerate not only in the sense that more than three particles can lie on the same straight line or more than four on a circle, leading to vertices with more than three polygons meeting at the vertex, but many different pairs of particles have the same perpendicular bisector. Hence instead of a point $\underline{x} \in \langle\omega_1\omega_2\rangle$ belonging to a unique V_n, if $Q(\underline{x}, |\underline{x} - \omega_1|)$ is (n - 1)-filled, it in general belongs to a whole sequence of V_n segments, but relative to different generating particle pairs for $\langle\omega_1\omega_2\rangle$ (see Figure 9).

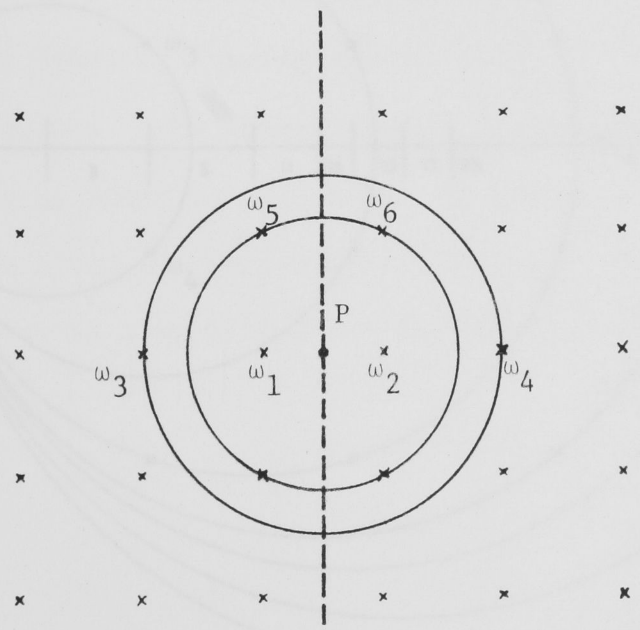

P on $\langle\omega_1\omega_2\rangle$ is in $\mathcal{L}_1$

P on $\langle\omega_3\omega_4\rangle$ is in $\mathcal{L}_7$

P on $\langle\omega_5\omega_6\rangle$ is between $\mathcal{L}_3$ and $\mathcal{L}_5$

Figure 9

(ii) unlike $n_d(\underline{x})$ on $\langle\omega_1\omega_2\rangle$ for the general position case, the jump between successive V_n segments on a perpendicular bisector can and often does exceed one, since more than three particles can be on the one circle (see Figure 10). This effect is easily accomodated into the previous program however. The circumcentres are stored for each particle as before, so if, as in Figure 10, two particles (ω_3 and ω_4 say) lie on the same circle as ω_1 and ω_2, the circumcentre list would be

$$-1,\ -\tfrac{1}{2},\ -\tfrac{1}{2},\ \tfrac{1}{2},\ \tfrac{1}{2},\ 1\ .$$

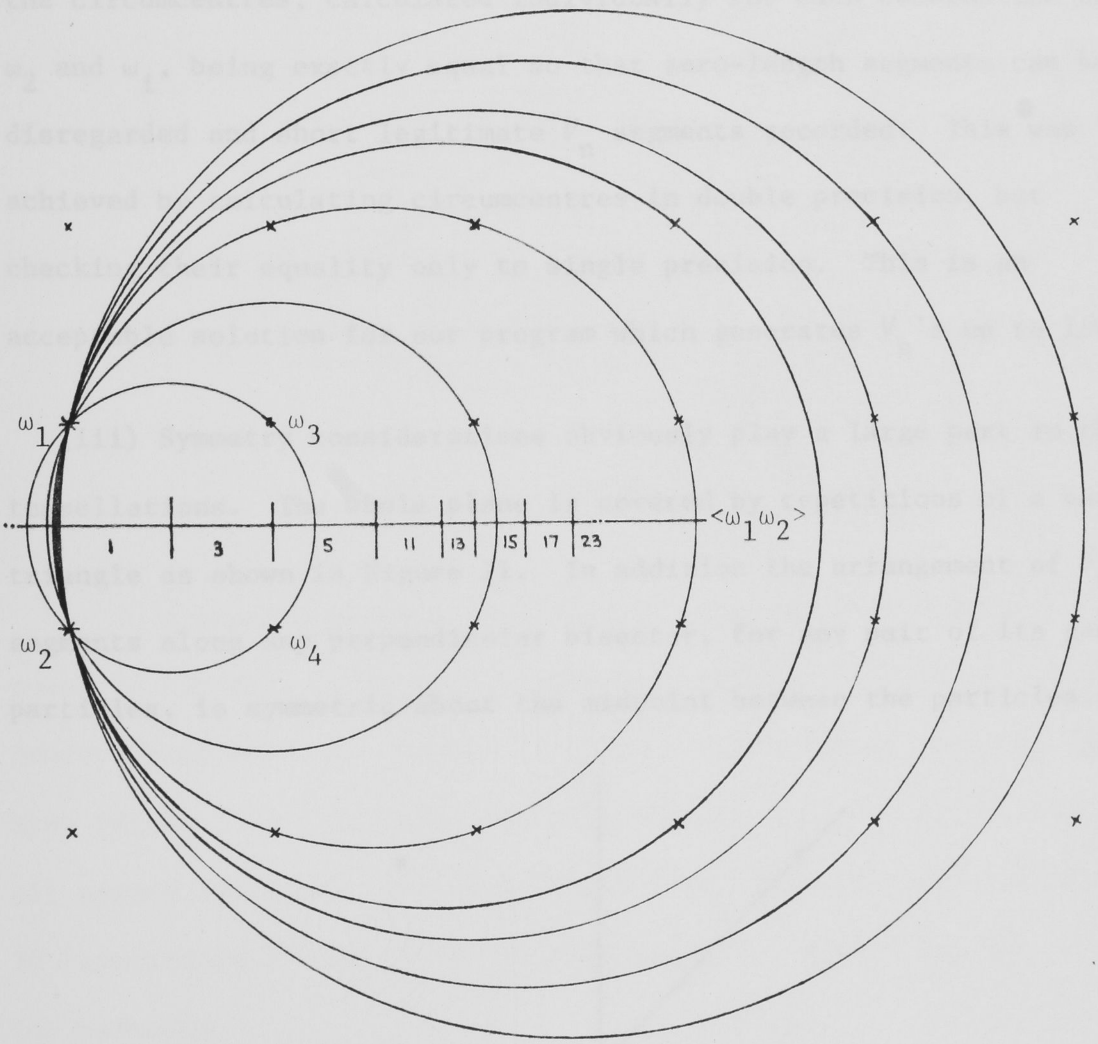

$<\omega_1\omega_2>$ is numbered with $\mathcal{L}_n$ segments.

Figure 10

Since the base circle is zero-filled $(-\frac{1}{2},\frac{1}{2})$ is a V_1 segment. Since the particle generating the first $\frac{1}{2}$, ω_3, was not a base circle particle, we add one to the n value and have a V_2 segment $(\frac{1}{2},\frac{1}{2})$; this segment is not stored however being of zero-length. The n value again rises by one, since ω_4 is not a base circle particle and we have a V_3 segment $(\frac{1}{2},1)$.

For higher n values this effect is magnified with large numbers of particles on the one circle. The solution here depends on the circumcentres, calculated individually for each combination of ω_1, ω_2 and ω_i, being exactly equal so that zero-length segments can be disregarded and short legitimate V_n segments recorded. This was achieved by calculating circumcentres in double precision, but checking their equality only to single precision. This is an acceptable solution for our program which generates V_n's up to 150.

(iii) Symmetry considerations obviously play a large part in these tessellations. The whole plane is covered by repetitions of a basic triangle as shown in Figure 11. In addition the arrangement of V_n segments along any perpendicular bisector, for any pair of its generating particles, is symmetric about the midpoint between the particles.

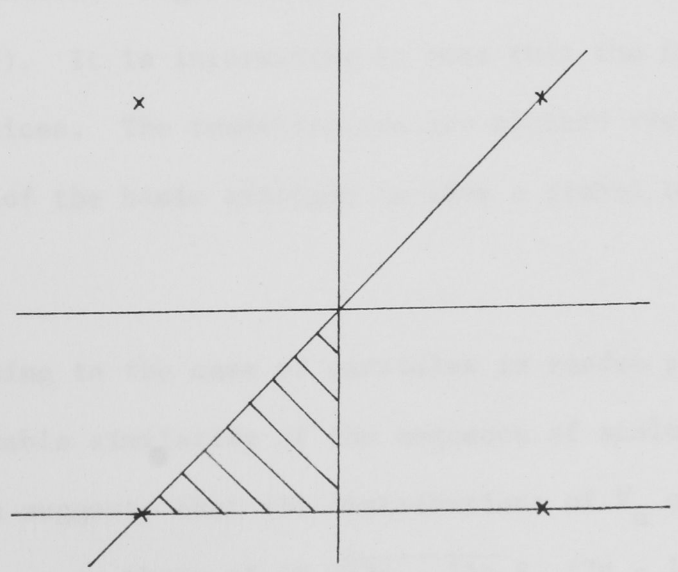

Figure 11

(iv) To ensure that complete tessellations were generated, i.e. that no edge-contiguous particle pairs were missed, the tessellation was generated over a single square region S inside a square grid large enough to ensure that all points in S have at least their nearest n particles determined by the larger grid - a twenty by twenty grid ensures valid V_n in the central region up to approximately 240 (see Figure 12).

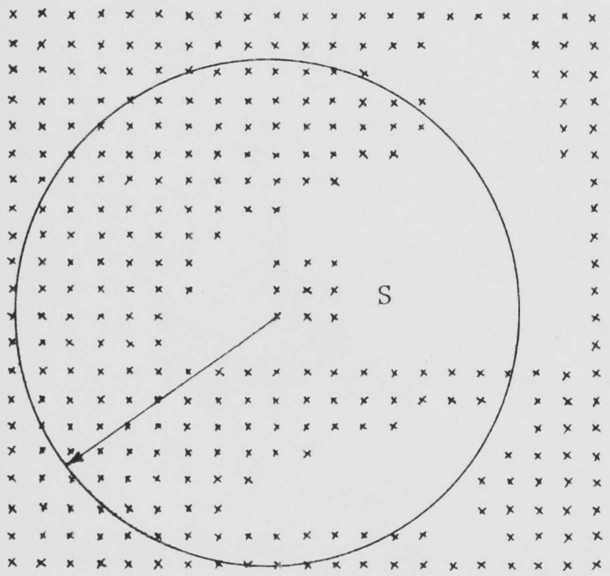

Figure 12

A program using a 20 × 20 grid of particles, over which all possible particle pairs were considered, generated $V_1, V_2, \ldots, V_{150}$ in twenty three minutes. Figure 13 shows a selection of these V_n (see also Figure 3.2). It is interesting to note that the first three are all square lattices. The tessellations are plotted over 9 squares or 36 repetitions of the basic triangle to give a global impression of the patterns.

Returning to the case of particles in random position, we note the remarkable similarity of the sequence of scaled V_n's in Figure 5, which suggests that the distributions of V_n cell characteristics, e.g. those of $(N, \sqrt{(2n - 1)\rho}\ S, (2n - 1)\rho A)$, tend rapidly to non-degenerate limits. This prompted the investigations of limiting distributions undertaken in Chapter 6.

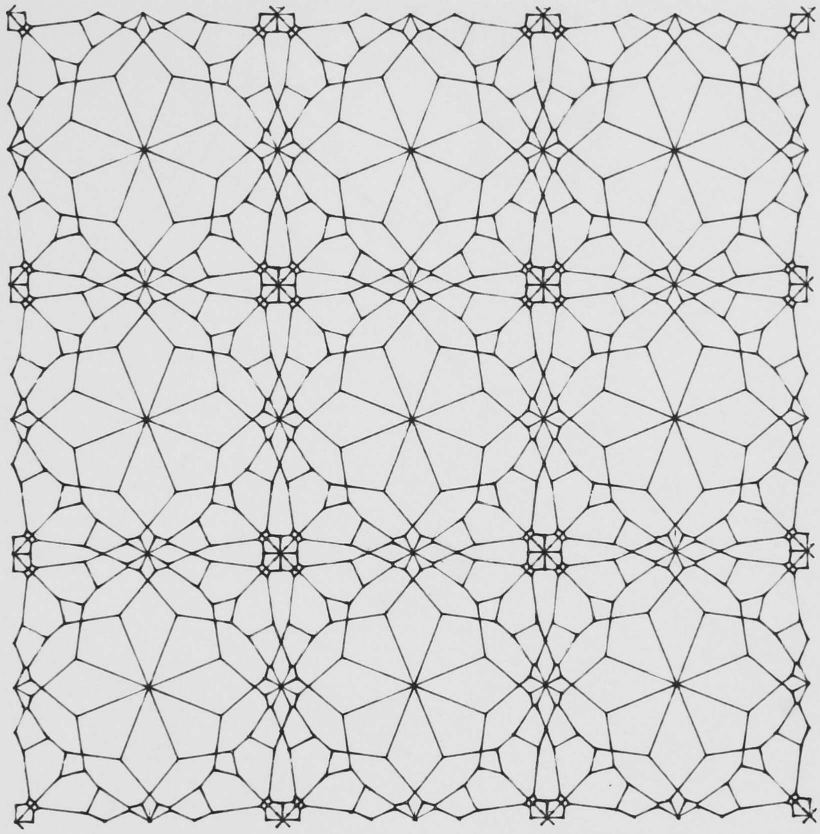

VORONOI - 50

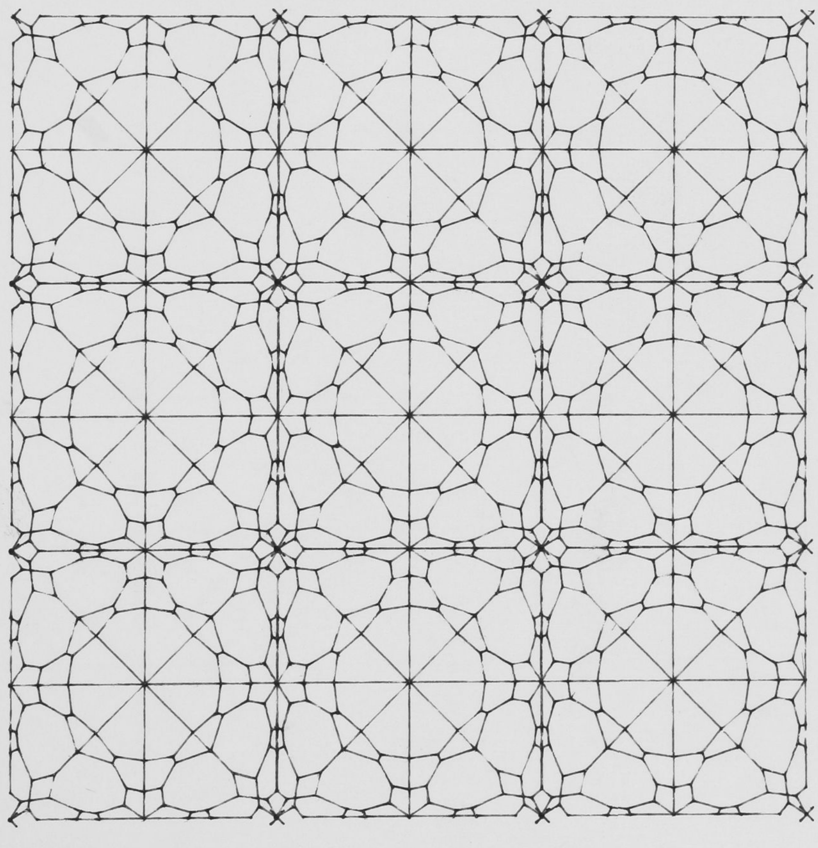

VORONOI - 51

Figure 13 (i). V_n*'s based on a square grid of particles*

The particles are shown by crosses.

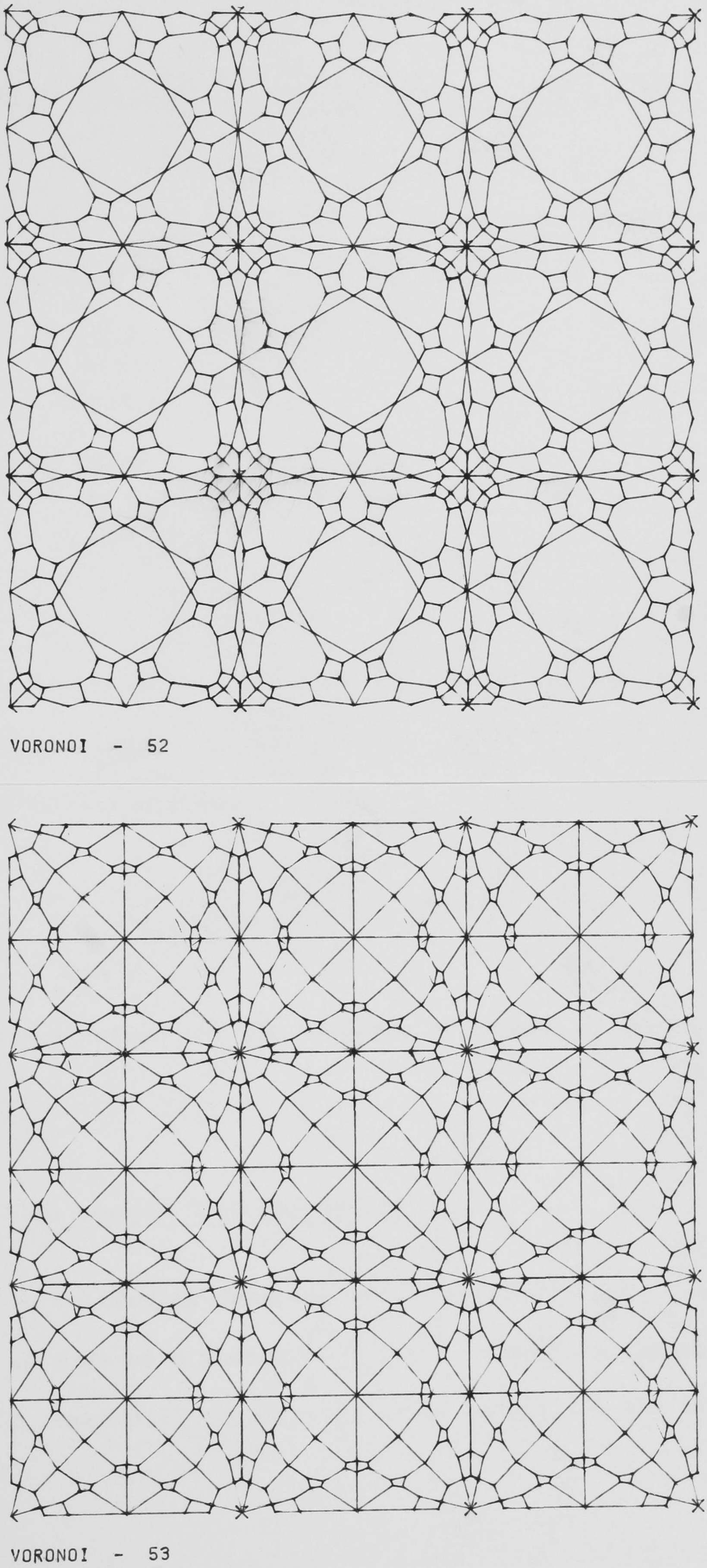

Figure 13 (ii). V_n*'s based on a square grid of particles*

The particles are shown by crosses.

CHAPTER 6

GENERALIZED VORONOI TESSELLATIONS - LIMITING RESULTS

In this chapter we establish some limiting distributions relating to a sequence of scaled V_n tessellations. If we scale the tessellation by $\sqrt{n}$ along both axes the mean cell area is normed to $n[(2n-1)\rho]^{-1}$. This scaling is used for convenience in the derivations and we refer to

$$V'_\infty = \lim_{n\to\infty} \sqrt{n}\, V_n \quad ,$$

as the limiting tessellation, in which the polygon characteristics have the calculated limiting distributions. However the calculated moments are given relative to

$$V_\infty = \lim_{n\to\infty} \sqrt{(2n-1)\rho}\, V_n \quad ,$$

the limiting tessellation for the sequence of normed V_n having unit mean cell area.

6.1 Limiting Side-Length Distribution for V'_∞

In this section we make use of the stochastic construction of a uniform random side of a member of V_n, i.e. a uniform random member of $\mathcal{L}_n$, given in Lemma 3.11, to prove a limit result for the ergodic side-length distribution of V'_∞.

From Lemma 3.10 we have the following ergodic results for an N-filled vertex of V_n (see Figure 1).

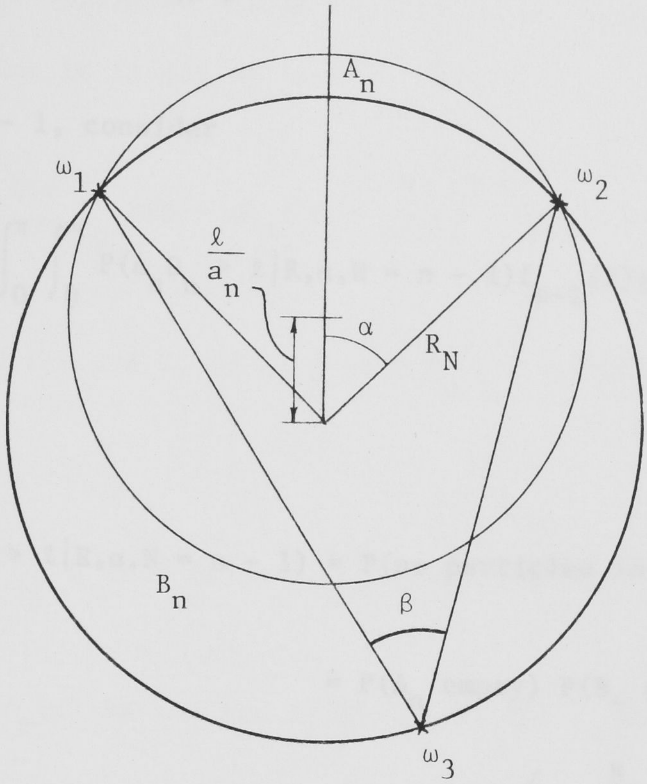

Figure 1

$$R_N \sim \Gamma_2(2N + 4, \pi\rho) \text{ with p.d.f. } f_N(R)$$

$$N = \begin{cases} n - 1 \text{ with probability } p_{n-1} = {}^{n}/(2n-1) \to \tfrac{1}{2} \text{ as } n \to \infty \\ n - 2 \quad '' \quad\quad '' \quad\quad p_{n-2} = {}^{(n-1)}/(2n-1) \to \tfrac{1}{2} \text{ as } n \to \infty. \end{cases}$$

α, half the angular separation of two circumferential particles, has the same distribution as a random angle in a Delaunay tessellation (since $2\alpha = 2\beta$ in Figure 1).

Hence $\quad g(\alpha) = \text{p.d.f. of } \alpha = \dfrac{4 \sin \alpha}{3\pi} (\sin \alpha + (\pi - \alpha)\cos \alpha) \quad .$

Let D_n denote the length of a random side of V_n, and consider $P(a_n D_n > \ell)$, where $a_n > 0$ and $a_n \to \infty$ as $n \to \infty$, $\ell > 0$.

$$P(a_nD_n > \ell) = \sum_{i=n-1,n-2} \iint P(a_nL_n > \ell \mid R,\alpha,N = i) f_i(R)g(\alpha)d\alpha dR \tag{1.1}$$

Assuming i = n - 1, consider

$$\lim_{n\to\infty} \int_0^{\pi}\int_0^{\infty} P(a_nD_n > \ell \mid R,\alpha,N = n-1) f_{n-1}(R)g(\alpha)dRd\alpha \tag{1.2}$$

From Figure 1,

$$\begin{aligned} P(a_nD_n > \ell \mid R,\alpha,N = n-1) &= P(\text{no particles in } A_n \text{ or } B_n) \\ &= P(A_n \text{ empty})\, P(B_n \text{ empty}) \\ &= \exp\{-\rho A_n\}\left(1 - \frac{B_n}{\pi R^2}\right)^{n-1} \quad , \end{aligned}$$

where A_n and B_n are functions of ℓ, a_n, α and R. Hence (1.2) becomes

$$\int_0^{\pi}\left[\lim_{n\to\infty}\int_0^{\infty} \exp\{-\rho A_n\}\left(1 - \frac{B_n}{\pi R^2}\right)^{n-1} f_{n-1}(R)dR\right]g(\alpha)d\alpha \tag{1.3}$$

where, since the inner integral in (1.2) is bounded by one, which is integrable on $[0,\pi]$, we have interchanged the limit and integration by Lebesque's dominated convergence theorem.

As $R_{n-1} \sim \Gamma_2(2n + 2,\pi\rho)$,

$$E(R_{n-1}) = \frac{\Gamma\left(\frac{2n+3}{2}\right)}{\Gamma(n+1)} \frac{1}{\sqrt{\pi\rho}} \to \sqrt{\frac{n}{\pi\rho}} \quad \text{as} \quad n \to \infty$$

$$\mathrm{Var}(R_{n-1}) = \frac{n+1}{\pi\rho} - (ER_{n-1})^2 \to \frac{1}{\pi\rho}, \quad \text{as} \quad n \to \infty \quad .$$

Hence for $C_{n-1} = R_{n-1}/\sqrt{n}$, as $n \to \infty$ $E(C_{n-1}) \to \frac{1}{\sqrt{\pi\rho}}$ and $Var(C_{n-1}) \to \frac{1}{n\pi\rho}$. Therefore making the change of variable $r = R/\sqrt{n}$ in the inner integral in (1.3), we have

$$\lim_{n\to\infty} \int_0^\infty \exp\{-\rho A_n\}\left(1 - \frac{B_n}{n\pi r^2}\right)^{n-1} f^*_{n-1}(r)dr \quad , \tag{1.4}$$

where $f^*_{n-1}(r)$ is the p.d.f. of C_{n-1} with $C_{n-1} \xrightarrow{p} 1/\sqrt{\pi\rho}$ as $n \to \infty$. We need the

<u>Lemma 1</u> $$\lim_{n\to\infty} \int g_n(x) f_n(x)dx = \lim_{n\to\infty} g_n(a), \quad \text{if} \quad X_n \xrightarrow{p} a$$

as $n \to \infty$, where $f_n(x)$ is the p.d.f. of X_n and the g_n are continuous and bounded.

A proof of Lemma 1 is appended to this section. Applying Lemma 1 to (1.4) we have

$$\lim_{n\to\infty} \int_0^\infty \exp\{-\rho A_n\}\left(1 - \frac{B_n}{n\pi r^2}\right)^{n-1} f^*_{n-1}(r)dr$$

$$= \lim_{n\to\infty} \exp\{-\rho A_n\}\left(1 - \frac{B_n}{n\pi r^2}\right)^{n-1}\Bigg|_{r=\frac{1}{\sqrt{\pi\rho}}}$$

$$= \lim_{n\to\infty} \exp\left\{-\rho A_n(\ell,\alpha,a_n,R)\right\}\left(1 - \frac{B_n(\ell,\alpha,a_n,R)}{\pi R^2}\right)^{n-1}\Bigg|_{R=\sqrt{\frac{n}{\pi\rho}}}$$

We now consider the limits of $A_n(\ell,\alpha,a_n,R)$ and $B_n(\ell,\alpha,a_n,R)$ (see Figure 2)

$$A_n = R'^2(\theta - \sin\theta\cos\theta) - R^2(\alpha - \sin\alpha\cos\alpha) \quad ,$$

where $R'^2 = (R \sin \alpha)^2 + (R \cos \alpha - \ell/a_n)^2 = R^2 - \dfrac{2\ell \cos \alpha}{a_n} + \dfrac{\ell}{a_n^2}$

and $\sin \theta = \dfrac{R \sin \alpha}{R'}$, $\cos \theta = \dfrac{(R \cos \alpha - \ell/a_n)}{R'}$

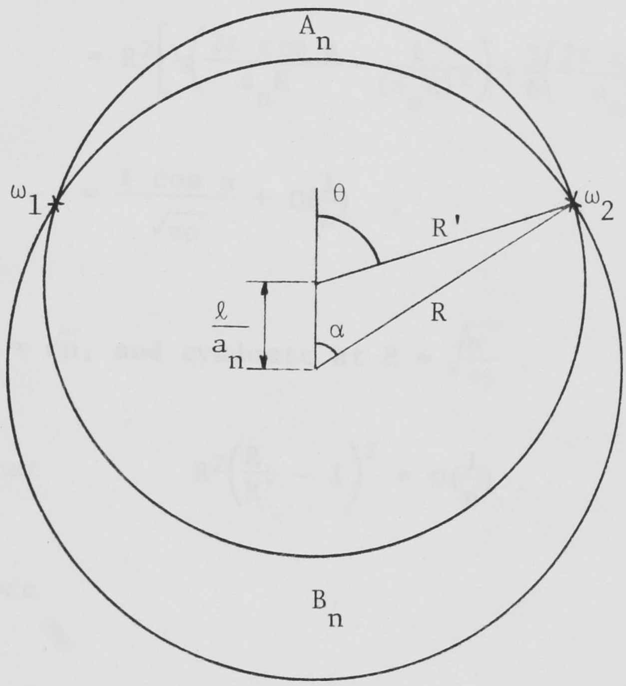

Figure 2

Hence $A_n = \theta R'^2 - R \sin \alpha (R \cos \alpha - \ell/a_n) - \alpha R^2 + R^2 \sin \alpha \cos \alpha$

$$= \sin^{-1}\left(\frac{R \sin \alpha}{R'}\right) R'^2 + \frac{R\ell \sin \alpha}{a_n} - \alpha R^2$$

$$= R^2\left\{\sin^{-1} \frac{R \sin \alpha}{R'} - \alpha\right\} - \left(\frac{2\ell R \cos \alpha}{a_n} - \frac{\ell}{a_n^2}\right)\sin^{-1}\left(\frac{R \sin \alpha}{R'}\right) + \frac{R\ell \sin \alpha}{a_n}$$

Expanding $\sin^{-1}$ as a Taylor series about $\sin \alpha$,

$$A_n = R^2\left(\alpha + \tan\alpha\left(\frac{R}{R'} - 1\right) - \tan^3\alpha\left(\frac{R}{R'} - 1\right)^2 + \ldots - \alpha\right)$$

$$- \left(\frac{2\ell R \cos\alpha}{a_n} - \frac{\ell}{a_n^{\,2}}\right)\sin^{-1}\left(\frac{R \sin\alpha}{R'}\right) + \frac{R\ell \sin\alpha}{a_n}$$

Consider $R^2\left(\frac{R}{R'} - 1\right) = R^2\left[\frac{1}{\sqrt{1 - \frac{2\ell\cos\alpha}{a_n R} + \frac{\ell}{(a_n R)^2}}} - 1\right]$

$$= R^2\left[\tfrac{1}{2}\left(\frac{2\ell\cos\alpha}{a_n R} - \frac{\ell}{(a_n R)^2}\right) + \frac{3}{6}\left(\frac{2\ell\cos\alpha}{a_n R} - \frac{\ell}{(a_n R^2)}\right)^2 - \ldots\right]$$

$$= \frac{\ell\cos\alpha}{\sqrt{\pi\rho}} + O(\tfrac{1}{n}) \quad ,$$

if we choose $a_n = \sqrt{n}$, and evaluate at $R = \sqrt{\frac{n}{\pi\rho}}$.

Note that $\qquad R^2\left(\frac{R}{R'} - 1\right)^2 = O(\frac{1}{n})$.

Therefore

$$A_n = \tan\alpha\left(\frac{\ell\cos\alpha}{\sqrt{\pi\rho}}\right) - \left(\frac{2\ell\cos\alpha}{\sqrt{\pi\rho}} - \frac{\ell}{n}\right)\left(\alpha + O(\tfrac{1}{n})\right) + \frac{\ell\sin\alpha}{\sqrt{\pi\rho}}$$

$$= \frac{2\ell\sin\alpha}{\sqrt{\pi\rho}} - \frac{2\ell\alpha\cos\alpha}{\sqrt{\pi\rho}} + O(\tfrac{1}{n})$$

$$B_n = \pi(R^2 - R'^2) + A_n$$

$$= \frac{2\ell}{\sqrt{\pi\rho}}(\sin\alpha + (\pi - \alpha)\cos\alpha) + O(\tfrac{1}{n})$$

and $\qquad \lim_{n\to\infty} A_n\left(\ell,\alpha,\sqrt{n},\sqrt{\frac{n}{\pi\rho}}\right) = \frac{2\ell}{\sqrt{\pi\rho}}(\sin\alpha - \alpha\cos\alpha)$

$$\lim_{n\to\infty} B_n\left(\ell,\alpha,\sqrt{n},\sqrt{\frac{n}{\pi\rho}}\right) = \frac{2\ell}{\sqrt{\pi\rho}}(\sin\beta - \beta\cos\beta) = B \text{ say} \quad ,$$

where $\beta = \pi - \alpha$.

Substituting the above in (1.5),

$$\lim_{n\to\infty} \exp\{-\rho A_n\}\left(1 - \frac{\rho B_n}{n}\right)^{n-1}\Bigg|_{R=\sqrt{\frac{n}{\pi\rho}}}$$

$$= \exp\left\{-\rho.\frac{2\ell}{\sqrt{\pi\rho}}(\sin\alpha - \alpha\cos\alpha)\right\}\lim_{n\to\infty}\left(1 - \frac{\rho B_n}{n}\right)^{n-1}$$

$$= \exp\left\{-2\ell\sqrt{\frac{\rho}{\pi}}(\sin\alpha - \alpha\cos\alpha)\right\}\lim_{n\to\infty}\left(1 - \frac{\rho B}{n} + \frac{O(\frac{1}{n})}{n}\right)^{n-1}$$

$$= \exp\left\{-2\ell\sqrt{\frac{\rho}{\pi}}(\sin\alpha - \alpha\cos\alpha)\right\}\exp\{-\rho B\}$$

$$= \exp\left\{-4\ell\sqrt{\frac{\rho}{\pi}}\left(\sin\alpha + (\frac{\pi}{2} - \alpha)\cos\alpha\right)\right\} \qquad (1.6)$$

Clearly $\lim P(a_n D_n > \ell|R,\alpha,N)$ is the same for both $N = n - 1$ and $N = n - 2$, and since $p_{n-1}, p_{n-2} \to \frac{1}{2}$ as $n \to \infty$, (1.1), (1.3), (1.5) and (1.6) combined give

$$\lim_{n\to\infty} P(\sqrt{n}D_n > \ell) = \int_0^\pi \exp\left\{-4\ell\sqrt{\frac{\rho}{\pi}}\left(\sin\alpha + (\frac{\pi}{2} - \alpha)\cos\alpha\right).g(\alpha)d\alpha\right\}.$$

Hence we have established the

<u>Theorem 1</u>

Let D_n denote the length of a <u>uniform random</u> member of $\mathcal{L}_n$. Then the sequence $\{\sqrt{n}D_n\}$ converges in distribution to D'_∞, the side length for a <u>uniform random</u> member of V'_∞, with

$$P(D'_\infty > \ell) = \int_0^\pi \exp\left\{-4\ell\sqrt{\frac{\rho}{\pi}}\left(\sin\alpha + (\frac{\pi}{2} - \alpha)\cos\alpha\right)\right\}\frac{4\sin\alpha}{3\pi}(\sin\alpha + (\pi-\alpha)\cos\alpha)d\alpha.$$

Since D'_∞ is positive, we can calculate the mean as

$$E(D'_\infty) = \int_0^\infty P(D'_\infty > x)dx$$

$$= \int_0^\pi \int_0^\infty \exp\left\{-4x\sqrt{\frac{\rho}{\pi}}\left(\sin\alpha + (\frac{\pi}{2}-\alpha)\cos\alpha\right)\right\}dx\ \frac{4\sin\alpha}{3\pi}(\sin\alpha + (\pi-\alpha)\cos\alpha)d\alpha$$

$$= \int_0^\pi \frac{\sin\alpha(\sin\alpha + (\pi-\alpha)\cos\alpha)}{3\sqrt{\rho\pi}\left(\sin\alpha + (\frac{\pi}{2}-\alpha)\cos\alpha\right)}\, d\alpha$$

$$= (3\sqrt{\rho\pi})^{-1}\left[\int_0^\pi \sin\alpha d\alpha + \int_0^\pi \frac{\pi}{2}.\frac{\sin\alpha\cos\alpha}{\left(\sin\alpha + (\frac{\pi}{2}-\alpha)\cos\alpha\right)}\, d\alpha\right]$$

$$= 2/3\sqrt{\rho\pi} \quad .$$

This result checks with the known results for $E(S)$ and $E(N)$ from section 3.1, since, from section 1.2 we have

$$E(S) = \lim_{R\to\infty} \sum_{\text{cells in } Q(R)} S_i/N(R)$$

$$E(N) = \lim_{R\to\infty} \sum_{\text{cells in } Q(R)} N_i/N(R)$$

and

$$E(L) = \lim_{R\to\infty} \sum_{\text{edges in } Q(R)} L_i/N_\ell(R) \quad ,$$

where the S_i denotes perimeter, N_i number of sides and L_i edge length of cells, $N(r)$ = total number of cells in $Q(R)$ and $N_\ell(R)$ = total number of edges in $Q(R)$.

Also $\quad N_\ell(R) = \tfrac{1}{2}\Sigma N_i$ and $\Sigma S_i = 2\Sigma L_i$, so

$$\frac{\Sigma S_i}{N(r)} = \frac{2\Sigma L_i}{N(r)}\frac{\tfrac{1}{2}\Sigma N_i}{\tfrac{1}{2}\Sigma N_i} = \frac{\Sigma L_i}{N_\ell(R)}\frac{\Sigma N_i}{N(r)} \quad ,$$

and hence $\quad E(L) = E(S)/E(N) \quad .$

Higher moments for D'_∞ can be obtained numerically.

$$E(D'^m_\infty) = m\int_0^\infty x^{m-1}P(D'_\infty > x)dx$$

$$= \frac{4m!}{3\pi\left(4\sqrt{\frac{\rho}{\pi}}\right)^m}\int_0^\pi \frac{\sin\alpha(\sin\alpha + (\pi-\alpha)\cos\alpha)}{\left[\sin\alpha + (\frac{\pi}{2}-\alpha)\cos\alpha\right]^m}\,d\alpha$$

$$= \frac{m!\,\pi^{m/2-1}}{3.4^{m-1}\rho^{m/2}}\left[\int_0^\pi \frac{\sin\alpha d\alpha}{\left(\sin\alpha + (\frac{\pi}{2}-\alpha)\cos\alpha\right)^{m-1}} + \frac{\pi}{2}\int_0^\pi \frac{\sin\alpha\cos\alpha}{\left[\sin\alpha + (\frac{\pi}{2}-\alpha)\cos\alpha\right]^m}\right]$$

The second integral disappears since the integrand is odd about $\frac{\pi}{2}$. Hence

$$E(D'^m_\infty) = \frac{2m!\,\pi^{m/2-1}}{3.4^{m-1}}\int_0^{\pi/2} \frac{\sin\alpha d\alpha}{\left(\sin\alpha + (\frac{\pi}{2}-\alpha)\cos\alpha\right)^{m-1}} \qquad (1.7)$$

In Table 1 we list the moments of D_∞, the side length for a uniform random member of V_∞, numerically calculated from (1.7).

Table 1

m	$E(D_\infty{}^m)$
1	0.532
2	0.576
3	0.952
4	2.13
$\mathrm{Var}(D_\infty)$	0.293

Proof of Lemma 1

Let $\quad \ell = \lim_{n\to\infty} g_n(a)$, and $F_n(x)$ the d.f. of X_n .

Consider

$$\left|\int g_n(x) f_n(x)dx - \ell\right|$$

$$= \left|\int g_n(x) f_n(x)dx - \int g_N(x) f_n(x)dx + \int g_N(x) f_n(x)dx - g_N(a) + g_N(a) - \ell\right|$$

$$\leq \left|\int g_n(x) f_n(x)dx - \int g_N(x) f_n(x)dx\right| + \left|\int g_N(x) f_n(x)dx - g_N(a)\right| + \left|g_N(a) - \ell\right|$$

$$\leq \int \left|g_n(x) - g_N(x)\right| f_n(x)dx + \left|\int g_N(x)dF_n(x) - g_N(a)\right| + \left|g_N(a) - \ell\right|$$

Let $\varepsilon > 0$.

As $\lim_{n\to\infty} g_n(a) = \ell$, $\exists N_1$ such that $\forall n > N_1$, $|g_n(a) - \ell| < \varepsilon/3$.

As $F_n \to F(x)$, the d.f. for a random variable degenerate at 'a', and the g_n are bounded and continuous, we can apply the Helly-Bray Theorem to obtain

$$\int g_N(x)dF_n(x) \to \int g_N(x)dF(x) = g_N(a)$$

i.e. $\quad \exists N_2$ such that $\forall n > N_2$, $\left|\int g_N(x)dF_n(x) - g_N(a)\right| < \varepsilon/3$.

Finally as $\{g_n(a)\}$ is a Cauchy sequence,

$$\exists N_3 \text{ such that } \forall n,m > N_3,\ |g_n(a) - g_m(a)| < \varepsilon/3 .$$

Hence $\forall\varepsilon > 0$, choosing $N > \max\{N_1,N_3\}$ and $n > \max\{N_2,N_3\}$ ensures that

$$\left|\int g_n(x)f_n(x)dx - \ell\right| < \varepsilon/3 + \varepsilon/3 + \varepsilon/3 < \varepsilon$$

i.e. $$\lim_{n\to\infty} \int g_n(x)f_n(x)dx = \lim_{n\to\infty} g_n(a) \quad ,$$

which completes the lemma.

6.2 Limiting Transect Distribution for V'_∞

In section 4.5 we defined J'_n as $\sqrt{n}J_n$, where J_n is the distance from an arbitrary point to the next 'event', or intersection with the tessellation, on a linear transect of V_n. We now establish the limiting distribution of J'_n; $J'_n \xrightarrow{d} J'_\infty$, the transect distribution for the scaled aggregate $V'_\infty = \lim_{n\to\infty} \sqrt{n}V_n$.

Now, from (4.5.2) and using the notation of section 4.5 (see Figure 4.19)

$$P(J'_\infty > x) = \lim_{n\to\infty} P(\sqrt{n}J_n > x)$$

$$= \lim_{n\to\infty} \int_0^\infty \int_0^{r_{n+1}+x/\sqrt{n}} P(\text{An empty, } w_{n+1} \notin q(\alpha) | r_{n+1}, s_n) f(s_n | r_{n+1}) ds_n h(r_{n+1}) dr_{n+1} . \tag{2.1}$$

Since $R_{n+1} \sim \Gamma_2(2n + 2, \pi\rho)$,

$$E(R_{n+1}) = \sqrt{\frac{n}{\pi\rho}}$$

$$\mathrm{Var}(R_{n+1}) \to {}^1/_{\pi\rho} \quad \text{as} \quad n \to \infty .$$

So $R'_{n+1} = R_{n+1}/\sqrt{n} \xrightarrow{p} {}^1/_{\sqrt{\pi\rho}}$, and

$$P(J'_\infty > x) = \lim \int_0^\infty \left[\int_0^{\sqrt{n}r'_{n+1}+x/\sqrt{n}} P(\text{An empty, } w_{n+1} \notin q(\alpha) \,|\, r_{n+1}, s_n) f(s_n \,|\, r_{n+1}) ds_n \right].$$

$$h^*(r'_{n+1}) dr'_{n+1} \quad ,$$

where h^* is the p.d.f. of R'_{n+1}. The inner integral is bounded and continuous, so, by lemma 1,

$$P(J'_\infty > x) = \lim_{n\to\infty} \int_0^{\sqrt{\frac{n}{\pi\rho}}+x/\sqrt{n}} P\left(\text{An empty, } w_{n+1} \notin q(\alpha) \,|\, r_{n+1} = \sqrt{\frac{n}{\pi\rho}}, s_n\right).$$

$$f\left(s_n \,|\, r_{n+1} = \sqrt{\frac{n}{\pi\rho}}\right) ds_n \ .$$

Since x is fixed, eventually $\sqrt{\frac{n}{\pi\rho}} > x/\sqrt{n}$, so $f\left(s_n \,|\, r_{n+1} = \sqrt{\frac{n}{\pi\rho}}\right)$ has support $\left(0, \sqrt{\frac{n}{\pi\rho}} + x/\sqrt{n}\right)$. Using (4.5.3) and (4.5.5),

$$P(J'_\infty > x) = \lim_{n\to\infty} \left\{ P\left(S_n < \sqrt{\frac{n}{\pi\rho}} - x/\sqrt{n} \,|\, r_{n+1} = \sqrt{\frac{n}{\pi\rho}}\right) \right.$$

$$\left. + \int_{\sqrt{\frac{n}{\pi\rho}}-x/\sqrt{n}}^{\sqrt{\frac{n}{\pi\rho}}+x/\sqrt{n}} \left(1 - \frac{\alpha}{\pi}\right) e^{-\rho|A_n|} \frac{2n\beta}{\pi.\left(\sqrt{\frac{n}{\pi\rho}}\right)^2} \left(1 - \frac{|B_n|}{\pi\left(\sqrt{\frac{n}{\pi\rho}}\right)^2}\right)^{n-1} s_n ds_n \right\}$$

From Figure 20 and (4.5.6),

$$P\left(S_n < \sqrt{\frac{n}{\pi\rho}} - x/\sqrt{n} \,|\, r_{n+1} = \sqrt{\frac{n}{\pi\rho}}\right) = \left(1 - \frac{|C_n|}{\pi r_{n+1}^2}\right)^n$$

$$= \left(1 - \frac{2x\sqrt{\pi\rho}}{n} + \frac{x^2\pi\rho}{n^2}\right)^n \to \exp\{-\,2x\sqrt{\pi\rho}\}$$

$$\text{as } n \to \infty \quad .$$

In the integral we make the change of variable to $y_n = \sqrt{\frac{n}{\pi\rho}}\, s_n - \frac{n}{\pi\rho}$, giving

$$\lim_{n\to\infty}\int_{-x/\sqrt{\pi\rho}}^{x/\sqrt{\pi\rho}}\left(1-\frac{\alpha}{\pi}\right)\exp\left\{-\rho A_n\left(\sqrt{\frac{n}{\pi\rho}},\sqrt{\frac{\pi\rho}{n}}(y_n+\frac{n}{\pi\rho}),\frac{x}{\sqrt{n}}\right)2\beta\rho\left(1-\rho\frac{|B_n|}{n}\right)^{n-1}\left(1+\frac{\pi\rho y_n}{n}\right)dy_n\right.$$

$$=\int_{-x/\sqrt{\pi\rho}}^{x/\sqrt{\pi\rho}}\lim_{n\to\infty}\left(1-\frac{\alpha}{\pi}\right)\exp\{-\rho|A_n|\}2\beta\rho\left(1-\rho\,\frac{|B_n|}{n}\right)^{n-1}\left(1+\frac{\pi\rho y_n}{n}\right)dy_n$$

since the integrand is bounded on a finite interval.

Using Lemma 4.4 we can establish that

$$A_n\left(\sqrt{\frac{n}{\pi\rho}},\sqrt{\frac{\pi\rho}{n}}(y_n+\frac{n}{\pi\rho}),x/\sqrt{n}\right)=\frac{2x}{\sqrt{\pi\rho}}\left(1-\frac{y_n{}^2\pi\rho}{x^2}\right)^{\frac{1}{2}}+2y_n\cos^{-1}\left(-\frac{y_n\sqrt{\pi\rho}}{x}\right)+O(\frac{1}{n})$$

$$=A(y_n)+O(\frac{1}{n})\ ,$$

$$B_n\left(\sqrt{\frac{n}{\pi\rho}},\sqrt{\frac{\pi\rho}{n}}(y_n+\frac{n}{\pi\rho}),x/\sqrt{n}\right)=A(y_n)-2\pi y_n+O(\frac{1}{n}),$$

and

$$\lim_{n\to\infty}\beta\left(\sqrt{\frac{n}{\pi\rho}},\sqrt{\frac{\pi\rho}{n}}(y_n+\frac{n}{\pi\rho}),x/\sqrt{n}\right)=\cos^{-1}\left(\frac{y_n\sqrt{\pi\rho}}{x}\right)$$

$$\lim_{n\to\infty}\alpha\left(\sqrt{\frac{n}{\pi\rho}},\sqrt{\frac{\pi\rho}{n}}(y_n+\frac{n}{\pi\rho}),x/\sqrt{n}\right)=\cos^{-1}\left(-\frac{y_n\sqrt{\pi\rho}}{x}\right)\ .$$

Note also that $\lim_{n\to\infty}\left(1-\frac{\rho B_n}{n}\right)^{n-1}=\lim_{n\to\infty}\left(1-\frac{\rho}{n}(A(y_n)-2\pi y_n)+\frac{O(\frac{1}{n})}{n}\right)^{n-1}$

$$=\exp\{-\rho(A(y_n)-2\pi y_n)\}\ .$$

Hence the integral becomes

$$\int_{-x/\sqrt{\pi\rho}}^{x/\sqrt{\pi\rho}}\exp\left\{-2\rho(A(y_n)-\pi y_n)\frac{2\rho}{\pi}\left\{\cos^{-1}(y_n\sqrt{\pi\rho}/x)\right\}^2dy_n\right.$$

$$=\frac{2\sqrt{\rho}}{\pi^{3/2}}\int_{-1}^{1}x\exp\left\{-2\sqrt{\frac{\rho}{\pi}}(A(p)-\pi p)x\right\}(\cos^{-1}p)^2dp\quad,$$

where $\quad A(p) = 2(1 - p^2)^{\frac{1}{2}} + 2p\cos^{-1}(-p)$.

Collecting the above results gives the

Theorem 2 Let J_n denote the transect length from an arbitrary point to the first intersection with the tessellation on a linear transect of V_n. Then the sequence $\{\sqrt{n}J_n\}$ converges in distribution to J'_∞, the transect length for a uniform random member of V'_∞, with

$$P(J'_\infty > x) = \exp\{-2\sqrt{\pi\rho}x\} + \frac{2\sqrt{\rho}}{\pi^{3/2}} \int_{-1}^{1} x \exp\left\{-2\sqrt{\frac{\rho}{\pi}}[A(p) - \pi p)]x\right\}(\cos^{-1}p)^2 dp$$

We are interested in the moments of J'_∞.

$$E(J'^m_\infty) = m \int_0^\infty x^{m-1} P(J'_\infty > x)dx$$

$$= \frac{m!}{2^m \pi^{m/2}} \left[1 + m.\pi^{m-1} \int_{-1}^{1} \frac{(\cos^{-1}p)^2 dp}{(A(p) - \pi p)^{m+1}}\right]\rho^{-m/2} \quad . \tag{2.2}$$

In Table 2 we list the moments of J_∞, the transect length for a uniform random member of V_∞, numerically calculated from (2.2), together with the same moments for D_∞, the side length.

Table 2

m	$E(J_\infty^m)$	$E(D_\infty^m)$
1	0.826	$2/\sqrt{2}/3\sqrt{\pi} = 0.532$
2	1.26	0.576
3	2.74	0.952
4	7.71	2.13

Utilizing these values, and (1.3.4), we can obtain the moments listed in Table 3, all of which refer to the limiting tessellation V_∞.

Table 3

$E(\Phi_\infty)$	5.19
$E(A_\infty^{\ 2})$	3.946
$E(A_\infty^{\ 2}R_\infty)$	5.73
$E(A_\infty I_\infty)$	12.1
$Var(J_\infty)$	0.574
$Var(D_\infty)$	0.293
$Var(A_\infty)$	2.946

BIBLIOGRAPHY

Ambartzumian, R.V. (1970). Random fields of segments and random mosaics on a plane. *Proc.* 6^{th} *Berkeley Symp. Math. Statist. Prob.* 3, 369-381.

Ambartzumian, R.V. (1974). Convex polygons and random tessellations. In Harding and Kendall (1974), 176-191.

Barlow, G.W. (1974). *Anim. Behav.* 22, 876-878.

Bernal, J.D. (1959). A geometrical approach to the structure of liquids. *Nature* 183, 141-147.

Besag, J. (1974). Spatial interaction and the statistical analysis of lattice systems. *J.R.S.S. B*, 36, 192-225.

Boots, B.N. (1974). Delaunay triangles: an alternative approach to point pattern analysis. *Proc. Assoc. Amer. Geographers* 6, 26-29.

Bowyer, A. (1981). Computing Dirichlet tessellations. *Comp. J.* 24, 162-166.

Cowan, R. (1978). The Use of the Ergodic Theorems in Random Geometry. *Suppl. Adv. Appl. Prob.* 10, 47-57.

Crain, I.K. and Miles, R.E. (1976). Monte Carlo estimates of the distributions of the random polygons determined by random lines in the plane. *J. Statist. Comp. Sim.* 4, 293-325.

Cruz-Orive, L.M. (1979). Distortion of Certain Voronoi Tessellations when one particle moves. *J. Appl. Prob.* 16, 95-103.

Davidson, R. (1974). See Harding and Kendall (1974).

Dirichlet, P.G. (1850). Über die Reduction der positiven quadratischen Formen mit drei unbestimmten ganzen Zahlen. *J. für die reine und angewandte Mathematik* 40, 216-219.

Fischer, R.A. and Miles, R.E. (1973). The Role of Spatial Pattern in the Competition between Crop Plants and Weeds - A Theoretical Analysis. *Math. Biosci.* 18, 335-350.

Gates, D.J., O'Conner, A.J., and Westcott, M. (1979). Partitioning the union of disks in plant competition models. *Proc. R. Soc. Lond. A.* 367, 59-79.

Gilbert, E.N. (1962). Random Subdivisions of space into crystals. *Ann. Math. Statist.* 33, 958-972.

Gilbert, E.N. (1967). Random Plane Networks and needle-shaped crystals. *Chap. 16 of Applications of Undergraduate Mathematics in Engineering,* B. Noble. Macmillan, New York.

Goudsmit, S.A. (1945). Random Distribution of Lines in a Plane. *Rev. Mod. Phys.* 17, 321-322.

Grant, P.R. (1968). *Amer. Naturalist.* 102, 75-80.

Green, P.J. and Sibson, R. (1978). Computing Dirichlet tessellations in the plane. *Comp. J.* 21, 168-173.

Hamilton, W.D. (1971). Geometry for the selfish herd. *J. Theor. Biol.* 31, 295-311.

Harding, E.F., and Kendall, D.G. (1974). *Stochastic Geometry: A Tribute to the Memory of Rollo Davidson.* Wiley, London.

Hasegawa, M. and Tanemura, M. (1976). On the pattern of space division by territories. *Ann. Inst. Statist. Math.* 28, Part B, 509-519.

Hasegawa, M. and Tanemura, M. (1977a). *Japanese. J. Appl. Statist.* 5, 47-61.

Hasegawa, M. and Tanemura, M. (1977b). *Hoppoh Ringyo (Northern Forestry).* 29, 115-119.

Hasegawa, M. and Tanemura, M. (1978). Mathematical Models on Spatial Patterns of Territories. *Proc. Int. Sym. on Math. Topics in Biology,* Kyoto, Japan, September 1978.

Hinde, A.L. and Miles, R.E. (1980). Monte Carlo estimates of the distributions of the random polygons of the Voronoi tessellation with respect to a Poisson process. *J. Statist. Comput. Simul.* 10, 205-223.

Horspool, N. (1979). Constructing the Voronoi diagram in the plane, *Technical Report SOCS 79.12*, July 1979, McGill Univ.

Hudspeth, A.J. (1975). *Proc. Nat. Acad. Sci. U.S.A.* 72, 2711-2713.

Kallenberg, O. (1976). On the structure of stationary flat processes. *Z. Wahrscheinlichkeitstheorie verw. Gebiete.* 37, 157-174.

Krickeberg, K. (1973). Moments of Point Processes. *Lecture Notes in Mathematics* 296, Springer-Verlag, Berlin, 70-101.

Lewis, F.T. (1946). The shape of cells as a mathematical problem. *Amer. Scientist* 34, 359-369.

Lewis, P.A.W. (Ed) (1972). *Stochastic Point Processes: Statistical Analysis, Theory and Applications*, Wiley.

Mardia, K.V., Edwards, R. and Puri, M.L. (1978). Analysis of central place theory. *Bull. I.S.I.* 47 (2), 93-110.

Matheron, G. (1975). *Random Sets of Integral Geometry*, Wiley, New York.

Matschinski, M. (1954). Considérations statistiques sur les polygones et les polyèdres. *Publ. Inst. Stat. Univ. Paris.* 3, 179-201.

Maynard-Smith, J. (1974). *Models in Ecology* (C.U.P.).

Mead, R. (1971). Models for interplant competition in irregularly spaced populations. In *Statist. Ecology* (Patil et al., eds.) Penn. State. U.P., Vol 2, 13-30.

Meijering, J.L. (1953). Interface area, edge length, and number of vertices in crystal aggregates with random nucleation. *Phillips. Res. Rep.* 8, 270-290.

Miles, R.E. (1961). Random Polytopes: the generalization to n dimensions of the intervals of a Poisson process. *PhD Thesis*, Cambridge Univ.

Miles, R.E. (1964). Random Polygons determined by random lines in a plane. *Proc. Nat. Acad. Sci. U.S.A.* 52, I 901-907, II 1157-1160.

Miles, R.E. (1970). On the Homogeneous Planar Poisson Point Process. *Math. Biosci.* 6, 85-127.

Miles, R.E. (1971). Poisson flats in Euclidean spaces. Part II: Homogeneous Poisson flats and the Complementary Theorem. *Adv. Appl. Prob.* 3, 1-43.

Miles, R.E. (1972). The Random Division of Space. *Suppl. Adv. Appl. Prob.* 243-266.

Miles, R.E. (1973). The Various Aggregates of Random Polygons determined by Random lines in a plane. *Adv. Math.* 10, 256-290.

Miles, R.E. (1974). A Synopsis of 'Poisson flats in Euclidean spaces'. In Harding and Kendall (1974), 202-227.

Miles, R.E. and Maillardet, R.J. (1982). The basic structures of Voronoi and generalized Voronoi polygons. *Essays in Statistical Science* (ed. J. Gani and E.J. Hannan), *Applied Prob. Trust, J. Appl. Prob.* 19A, 97-111.

Ogawa, T. and Tanemura, M. (1974). Geometrical Considerations on Hard Core Problems. *Prog. Theo. Phy.* 51, 399-417.

Ore, O. (1963). *Graphs and their uses.* Random House.

Papangelou, F. (1972). Summary of some results on point and line processes. In Lewis (1972), 522-532.

Rhynsburger, D. (1973). Analytic delineation of Thiessen polygons. *Geographical Analysis.* 5, 133-144.

Richards, P.I. (1964). Averages for Polygons formed by Random Lines. *Proc. Nat. Acad. Sci. U.S.A.* 52, 1160-1164.

Ripley, B.D. (1977). Modelling Spatial Patterns. *J.R.S.S. B,* 39, 172-192.

Robbins, H.E. (1944). On the measure of a random set. *Ann. Math. Statist.* 15, 70-74.

Santalo, L.A. (1976). *Integral Geometry and Geometric Probability,* Vol 1, Encyclopedia of Mathematics and its Applications, Addison-Wesley, Reading, Mass.

Sato, T. (1978). *Japanese J. Ophthalmol.* 22, 114-126.

Shamos, M.I. and Hoey, D. (1975). Closest point problems. *Proc. 16th Annual IEEE Symp. on Foundations of Computer Science (1975)*, 151-162.

Sibson, R. (1978). Locally equiangular triangulations. *Comp. J.* 21, 243-245.

Sibson, R. (1980a). A vector identity for the Dirichlet tessellation. *Math. Proc. Camb. Phil. Soc.* 87, 151-155.

Sibson, R. (1980b). The Dirichlet tessellation as an aid in data analysis. *Scand. J. Statist.* 7, 14-20.

Smalley, I.J. (1966). Contraction crack networks in basalt flows. *Geol. Mag.* 103, 110-114.

Solomon, H. (1978). *Geometric Probability* CBMS-NSF Regional Conference Series in Applied Mathematics, No. 28. Society for Industrial and Applied Mathematics, Philadelphia.

Tanemura, M. et al. (1977). Geometrical Analysis of Crystallization of the Soft-Core Model. *Prog. Theor. Phys.* 58, 1079-1095.

Watson, D.F. (1981). Computing the n-dimensional Delaunay tessellation with application to Voronoi polytopes. *Comp. J.* 24, 167-172.

Weiner, N. (1939). The Ergodic Theorem. *Duke Math. J.* 5, 1-18.